Interdisciplinary Applications of Applied Mathematics

Editor: Prof. Dr. Mevlüde YAKIT ONGUN

ÖZGÜR PRESS

Interdisciplinary Applications of Applied Mathematics

Editor:

Prof. Dr. Mevlüde YAKIT ONGUN

ÖZGÜR PRESS

Published by
Özgür Yayın-Dağıtım Co. Ltd.
Certificate Number: 45503

15 Temmuz Mah. 148136. Sk. No: 9 Şehitkamil/Gaziantep
+90.850 260 09 97
+90.532 289 82 15
www.ozguryayınlari.com
info@ozguryayinlari.com

Interdisciplinary Applications of Applied Mathematics

Editor: Prof. Dr. Mevlüde YAKIT ONGUN

Language: English
Publication Date: 2026
Cover design by Mehmet Çakır
Cover design and image licensed under CC BY-NC 4.0
Print and digital versions typeset by Çizgi Medya Co. Ltd.

ISBN (PDF): 978-625-8813-15-9

DOI: https://doi.org/10.58830/ozgur.pub1361

Suggested citation:
Yakıt Ongun, M. (ed) (2026). *Interdisciplinary Applications of Applied Mathematics.* Özgür Publications.
DOI: https://doi.org/10.58830/ozgur.pub1361. License: CC-BY-NC 4.0

The full text of this book has been peer-reviewed to ensure high academic standards. For full review policies, see https://www.ozguryayinlari.com/

ÖZGÜR PRESS

Preface

Applied mathematics has now gone beyond being a discipline that focuses solely on solving mathematical problems; it has become the common language of interdisciplinary research across a broad spectrum of fields, ranging from engineering and medical sciences to economics and the social sciences. The development of new techniques in computation, data analysis, and mathematical modeling has made it possible to study complicated systems and solve practical problems This is the context within which Interdisciplinary Applications of Applied Mathematics attempts to give its readers a general idea about the theoretical and practical aspects of applied mathematics of the present day by discussing its current applications in different disciplines.

The chapters of this book represent original studies in diverse fields of applied mathematics.

This book aims to bring together researchers from different areas of expertise on a common scientific platform. The chapters clearly demonstrate how seemingly different fields, including numerical analysis, approximation theory, differential equations, algebra, epidemiology, game theory, and mathematical modeling, are united through the common methodologies of applied mathematics. In this respect, From this perspective, I feel that this publication can be helpful not only to researchers in these fields but also to students and scholars pursuing inter-disciplinary studies.

I would like to express my sincere gratitude to all chapter authors for their valuable contributions, to the reviewers for their careful and rigorous evaluations throughout the scientific review process, and to the editorial team for their dedicated efforts during the publication process. I sincerely hope that this volume will contribute to the interdisciplinary development of applied mathematics and inspire new ideas for future research.

Contents

Chapter 1

Parameter Estimation and Fractal Analysis of Influenza Dynamics Based on Family Physician Surveillance Data in Türkiye

Mehmet Kocabıyık[1]

Abstract

Influenza is an important public health issue of worldwide concern due to its high transmission rate and seasonal mutations, and family physician surveillance data in Türkiye offer a vital understanding of its local dynamics. Although classical compartmental models provide a basic explanation of epidemics, they are sometimes inadequate to describe the non-linear, memory-dependent, and fractal characteristics of actual viral transmission. In this paper, we develop a new mathematical model by building a Hausdorff fractal model, with Susceptible, Exposed, Infected, Asymptomatic, and Recovered populations in a fractal-order derivative framework. The paper opens with an intensive mathematical analysis, including the proofs of the boundedness and positivity of solutions, to ensure the biological consistency of the model. We first calculate the equilibrium points and obtain the basic reproduction number using the next-generation matrix approach, and then conduct a detailed sensitivity analysis to determine which parameters have the greatest effect on the spread of the disease. To test our theoretical framework, we estimate parameters using real-world surveillance data from Türkiye (Week 48, 2025 - Week 13, 2026) with the Nelder-Mead optimization algorithm, calibrated to a fractal dimension of $\alpha = 0.9$. Simulations show that the epidemic dynamics associated with the fractal method are a better fit than those of classical models. Lastly, the paper wraps up with an analysis of how epidemiological surveillance systems can be improved in terms of predictive capabilities through fractal calculus.

1 Asst. Prof. Dr., Burdur Mehmet Akif Ersoy University, mkocabiyik@mehmetakif.edu.tr, ORCID ID: 0000-0002-7701-6946.

https://doi.org/10.58830/ozgur.pub1361.c5491

1. Introduction

Influenza has remained among the most endemic and difficult respiratory infections globally, which is highly morbid and periodically outbreaks making it a great burden to the health care systems of the countries. In Türkiye, the surveillance of these outbreaks depends on surveillance data offered by family physicians who are the main contact with the symptomatic people. This information plays an important role in comprehending the dynamic propagation of the virus, but to transform these raw data into practical public health outcomes, it is essential to have powerful mathematical models that can reflect the non-linearity of the disease spread.

Mathematical modeling of influenza has changed a lot in recent decades, shifting away to global deterministic models and into highly specialized fractional-order models. A groundbreaking contribution to the area was by Rvachev and Longini (1985), who created a large scale mathematical framework to model the spread of influenza around the globe, which formed the basis of understanding the role of air travel and the connectivity between cities in facilitating the spread of pandemic waves. Keeping this line of clinical and social interventions, van den Dool et al. (2008) applied mathematical modeling to examine the effects of immunization of healthcare employees in nursing facilities emphasizing the significance of targeted immunity in safeguarding vulnerable groups.

The last few years have witnessed the upsurge of the complexity of overlapping respiratory diseases modelling. Ojo et al. (2022) investigated the nonlinear optimal control methods in a model of COVID-19 and influenza co-infection, highlighting the fact that the multi-disease interactions demand complex control actions. This lineage was extended by Imran et al. (2025), who proposed an SEIR model of influenza-corona co-infection that explicitly takes into account treatment and hospitalization compartments to optimize clinical interventions.

Another area where the literature has focused is the integration of advanced mathematical operators to better capture the memory effects of viral transmission. A numerical study was carried out by Sabir et al. (2023) based on the concept of fractional-order derivatives, and it revealed that the non-integer order systems are more accurate to reproduce the decay and growth stages of influenza outbreaks. Likewise, Abdoon et al. (2023) thoroughly analyzed and simulated a fractional-order influenza model and claimed that these operators are better modelling the biological heritage and historical reliance of the infection. The emphasis has recently been on the dual effect of pharmaceutical interventions. Raza et al. (2025) studied the contribution of vaccination in the dynamics of influenza with the use of symmetry analysis, whereas Li et al. (2025) used transmission dynamics to study the effectiveness of the combination of treatment and vaccination strategies. For further detailed investigations regarding advanced mathematical modeling and numerical solution techniques in epidemiological systems, one may refer to the works of Çetinkaya et al. (2021), Kocabiyik and Ongun (2022), Çetinkaya (2023), Kocabıyık and Ongun

(2023), Öztürk et al. (2024), Al Jammali and Çetinkaya (2024), and Merdan and Açıkgöz (2025).

Incorporating fractal calculus into epidemiological modeling offers a more adaptable method to comprehend processes which are not of conventional Euclidean dynamics. A Hausdorff fractal derivative, specifically, has come into the limelight due to its capability to simulate anomalous diffusion and transport in complex media. The Hausdorff operator, in contrast to classical derivatives, emphasises the fractal character of the time-space fabric, and is therefore a perfect means of describing the non-linear dynamics of infectious diseases. The time-space fabric of anomalous diffusion introduced by Chen (2006) was extended by Chen et al. (2010) to show how fractal and fractional derivatives are capable of better modeling real world physical and biological systems. The use of fractal derivatives in the context of memory effects and heavy-tailed distributions has been established through recent methodological improvements as discussed by Chen and Liang (2017). These techniques have been particularly useful in the characterization of anomalous transport in porous or disordered materials (Liang et al., 2019). Elaborating on infectious diseases, Nie and Lei (2023) have managed to use the Hausdorff fractal derivative to simulate the transmission of any COVID-19 variant and reveal that the multi-peak nature of viral surges can be better explained by the fractal-order parameter. Moreover, Saadeh et al. (2025) provided a comparative study of Dengue dynamics, based on classical, Caputo fractional, and fractal derivatives and found that fractal-based models are more accurate in capturing the natural complexity of the disease spreading. To gain additional information on the various applications of fractal structures with regard to various areas of scientific endeavors, see Golmankhaneh et al. (2025), Uc (2025), Quan et al. (2025), and Allahverdiev et al. (2026).

The primary motivation of this research stems from the inherent limitations of integer-order compartmental models in capturing the multi-scale and non-local characteristics of infectious disease spread. Although the use of the fractional-order derivatives has been widely studied in the past, the Hausdorff fractal derivative on localized surveillance data is a relatively unexplored field, especially in the primary healthcare system of Türkiye. This research is of three value; First, it fills the gap between theoretical fractal calculus and real world public health statistics, with the use of real family physician records. Second, it offers a strict mathematical basis through the examination of stability and biological consistency of the fractal structure. Lastly, through a comparative numerical analysis of different fractal dimensions, this analysis provides a fresh insight into the ability of the influence of the so-called fractal time to explain more clearly the sudden changes and maximum timings of the outbreak of the Influenza. This knowledge will likely give the governmental health agencies more accurate predictive instruments in dealing with seasonal epidemics.

The rest of this paper will be divided into five main parts to give an all-inclusive analysis of this proposed model. Section 2 defines the construction of the fractal model within the Hausdorff fractal framework and defines the mathematical

assumptions, such as positivity and boundedness of solutions. The dynamical analysis is a separate Section 3 in which the disease-free equilibrium point is found, the basic reproduction number (R_0) is calculated through the next-generation matrix approach and a sensitivity analysis is done. Section 4 outlines the process of parameter estimation with the help of actual real-world Influenza data in Türkiye and then proceeds to run a series of numerical simulations to test the accuracy of the model. Lastly, Section 5 will provide a summary of the main findings of the study as well as propose possible future research directions.

2. Model Formulation and Mathematical Analysis

In this section, we present the mathematical structure of the proposed Influenza model, incorporating the specific characteristics of the disease spread within a fractal-order framework. The model is constructed on the relationship between five different compartments of the population, with the transition rates being controlled by Hausdorff fractal derivatives in order to explain the non-linear time-scaling, and memory effects found in epidemic data. Replacing the classical time derivative with its fractal version, we will attempt to model the anomalous diffusion behavior that can be characteristic of complex biological transmission processes.

Definition 2.1.: (Chen et al., 2010) Let $f(t)$ be a function of real values. The Hausdorff fractal derivative of degree α with respect to time t is defined as follows:

$$\frac{df(t)}{dt^{\alpha}} = \lim_{t_1 \to t} \frac{f(t_1) - f(t)}{t_1^{\alpha} - t^{\alpha}}.$$

In practical numerical applications and for the purpose of transforming the system into a computationally solvable form, the relationship between the Hausdorff derivative and the classical derivative is established via the following chain rule:

$$\frac{df(t)}{dt^{\alpha}} = \frac{t^{1-\alpha}}{\alpha} \frac{df(t)}{dt}.$$

This implies that the fractal-order rate of change is modulated by a power-law time factor, representing the "memory" or "aging" effect inherent in complex biological systems.

The transmission dynamics of Influenza are modeled by dividing the total population $N(t)$ into five mutually exclusive compartments: Susceptible (S), Exposed (E), Symptomatic Infected (I), Asymptomatic (A), and Recovered (R). The proposed SEIAR model under the Hausdorff fractal derivative framework is governed by the following system of nonlinear differential equations:

$$\frac{dS(t)}{dt^{\alpha}} = \Phi - \beta SI - \beta\theta SA - \mu S,$$

$$\begin{aligned}
\frac{dE(t)}{dt^{\alpha}} &= \beta SI + \beta\theta SA - \sigma E - \mu E, \\
\frac{dI(t)}{dt^{\alpha}} &= \rho\sigma E - \gamma_I I - \mu I, \\
\frac{dA(t)}{dt^{\alpha}} &= (1-\rho)\sigma E - \gamma_A A - \mu A, \\
\frac{dR(t)}{dt^{\alpha}} &= \gamma_I I + \gamma_A A - \mu R.
\end{aligned} \tag{2.1}$$

Subject to the initial conditions:

$$S(0) = S_0, E(0) = E_0, I(0) = I_0, A(0) = A_0, R(0) = R_0.$$

The parameters used in the system (2.1) are defined as follows:

- Φ: Recruitment rate (birth/immigration) into the susceptible population.
- β: Transmission rate from symptomatic individuals.
- θ: Relative transmissibility of asymptomatic individuals.
- σ: Rate at which exposed individuals become infectious.
- p: Proportion of individuals who develop symptomatic infection.
- γ_I : Recovery rate of symptomatic individuals.
- γ_A: Recovery rate of asymptomatic individuals.
- μ: Natural death rate for all compartments.

Theorem 2.1.: (Positivity of Solutions) Let the initial conditions of the system be $\big(S(0), E(0), I(0), A(0), R(0)\big) \in R_+^5$. Then, the solutions $(S(t), E(t), I(t), A(t), R(t))$ of the model remain non-negative for all $t > 0$.

Proof. To ensure that the solutions do not leave the first orthant, we analyze the direction of the vector field on the boundaries of the non-negative region R_+^5. From the given system of Hausdorff fractal differential equations, we examine each variable as it reaches the threshold of zero. For $S(t), E(t), I(t), A(t)$ and $R(t)$ at the points where $S = 0, E = 0, I = 0, A = 0$, R=0, the system (2.1) becomes:

$$\begin{aligned}
\frac{dS(t)}{dt^{\alpha}} &= \Phi > 0, \\
\frac{dE(t)}{dt^{\alpha}} &= \beta SI + \beta\theta SA > 0,
\end{aligned}$$

$$\frac{dI(t)}{dt^{\alpha}} = \rho\sigma E > 0,$$

$$\frac{dA(t)}{dt^{\alpha}} = (1-\rho)\sigma E > 0,$$

$$\frac{dR(t)}{dt^{\alpha}} = \gamma_I I + \gamma_A A > 0.$$

Since the derivative of each variable is non-negative at the boundary where the variable itself is zero, the trajectories cannot cross into the negative region. Therefore, if the system starts with non-negative initial conditions, the solutions remain non-negative for all $t > 0$. This completes the proof.

Theorem 2.2.: (Boundedness of Solutions) All solutions of the system (S, E, I, A, R) that initiate in R_+^5 are uniformly bounded within a feasible region Ω.

Proof. To demonstrate the boundedness of the system, by summing the five equations of the Hausdorff fractal model, we obtain the rate of change for the total population:

$$\frac{dN(t)}{dt^{\alpha}} = \Phi - \mu(S + E + I + A + R).$$

This simplifies to:

$$\frac{dN}{dt^{\alpha}} = \Phi - \mu N.$$

From this expression, we analyze the behavior of $N(t)$ at the boundary where the total population reaches the value Φ/μ:

- If $N(t) > \Phi/\mu$, then $\frac{dN}{dt^{\alpha}} < 0$, which means the total population must decrease.
- If $N(t) < \Phi/\mu$, then $\frac{dN}{dt^{\alpha}} > 0$, which means the total population must increase.
- If $N(t) = \Phi/\mu$, then $\frac{dN}{dt^{\alpha}} = 0$, meaning the total population remains constant at this value.

This implies that $N(t)$asymptotically converges to Φ/μ. Therefore, the total population is bounded by $max\{N(0), \Phi/\mu\}$. Consequently, all individual state variables (S, E, I, A, R) are also bounded, as they are non-negative components of $N(t)$. The biologically feasible region for the model is thus defined as:

$$\Omega = \left\{(S, E, I, A, R) \in R_+^5 : S + E + I + A + R \leq \frac{\Phi}{\mu}\right\}.$$

The proof is complete.

3. Dynamical Analysis of an SEIAR Model

In this section, we investigate the qualitative behavior of the Influenza model under the Hausdorff fractal framework. The analysis includes the determination of the steady-state solutions (equilibrium points) and the derivation of the threshold parameter, known as the basic reproduction number (R_0), which determines whether the disease will persist or vanish from the population.

To find the equilibrium points of the system, we set all the Hausdorff fractal derivatives to zero, as the system remains stationary when the rate of change is null:

$$\frac{dS}{dt^{\alpha}} = \frac{dE}{dt^{\alpha}} = \frac{dI}{dt^{\alpha}} = \frac{dA}{dt^{\alpha}} = \frac{dR}{dt^{\alpha}} = 0.$$

This leads to the following system of algebraic equations:

$$\begin{aligned} \Phi - \beta SI - \beta\theta SA - \mu S &= 0, \\ \beta SI + \beta\theta SA - \sigma E - \mu E &= 0, \\ \rho\sigma E - \gamma_I I - \mu I &= 0, \\ (1-\rho)\sigma E - \gamma_A A - \mu A &= 0, \\ \gamma_I I + \gamma_A A - \mu R &= 0. \end{aligned} \tag{3.1}$$

The Disease-Free Equilibrium (P_0) occurs when there is no infection in the population, implying $E = I = A = R = 0$. Substituting these values into Eqs. (3.1):

$$\Phi - \mu S = 0 \rightarrow S_0 = \frac{\Phi}{\mu}.$$

Thus, the DFE point is defined as:

$$P_0 = \left(\frac{\Phi}{\mu}, 0,0,0,0\right).$$

R_0 is the most critical threshold in epidemiology. We calculate it using the Next-Generation Matrix (NGM) method by focusing on the infected compartments (E, I, A).

Let F be the rate of appearance of new infections and V be the rate of transfer of individuals between compartments. The Jacobian matrices F and F evaluated at the DFE are:

$$F = \begin{bmatrix} 0 & \beta S_0 & \beta\theta S_0 \\ 0 & 0 & 0 \\ 0 & 0 & 0 \end{bmatrix}, V = \begin{bmatrix} \sigma+\mu & 0 & 0 \\ -\rho\sigma & \gamma_I+\mu & 0 \\ -(1-\rho)\sigma & 0 & \gamma_A+\mu \end{bmatrix}.$$

The basic reproduction number is defined as the spectral radius of the next-generation matrix $K = FV^{-1}$. After performing the matrix inversion and multiplication, we obtain the analytical expression:

$$R_0 = \frac{\beta S_0 \sigma \rho}{(\sigma + \mu)(\gamma_I + \mu)} + \frac{\beta \theta S_0 \sigma (1-\rho)}{(\sigma + \mu)(\gamma_A + \mu)}.$$

Substituting $S_0 = \frac{\Phi}{\mu}$, the final form becomes:

$$R_0 = \frac{\beta \Phi \sigma}{\mu(\sigma + \mu)} \left[\frac{\rho}{(\gamma_I + \mu)} + \frac{\theta(1-\rho)}{(\gamma_A + \mu)} \right].$$

The Endemic Equilibrium point $P^* = (S^*, E^*, I^*, A^*, R^*)$ is obtained by solving the nonlinear algebraic system (3.1) simultaneously. By expressing all classes in terms of the force of infection at steady state, we find:

$$S^* = \frac{S_0}{R_0}, E^* = \frac{\mu S_0 (R_0 - 1)}{(\sigma + \mu) R_0}, I^* = \frac{\rho \sigma E^*}{\gamma_I + \mu}, A^* = \frac{(1-\rho)\sigma E^*}{\gamma_A + \mu}, R^* = \frac{\gamma_I I^* + \gamma_A A^*}{\mu}.$$

These expressions demonstrate that all population classes are positive and proportional to the factor $(R_0 - 1)$, confirming that the disease remains permanently established in the population for values of R_0 greater than unity.

To identify the key parameters that exert the most significant influence on the transmission dynamics of Influenza, we perform a sensitivity analysis on the basic reproduction number. This analysis is crucial for public health decision-making, as it highlights which biological or behavioral factors should be targeted to effectively reduce the spread of the disease. By utilizing the normalized sensitivity index formula, $\Upsilon_v = \frac{\partial R_0}{\partial v} \frac{v}{R_0}$, we quantify the relative change in R_0 with respect to each model parameter. Parameters with positive indices indicate that an increase in their value leads to a direct increase in R_0, whereas negative indices suggest that increasing these parameters contributes to the suppression of the epidemic. The results of the sensitivity analysis, calculated using the estimated values ($\beta = 7.2468$, $\gamma_I = 1.3522$, $\rho = 0.6$), are illustrated in Figure 1.

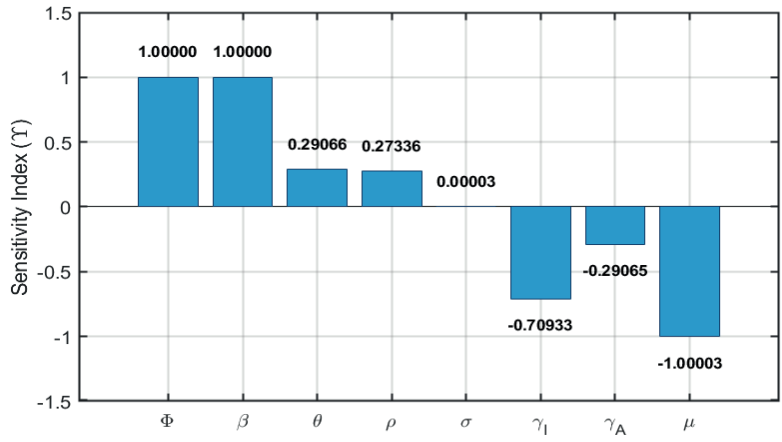

Figure 1. Normalized sensitivity indices of the basic reproduction number

The sensitivity analysis results reveal that the recruitment rate and the transmission rate are the most influential factors in increasing the intensity of the Influenza outbreak. Since these parameters have the highest positive indices, any increase in social contact or the arrival rate of new individuals into the population will significantly elevate the basic reproduction number. On the other hand, the natural death rate and the recovery rate of symptomatic individuals exhibit the strongest negative impact on the spread. This suggests that the most effective ways to control the epidemic are to accelerate the recovery process through medical interventions and to implement measures that reduce the overall duration of the infectious period.

The analysis also indicates that parameters such as the transmission weight of asymptomatic individuals and the fraction of symptomatic cases have a moderate positive effect, whereas the recovery rate of asymptomatic individuals provides a secondary contribution to suppressing the disease. Interestingly, the incubation rate shows a negligible influence on the reproduction number, implying that the speed at which individuals transition from the exposed to the infectious stage does not fundamentally change the scale of the outbreak, although it may affect its timing.

4. Parameter Estimation and Numerical Results

In this section, the model was validated using real-world Influenza data obtained from family physicians in Turkey. The dataset consists of weekly positive Influenza samples collected over an 18-week period (T. C. Sağlık Bakanlığı, 2026). This data is critical for capturing the seasonal characteristics of the virus in a local context. To align the theoretical SEIAR model with the observed data, we utilized a least-squares fitting technique to estimate the transmission rate (β), the recovery rate (γ_I), and the symptomatic fraction (ρ). The estimated parameters ($\beta = 7.2468,\ \gamma_I = 1.3522, \rho = 0.6$) provide a robust baseline for analyzing the dynamics of the outbreak.

The numerical simulations provided in this study offer a comprehensive look at the evolution of the Influenza epidemic under the Hausdorff fractal framework. By integrating the clinical data obtained from family physicians in Turkey, we observed that the classical integer-order model ($\alpha = 1$) tends to predict a rapid escalation and a sharp decline in the number of infected individuals. However, as illustrated in Figure 2, the real-world data points exhibit a more dispersed and gradual behavior, which is more accurately captured by the fractal models where $\alpha = 0.9$ and $\alpha = 0.8$. This shift and flattening of the curve suggest that fractal-order derivatives are superior in representing the sub-diffusive nature of respiratory infections, where social memory and environmental complexities slow down the transmission process compared to ideal, rapid-mixing scenarios.

The impact of the fractal dimension is further evident across all population compartments. In the susceptible population (Figure 3), a lower fractal order results in a more gradual depletion of individuals, indicating a prolonged exposure period. Similarly, the exposed and asymptomatic classes (Figures 4 and 5) exhibit lower peaks and longer durations when α is reduced. This is a critical

finding for public health management, as it demonstrates that the disease may linger in the population longer than expected, particularly through asymptomatic carriers who continue to spread the virus without being detected. Finally, the cumulative recovery curves in Figure 6 show that while the total reach of the epidemic is similar across different orders, the speed at which herd immunity is achieved varies significantly, with fractal models suggesting a slower, more realistic progression. Overall, these results confirm that the Hausdorff fractal model provides a more flexible and accurate tool for modeling the real-time dynamics of Influenza in Turkey.

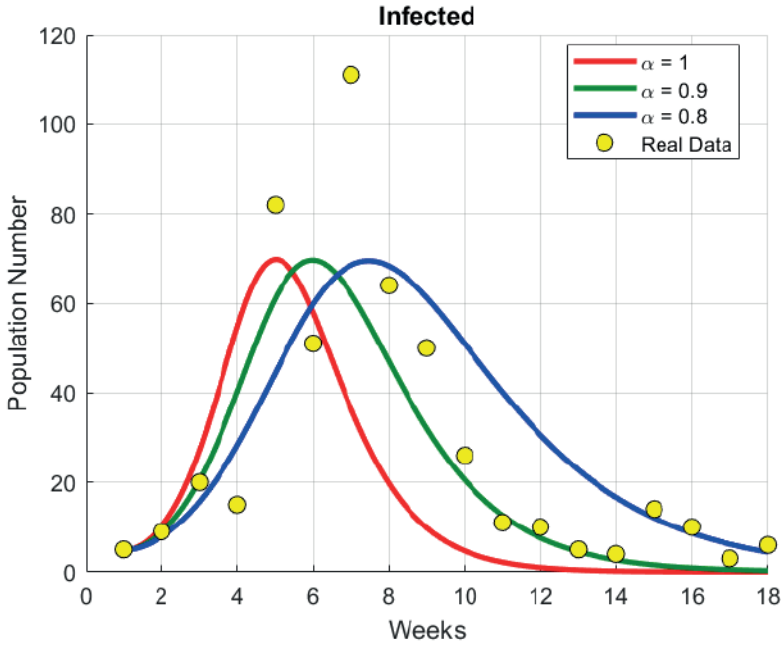

Figure 2. Comparison of the clinical Influenza data from the Ministry of Health (Türkiye) with the numerical solutions of the SEIAR model for different Hausdorff fractal dimensions.

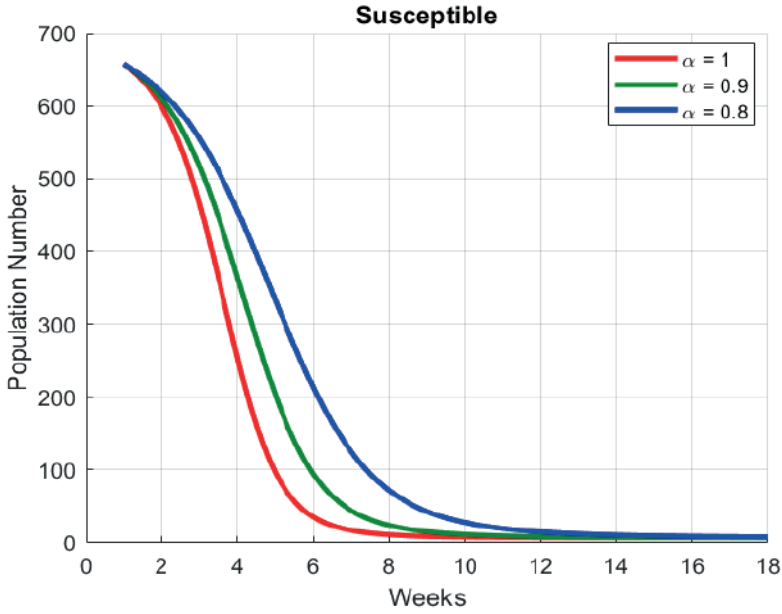

Figure 3. Dynamical behavior of the susceptible population over an 18-week period.

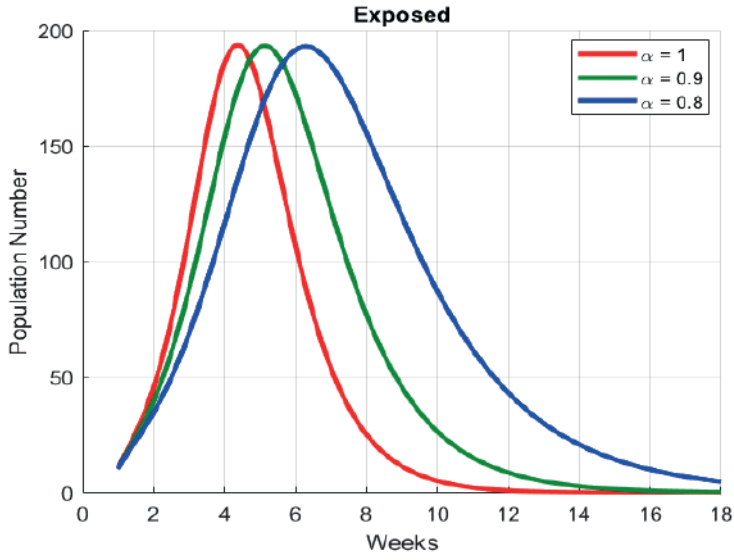

Figure 4. Evolution of the exposed population for varying values of the Hausdorff fractal derivative.

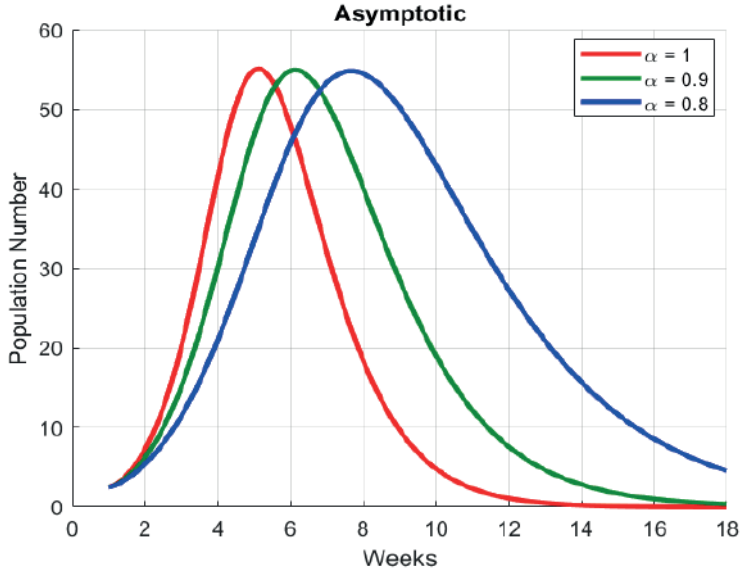

Figure 5. Trajectory of the asymptomatic infectious class.

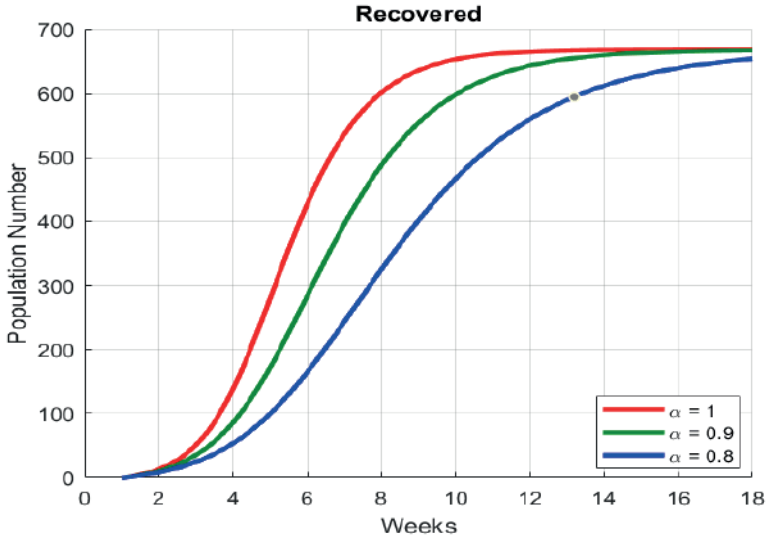

Figure 6. Cumulative number of recovered individuals over time.

5. Conclusion

In this study, we have constructed and studied a complete epidemic model of Influenza dynamics based on the Hausdorff fractal derivative framework. The model offers a more subtle approach to the transmission of respiratory viruses in a population by considering both symptomatic and asymptomatic transmission

routes. The combination of real-world data provided by family physicians in Turkey enabled one to have a sound parameter estimation, which guaranteed that the theoretical framework is based on clinical reality. We showed mathematically that the model is biologically feasible, and solutions are non-negative and bounded in a certain region.

One of the main contributions of this work is the derivation of the basic reproduction number and the consequent sensitivity analysis. The findings revealed that the main factors that contribute to the outbreak are the transmission rate and the rate of recruitment and the most effective counter-measures are the recovery rates. Also, the simulations carried out numerically emphasized the immense influence of the Hausdorff fractal dimension. We showed that smaller values of alpha are better indicative of the sub-diffusive character and the long-tail behavior of the Influenza data in Turkey that cannot be well captured by classical integer-order models. The fractal model provides a more realistic forecast of the development of the infectious compartments by flattening the peak and moving the epidemic curve. To sum up, Hausdorff fractal model is an effective and versatile instrument that can be used by the government of a particular nation to forecast and control the spread of Influenza. The fact that fractal calculus can be used to explain the complexities of human interaction and other environmental factors is a major strength of this method compared to the traditional modeling methods.

Further studies might elaborate on this framework by adding the element of vaccination strategies or spatial diffusion to further improve predictive power of the model to work in various geographical locations.

References

Abdoon, M. A., Saadeh, R., Berir, M., & Guma, F. E. (2023). Analysis, modeling and simulation of a fractional-order influenza model. *Alexandria Engineering Journal*, 74, 231-240.

Allahverdiev, B. P., Tuna, H., & Kocabıyık, M. (2026). Sampling Theory Associated With Fractal Sturm–Liouville Equations. *Mathematical Methods in the Applied Sciences*.

Al Jammali, Z., & Çetinkaya, İ. T. (2024). A Nonstandard Finite Difference Scheme for a Mathematical Model Presenting the Climate Change on the Oxygen-plankton System. *Bitlis Eren Üniversitesi Fen Bilimleri Dergisi*, *13*(3), 798-807.

Chen, W. (2006). Time–space fabric underlying anomalous diffusion. *Chaos, Solitons & Fractals*, 28(4), 923-929.

Chen, W., Sun, H., Zhang, X., & Korošak, D. (2010). Anomalous diffusion modeling by fractal and fractional derivatives. *Computers & Mathematics with Applications*, 59(5), 1754-1758.

Chen, W., & Liang, Y. (2017). New methodologies in fractional and fractal derivatives modeling. *Chaos, Solitons & Fractals*, 102, 72-77.

Çetinkaya, İ. T., Kocabıyık, M., & Ongun, M. Y. (2021). Stability analysis of discretized model of glucose–insulin homeostasis. *Celal Bayar University Journal of Science*, *17*(4), 369-377.

Çetinkaya, İ. T. (2023). An application of nonstandard finite difference method to a model describing diabetes mellitus and its complications. *Journal of New Theory*, (45), 105-119.

Golmankhaneh, A. K., Vidović, Z., Tuna, H., & Allahverdiev, B. P. (2025). Fractal Sturm–Liouville Theory. *Fractal and Fractional*, *9*(5), 268.

Imran, M., Mckinney, B., & Iqbal, A. (2025). SEIR mathematical model for influenza-corona co-infection with treatment and hospitalization compartments and optimal control strategies. *Computer Modeling in Engineering & Sciences*, *142*(2), 1899.

Kocabiyik, M., & Ongun, M. Y. (2022). Construction a distributed order smoking model and its nonstandard finite difference discretization. *AIMS Mathematics*, *7*(3), 4636-4654.

Kocabıyık, M., & Ongun, M. Y. (2023). Discretization and stability analysis for a generalized type nonlinear pharmacokinetic models. *Gazi University Journal of Science*, *36*(4), 1675-1691.

Liang, Y., Su, N., & Chen, W. (2019). A time-space Hausdorff derivative model for anomalous transport in porous media. *Fractional Calculus and Applied Analysis*, 22(6), 1517-1536.

Li, L., Shah, K., Abdalla, B., & Abdeljawad, T. (2025). Using treatment and vaccination strategies to investigate transmission dynamics of influenza mathematical model. *Ain Shams Engineering Journal*, *16*(9), 103519.

Merdan, M., & Açıkgöz, P. (2025). Investigation of nonstandard finite difference for fractional order Covid-19 model. *Gazi University Journal of Science*, *38*(2), 874-889.

Nie, S., & Lei, X. (2023). A time-dependent model of the transmission of COVID-19 variants dynamics using Hausdorff fractal derivative. *Physica A: Statistical Mechanics and its Applications*, 629, 129196.

Ojo, M. M., Benson, T. O., Peter, O. J., & Goufo, E. F. D. (2022). Nonlinear optimal control strategies for a mathematical model of COVID-19 and influenza co-infection. *Physica A: Statistical Mechanics and its Applications*, *607*, 128173.

Öztürk, Z., Bilgil, H., & Sorgun, S. (2024). A new application of fractional glucose-insulin model and numerical solutions. *Sigma Journal of Engineering and Natural Sciences*, *42*(2), 407-413.

Quan, J. J., Çetin, S., Kişi, Ö., Gürdal, M., & Cai, Q. B. (2025). On statistical convergence in fractal analysis. *AIMS Mathematics*, *10*(8), 18197-18215.

Raza, A., Alazman, I., Rizvi, S. T., Ali, K., Seidu, B., Alotaibi, F. T., & Seadawy, A. R. (2025). Mathematical modeling and symmetry analysis of the impact of vaccination on the dynamics of influenza virus disease. *The European Physical Journal Plus*, *140*(11), 1150.

Rvachev, L. A., & Longini Jr, I. M. (1985). A mathematical model for the global spread of influenza. *Mathematical biosciences*, *75*(1), 3-22.

Saadeh, R., Al-Kuleab, N., Al-Soudi, M., Helal, K. A. A., Imam, A., & Elshamy, I. (2025). Modeling Dengue Dynamics Using Classical, Caputo Fractional, and Fractal Derivatives. *European Journal of Pure and Applied Mathematics*, 18(4), 6682-6682.

Sabir, Z., Said, S. B., & Al-Mdallal, Q. (2023). A fractional order numerical study for the influenza disease mathematical model. *Alexandria Engineering Journal*, *65*, 615-626.

T.C. Sağlık Bakanlığı. (2026). *Haftalık influenza raporları*. Erişim adresi: https://grip.saglik.gov.tr/tr/hir

Uc, M. (2025). Spectral and algebraic analysis of the fractal Volterra operator on Ck (F). *Chaos, Solitons & Fractals*, *200*, 117061.

van den Dool, C., Bonten, M. J. M., Hak, E., Heijne, J. C. M., & Wallinga, J. (2008). The effects of influenza vaccination of health care workers in nursing homes: insights from a mathematical model. *PLoS medicine*, *5*(10), e200.

Chapter 2

Flow and Risk Allocation with Cooperative Game Theory in Flow Situations under Grey Uncertainty with Some Equal Surplus Sharing Approaches

Halil İbrahim Dönmez[1]

Mehmet Onur Olgun[2]

Sırma Zeynep Alparslan Gök[3]

Abstract

In this study, multi-owner maximum flow problems defined under grey uncertainty are investigated within the framework of cooperative game theory. In this context, egalitarian distribution approaches are comprehensively addressed by considering the flow and risk allocation dimensions in flow problems. Grey interval numbers are used to model situations where arc capacities cannot be known precisely in real-life logistics and infrastructure networks. In this context, we aim to overcome the limitations of both deterministic and probabilistic approaches.

Based on a single-source, single-sink and multi-owner network structure, where arc capacities are expressed by grey interval numbers, two separate games are formulated for all possible coalitions: the grey maximum flow game $\langle N, v' \rangle$ and the grey risk game $\langle N, c' \rangle$. The grey characteristic function of each coalition is obtained using the BWC algorithm and the Grey REILP method. Through this method, a quantitative balance is established between risk and system return.

Four Equal Surplus Sharing Approaches, namely the Grey Banzhaf value, Grey CIS-value ($\mathcal{G}$CIS), Grey ENSC-value ($\mathcal{G}$ENSC), and Grey ED-value ($\mathcal{G}$ED) are applied to both games. The results are evaluated comparatively in terms of efficiency, individual rationality, and coalitional rationality criteria. The findings demonstrate that the $\mathcal{G}$ENSC-value lies within the grey core and ensures coalition stability. The results provide significant contributions to cooperative models for the design of fair, stable, and risk-sensitive collaboration in infrastructure and logistics networks under grey uncertainty.

Keywords: Grey numbers, Cooperative game theory, Maximum flow problem, Egalitarian distribution approach, Risk allocation, Grey uncertainty.

1 Cand.PhD, Graduate School of Natural and Applied Sciences, Süleyman Demirel University, hidonmez35@gmail.com, ORCID ID: 0000-0002-2110-738X

2 Assoc. Dr., Department of Industrial Engineering, Faculty of Engineering and Natural Sciences, Süleyman Demirel University, onurolgun@sdu.edu.tr, ORCID ID: 0000-0002-7568-3235

3 Prof. Dr., Department of Mathematics, Faculty of Engineering and Natural Sciences, Süleyman Demirel University, sirmagok@sdu.edu.tr, ORCID ID: 0000-0001-9435-0527

https://doi.org/10.58830/ozgur.pub1361.c5492

1. Introduction

The most fundamental decision problem in transportation and logistics networks is maximizing the flow transmitted from a source node to a sink node. The maximum flow problem (MFP)is first solved by Ford and Fulkerson (1956) is used as a fundamental modeling tool in many engineering and management problems especially in electrical power systems, communication networks, computer networks and logistics networks (Asano & Asano, 2000). Although numerous effective solution algorithms have been developed for the deterministic MFP in the literature, the capacities of network components are often not known precisely in real-life applications. This uncertainty poses a critical decision difficulty, especially in structures where multiple operators control different network segments (Dantzig, 1955).

Various approaches have been proposed in the literature to model uncertainty, such as probability theory (Evans, 1976; Fishman, 1987; Goldberg & Tarjan, 1988), fuzzy set theory (Chanas & Kołodziejczyk, 1982; Chanas & Kołodziejczyk, 1984; Chanas & Kolodziejczyk, 1986; Ji et al., 2006), stochastic optimization (Hafezalkotob & Makui, 2015) and robust optimization (Ben-Tal et al., 2004; Minoux, 2009; Minoux, 2010). However, these methods have significant limitations. Estimating probability distributions relies on expert opinion and can lead to misleading results when evaluating rare events (Tversky & Kahneman, 1992). Fuzzy approaches require the selection of appropriate membership functions, whereas stochastic programming incurs high computational costs and may be infeasible (Hafezalkotob & Makui, 2015; Charnes & Cooper, 1959). In contrast, Interval Linear Programming (ILP) requires only the lower and upper bounds of the parameters, thus operating with less information and a lower computational burden, and with these features, it is becoming a preferred method in practical applications (Huang et al., 2013; Huang et al., 2015; Shaocheng, 1994).

In real life, different parts of the network may be owned by different individuals, companies, or countries. Natural gas pipelines, electrical transmission grids, and multi-operator logistics networks are typical examples of this situation (Koch et al., 2015; Tran et al., 2018). Collaboration among owners in such structures can significantly improve the network's overall performance. The fair allocation of the benefits from collaboration among the owners is the fundamental problem in cooperative game theory. Kalai and Zemel (1982a, 1982b) establish the theoretical foundation of flow games by revealing the structure of totally balanced games in multi-owner networks. Subsequently, Reyes (2005) perform fair flow allocation in transshipment networks via the Shapley value and Hafezalkotob and Makui (2015) solved the cooperative MFP under stochastic uncertainty, comparing different allocation concepts such as the Shapley value, the τ-value, and the core. Meanwhile, Baykasoğlu and Kubur Özbel (2019) solve the multi-owner maximum flow problem under interval uncertainty using the Risk-Explicit Interval Linear Programming (REILP) method and allocated both flow and risk among owners via the Shapley value.

On the other hand, grey system theory is introduced by Deng (1982) and has developed into a powerful tool for modeling systems that are partially known, have small sample sizes, or contain missing data (Deng, 1982). Grey numbers represent quantities whose exact values are unknown but whose containing intervals are known, and they naturally fit the structure of real-world data. Within this framework, Alparslan Gök et al. (2008, 2009, 2011) develope the fundamental concepts of cooperative grey game theory, while Olgun et al. (2016, 2017) define grey inventory games and examined cost allocation solutions. Dönmez et al. (2024) define egalitarian allocation solutions within the framework of grey numbers in grey inventory games and tested them on an application involving three arms factories.

The main contributions of this study can be summarized under three headings. First, the egalitarian allocation solution concepts used by Dönmez et al. (2024) in grey inventory games are applied to cooperative grey maximum flow games. Second, it is demonstrated that collaboration is a mechanism that not only increases the total flow but also reorganizes the uncertainty burden; two separate cooperative grey TU games, namely the grey flow game and the grey risk game are formulated, and simultaneous allocation is performed for both under four different fairness criteria. Third, it is numerically verified that the $\mathcal{G}$ENSC-value lies within the grey core, thereby demonstrating the transferability of the known compatibility between the core and ENSC (van den Brink & Funaki, 2009; Driessen & Funaki, 1991) for deterministic games to grey games.

The remainder of the chapter is organized as follows. In the second section, preliminary information regarding grey calculus and cooperative grey game theory is provided, while the grey egalitarian distribution framework is established. In the third section, a numerical application is presented for the logistics network example from Baykasoğlu and Kubur Özbel (2019). In the fourth section, the findings are discussed, theoretical and practical implications are presented, and future research directions are suggested.

2. Preliminaries

In this section, fundamental concepts related to grey system theory, cooperative grey game theory, and Equal Surplus Sharing Approaches used throughout the study are presented (Alparslan Gök et al., 2008; Dönmez et al., 2024; van den Brink & Funaki, 2009; Branzei et al., 2008).

2.1. Grey Arithmetic Operations

In this part, some grey calculus operations used in formulating cooperative grey games used in this chapter are presented. Numbers whose exact values are unknown but whose containing intervals are known are called grey numbers. For $\underline{a}, \overline{a} \in \mathbb{R}$, the number with lower bound $\underline{a}$ and upper bound $\overline{a}$ is denoted as $\otimes_a \in [\underline{a}, \overline{a}]$. For example, if the temperature of a room varies between 20 and 25 degrees, this situation is denoted as durum $\otimes_1 \in [20,25]$.

The set of all grey interval numbers in $\mathbb{R}$ is denoted by $\mathcal{G}(\mathbb{R})$, and for $\otimes_1,\otimes_2 \in \mathcal{G}(\mathbb{R})$, they are expressed as $\otimes_1 \in [\underline{a}, \overline{a}]$, $\otimes_2 \in [\underline{b}, \overline{b}]$, $|\otimes_1| = \underline{a} - \overline{a}$ and $\alpha \in \mathbb{R}_+$. Based on this, the following operations are defined:

1. $\otimes_1 + \otimes_2 \in [\underline{a} + \underline{b}, \overline{a} + \overline{b}]$ (2.1)
2. $\alpha \otimes_1 \in [\alpha\underline{a}, \alpha\overline{a}]$. (2.2)

So, $\mathcal{G}(\mathbb{R})$ has cone structure.

In this study we use a partial subtraction operator. Our partial subtraction operator $\otimes_1 - \otimes_2$ is only defined when $|\overline{a} - \underline{a}| \geq |\overline{b} - \underline{b}|$ and is calculated as $\otimes_1 - \otimes_2 \in [\underline{a} - \underline{b}, \overline{a} - \overline{b}]$ (Alparslan Gök et al., 2009).

The ordered pair approach is adopted in ordering grey interval numbers. For $\otimes_1 \in [\underline{a}, \overline{a}]$ and $\otimes_2 \in [\underline{b}, \overline{b}]$, $[\underline{a}, \overline{a}]$ being better than $[\underline{b}, \overline{b}]$ even in a weak sense implies the satisfaction of the conditions $[\underline{a}, \overline{a}] \geq [\underline{b}, \overline{b}] \Leftrightarrow \underline{a} \geq \underline{b}$ ile $\overline{a} \geq \overline{b}$. The reverse case is denoted by $[\underline{a}, \overline{a}] \leq [\underline{b}, \overline{b}]$ and is shown as $\underline{a} \leq \underline{b}$ and $\overline{a} \leq \overline{b}$ (Olgun et al., 2016).

In this context, fundamental concepts pertaining to cooperative grey game theory are now presented. A cooperative grey game is defined by the ordered pair $\langle N, w' \rangle$. Here, $N = \{1,2, \dots, n\}$ is the set of players and $w' : 2^N \to \mathcal{G}(\mathbb{R})$ denotes the characteristic function. Here, with $w'(\emptyset) \in [0,0]$, the value of the expected grey loss (cost) of coalition $S \in 2^N$, which is $w'(S) \in \left[\underline{w'(S)}, \overline{w'(S)}\right]$, is the grey loss function. While $\underline{w'(S)} \leq \overline{w'(S)}$, $\underline{w'(S)}$ and $\overline{w'(S)}$ indicate the minimum and maximum losses of the coalition. Therefore, a cooperative grey game can be considered as a classical cooperative game with $\otimes$ grey loss values. Grey solution methods are appropriate methods for solving loss (cost) problems using grey numbers for cooperative grey games. Grey solution methods and their elements are grey loss values defined in $G(\mathbb{R})$. $G(\mathbb{R})^N$ is defined as the set of all grey loss values, and $\mathcal{G}G^N$ is defined as the set of cooperative grey games.

Specifically, IG^N denotes the family of all cooperative interval games with player set N. For each $S \in 2^N$, when $w, w_1, w_2 \in IG^N$ and $w', w_1', w_2' \in GG^N$, if the condition $w_1'(S) \leq w_2'(S)$ is satisfied, we say $w_1' \in w_1 \leq w_2' \in w_2$. Here, $w_1'(S) \in w_1(S)$ and $w_2'(S) \in w_2(S)$ hold for each $S \in 2^N$. For $w_1', w_2' \in GG^N$ and $\lambda \in \mathbb{R}_+$, the games $(w_1' + w_2')$ and $(N, \lambda w')$ are defined by the relations $(w_1' + w_2')(S) = w_1'(S) + w_2'(S)$ and $(\lambda w')(S) = \lambda w'(S)$, respectively. Therefore GG^N is equipped with the $\leq$ ordering and has a cone structure with respect to addition and multiplication by non-negative scalars, as explained above. Furthermore, for $w_1', w_2' \in GG^N$, where $w_1' \in w_1$ ve $w_2' \in w_2$, when the condition $|w_1(S)| \geq |w_2(S)|$ is satisfied for each $S \in 2^N$, the game $(N, w_1' - w_2')$ is definied $(w_1' - w_2')(S) = w_1'(S) - w_2'(S) \in w_1(S) - w_2(S)$ (Alparslan Gök et al., 2019).

2.2. Equal Surplus Sharing Approaches

Four grey equal surplus sharing solution concepts for cooperative grey games are defined for Equal Surplus Sharing Approaches by utilizing the studies of van den Brink and Funaki (2009) and Dönmez et al. (2024).

The Grey Banzhaf value, grey *CIS*-value, grey *ENSC*-value, and grey *ED*-value solution are defined within the class $(SM\mathcal{G}G)^N$ just like the Grey Shapley value. The reason for this is that grey marginal operators are defined within the class $(SM\mathcal{G}G)^N$. The Grey Shapley value is defined and denoted as $\phi' : (SM\mathcal{G}G)^N \rightarrow G(\mathbb{R})^N$.

$$\phi_i'(c') = \frac{1}{n!}\sum_{\sigma\in\Pi(N)}\sum_{i\in N} m_i^{\sigma}(c') = \frac{1}{n!}n!\; c'(N) = c'(N) \in \left[\underline{a_N}, \overline{a_N}\right] \qquad (2.3)$$

Definition 2.1. (Grey Banzhaf Value): The Banzhaf value assumes that each player joins any coalition with equal probability. This value is defined by $\beta' : (SM\mathcal{G}G)^N \rightarrow G(\mathbb{R}^N)$ and is expressed as

$$\beta_i'(c') \in \left[\underline{\beta_i'(c')}, \overline{\beta_i'(c')}\right] = \frac{1}{2^{N-1}}\sum_{i\in S} c'(S) - c'(S\setminus\{i\}), c' \in \left[\underline{a_N}, \overline{a_N}\right] \quad (2.4)$$

This expression is valid for all $i \in N$ and all $c' \in (SM\mathcal{G}G)^N$.

Definition 2.2. ($\mathcal{G}$*CIS*-Value): The $\mathcal{G}$*CIS*-value allocates the individual grey value to each player and equally distributes the remainder of the grand coalition N among all players. The $\mathcal{G}$*CIS*-value is defined by $\mathcal{G}CIS' : (SM\mathcal{G}G)^N \rightarrow G(\mathbb{R}^N)$ and, where $| c'(N) | \leq \sum_{i\in N} c'(i)$, it is expressed as

$$\begin{aligned}\mathcal{G}CIS_i'(c') &\in \left[\underline{\mathcal{G}CIS_i'(c')}, \overline{\mathcal{G}CIS_i'(c')}\right] \\ &= c'(\{i\}) + \frac{1}{|N|}\left(c'(N) - \sum_{j\in N} c'(\{j\})\right), c' \in \left[\underline{a_N}, \overline{a_N}\right] \quad (2.5)\end{aligned}$$

This expression is valid for all $i \in N$ and all $c' \in (SM\mathcal{G}G)^N$.

Definition 2.3. ($\mathcal{G}$*ENSC*-Value): In a grey game extending from c' to $c'^* \in SM\mathcal{G}G^N$ in the class $SM\mathcal{G}G^N$, each coalition $S \subseteq N$ is assigned the grey value that the grand coalition N lose if coalition S are to leave N. For each $S \subseteq N$, it is defined as $c^{*\prime}(S) = c'(S) - c'(N \setminus S)$. The Grey *ENSC*-value ($\mathcal{G}$*ENSC*-value), assigns the *CIS*-value of the dual game c'^* to each game c'. It is defined by $\mathcal{G}ENSC' : SM\mathcal{G}G^N \rightarrow G(\mathbb{R}^N)$ and expressed as

$$\begin{aligned}\mathcal{G}ENSC_i'(c') \in \left[\underline{\mathcal{G}ENSC_i'(c')}, \overline{\mathcal{G}ENSC_i'(c')}\right] &= \mathcal{G}CIS_i'(c'^*) \in \left[\underline{\mathcal{G}CIS_i'(c'^*)}, \overline{\mathcal{G}CIS_i'(c'^*)}\right] \\ &= \frac{1}{|N|}\left(c'(N) + \sum_{j\in N} c'(N\setminus\{j\})\right) - c'(N), c' \in \left[\underline{a_N}, \overline{a_N}\right] \qquad (2.6)\end{aligned}$$

This expression is valid for all $i \in N$ and all $c' \in SM\mathcal{G}G^N$. It is observed that $| c'(N) + \sum_{j \in N} c'(N \setminus \{j\}) | \leq | N || c'(N \setminus \{i\})$. Therefore, the *GENSC*-value determines the grey marginal contribution of each player to the grand coalition and distributes the remainder equally among the players.

Definition 2.4. ($\mathcal{GED}$-Value): The Grey *ED*-value ($\mathcal{GED}$-value) is defined by $\mathcal{GED}' : \mathcal{G}G^N \to G(\mathbb{R}^N)$ and is expressed as

$$\mathcal{GED}'_i(c') \in \left[\underline{\mathcal{GED}'_i(c')}, \overline{\mathcal{GED}'_i(c')}\right] = \frac{c'(N)}{| N |}, c' \in \left[\underline{a_N}, \overline{a_N}\right] \tag{2.7}$$

This expression is valid for all $i \in N$ and all $c' \in \mathcal{G}G^N$.

3. Formulation of Maximum Flow Problems under Grey Uncertainty

In this section, the multi-owner maximum flow problem under grey uncertainty is expressed within the framework of cooperative grey game theory. The model is built on a three-layered structure: ***i.*** definition of the network structure with grey arc capacities, ***ii.*** formulation of the grey characteristic function for each coalition via the BWC algorithm and Grey REILP method, and ***iii.*** transformation of the obtained grey characteristic functions into the grey flow game $\langle N, v' \rangle$ and the grey risk game $\langle N, c' \rangle$.

3.1. Network Structure and Grey Capacity Model

Consider an acyclic directed graph $G(A, V)$ with a single source node s and a single sink node t. Here, A denotes the finite set of arcs, and V denotes the finite set of nodes. Let $N = \{1,2, \dots, n\}$ be the set of players; the set of arcs under the control of the k-th player is denoted by $A_{\{k\}}$, and they are united as $A = \bigcup_{k=1}^{n} A_{\{k\}}$. It is assumed that the arc sets of the players are disjoint, meaning $A_{\{k\}} \cap A_{\{l\}} = \emptyset$ when $k \neq l$.

In real-life applications, arc capacities are affected by structural sources of uncertainty such as weather conditions, equipment breakdowns, demand fluctuations and measurement errors. These capacities cannot be known precisely.

Definition 3.1. (Network Under Grey Uncertainty): When the capacity of each arc $(i, j) \in A$ is expressed by a grey interval number, we have

$$\otimes_{cap_{ij}} \in \left[\underline{cap_{ij}}, \overline{cap_{ij}}\right] \in G(\mathbb{R}),\ \underline{cap_{ij}} \leq \overline{cap_{ij}}. \tag{3.1}$$

(3.1) is called a network under grey uncertainty. Here, $\underline{cap_{ij}}$ represents the most pessimistic realization value of the capacity, and $\overline{cap_{ij}}$ represents the most optimistic one.

3.2. Coalition-Based Grey Maximum Flow Model

For any coalition $v_m \subseteq N$, the set of arcs used by the coalition is defined as $A_{v_m} = \bigcup_{k \in v_m} A_{\{k\}}$. The maximum flow problem for this coalition is formulated with the following grey ILP ($\mathcal{G}$ILP) model.

The objective function is defined by

$$\max \text{flow}\,(v_m) = \sum_{j \in F_s} \otimes_{x_{sj}} = \sum_{i \in E_t} \otimes_{x_{it}}. \tag{3.2}$$

Here, the capacity constraint for the flow on each arc $\forall (i,j) \in A_{v_m}$ cannot exceed the grey capacity of that arc with $\otimes_{x_{ij}} \preceq \otimes_{cap_{ij}}$. In the flow conservation constraint, for all intermediate nodes other than source s and sink t, when $\forall i \in V \setminus \{s,t\}$, we have

$$\sum_{l \in E_i} \otimes_{x_{li}} = \sum_{l \in F_i} \otimes_{x_{il}}\,. \tag{3.3}$$

The amount of incoming flow must equal the amount of outgoing flow. The non-negativity constraint is expressed as $\otimes_{x_{ij}} \succeq [0,0]$ when $\forall (i,j) \in A_{v_m}$, which establishes that the model is a $\mathcal{G}$ILP.

3.3. Solution of $\mathcal{G}$ILP with BWC Algorithm and Obtaining the Grey Characteristic Function

The $\mathcal{G}$ILP model is solved with the Best-Worst Case (BWC) algorithm proposed by Shaocheng (1994). This algorithm decomposes the grey model into two deterministic sub-models that represent the two extreme uncertainty conditions.

Most Optimistic Case (Upper Bound) is given by

$$\max f^{+} = \sum_{(i,j) \in A_{v_m}} \overline{cap_{ij}} \cdot z_{ij} \tag{3.4}$$

$$\sum_{j \in F_s} x_{sj}^{+} = \sum_{i \in E_t} x_{it}^{+} \tag{3.5}$$

$$x_{ij}^{+} \le \overline{cap_{ij}}, \sum_{l \in E_i} x_{li}^{+} = \sum_{l \in F_i} x_{il}^{+}\,, x_{ij}^{+} \ge 0. \tag{3.6}$$

The most optimistic case implies that the constraints define the widest solution space.

Most Pessimistic Case (Lower Bound) is given by

$$\max f^{-} = \sum_{(i,j) \in A_{v_m}} \underline{cap_{ij}} \cdot z_{ij} \tag{3.7}$$

$$\sum_{j\in F_s} x_{sj}^{-} = \sum_{i\in E_t} x_{it}^{-} \tag{3.8}$$

$$x_{ij}^{-} \le \underline{cap_{ij}}, \sum_{l\in E_i} x_{li}^{-} = \sum_{l\in F_i} x_{il}^{-}, x_{ij}^{-} \ge 0. \tag{3.9}$$

This most pessimistic case implies that the constraints define the narrowest solution space. From the solution of the two sub-models, the grey optimal flow value is obtained for each coalition v_m.

$$f_{opt}^{\pm}(v_m) \in \left[f_{opt}^{-}(v_m), f_{opt}^{+}(v_m)\right] \in G(\mathbb{R}) \tag{3.10}$$

The solution corresponding to f_{opt}^{-} indicates zero risk of constraint violation since it is obtained under the most pessimistic condition, where constraints are defined in the narrowest manner. The solution corresponding to f_{opt}^{+}, carries a high risk of violation in the event that uncertainty is realized, despite the capacities taking their widest values. The actual system will operate somewhere between these two extremes. This feature demonstrates that the grey interval is both a boundary of information and a carrier of risk.

3.4. Formulation of the $\mathcal{G}$REILP Model

The classical $\mathcal{G}$ILP approach has two main limitations: first, the obtained interval solutions can lead to infeasible or non-optimal decisions in practice and second, a quantitative link cannot be established between decision risk and system payoff (Zou et al., 2010). In order to overcome these limitations, the REILP approach (Zou et al., 2010) is adapted to the cooperative grey game framework.

Definition 3.2. (Grey Risk Function): For each arc (i,j) in A_{c_m}, the grey risk function is defined as follows, where $r_k \in [0,1]$ and $\forall(i,j) \in A_{c_m}$.

$$\xi_k = r_k \cdot \frac{\overline{cap_{ij}} - \underline{cap_{ij}}}{\overline{cap_{ij}} + \underline{cap_{ij}}} \tag{3.11}$$

Here, $r_k \in [0,1]$ represents the risk variable belonging to the k-th arc, the numerator $\left(\overline{cap_{ij}} - \underline{cap_{ij}}\right)$ represents the grey uncertainty width of the arc, and the denominator $\left(\overline{cap_{ij}} + \underline{cap_{ij}}\right)$ represents the center value. This normalization brings the risk contributions of arcs with capacities of different magnitudes to a comparable scale. When $\xi_k = 0$, $r_k = 0$, meaning the capacity limit for the given arc is defined by its most pessimistic value, and there is no risk of constraint violation. When $\xi_k > 0$, $r_k > 0$, the probability of constraint violation increases as the upper limit of the capacity is approached.

Definition 3.3. ($\mathcal{G}$REILP Model): For each coalition $c_m \subseteq N$, the $\mathcal{G}$REILP model is defined as follows:

$$\min \xi(c_m) = \sum_{(i,j)\in A_{c_m}} r_k \cdot \frac{\overline{cap_{ij}} - \underline{cap_{ij}}}{\overline{cap_{ij}} + \underline{cap_{ij}}} \tag{3.12}$$

$$\sum_{j\in F_s} x_{sj} \geq f_{opt}^{-}(c_m) + \lambda_0 \left(f_{opt}^{+}(c_m) - f_{opt}^{-}(c_m)\right) \tag{3.13}$$

$$x_{ij} - \underline{cap_{ij}} \leq \left(\overline{cap_{ij}} - \underline{cap_{ij}}\right) \cdot r_k, \forall (i,j) \in A_{c_m} \tag{3.14}$$

$$\sum_{l\in E_i} x_{li} = \sum_{l\in F_i} x_{il}\,, \forall i \in V \setminus \{s,t\} \tag{3.15}$$

$\lambda_0 = \lambda_{pre},\ \forall k$ iken $0 \leq r_k \leq 1$ ve $x_{ij} \geq 0$.

Definition 3.4. (Aspiration Level): $\lambda_0 \in [0,1]$ is the aspiration level that reflects the decision maker's attitude towards risk.

$\lambda_0 = 0$: The most pessimistic case; the system payoff is equal to f_{opt}^{-} and the risk is zero.

$\lambda_0 = 1$: The most optimistic case; the system payoff reaches f_{opt}^{+} and the risk is at a maximum level.

$0 < \lambda_0 < 1$: The decision maker strikes a balance between risk and payoff.

Definition 3.5. (Normalized Risk Level): In order to compare the risk values of different coalitions and different aspiration levels, the normalized risk level is defined.

$$NRL(c_m, \lambda_0) = \frac{\xi(c_m, \lambda_0) - \xi_{min}(c_m)}{\xi_{min}(c_m) - \xi_{min}(c_m)} \tag{3.16}$$

Here, $\xi_{min}(c_m) = \xi(c_m, \lambda_0 = 0)$ and $\xi_{max}(c_m) = \xi(c_m, \lambda_0 = 1)$.

$NRL = 0$ represents the most pessimistic case (zero risk), while $NRL = 1$ represents the most optimistic case (maximum risk).

3.5. Formulation of Cooperative Grey Games

The $\mathcal{G}$REILP model is solved at the values of $\lambda_0 = 0$ and $\lambda_0 = 1$ for each coalition $c_m \subseteq N$, directly obtaining the lower and upper bounds of the grey characteristic functions. This step is an important structure connecting REILP solutions to cooperative grey game theory.

Definition 3.6. (Grey Maximum Flow Game): The grey maximum flow game $\langle N, v' \rangle$ is the game $\langle N, v' \rangle \in \mathcal{IG}^N$ where, with $N = \{1,2,\dots,n\}$, the grey

characteristic function for each $c_m \subseteq N$ is defined as $v'(c_m) \in \left[f_{opt}^{-}(c_m), f_{opt}^{+}(c_m)\right] \in G(\mathbb{R})$. It is clear that $v'(\emptyset) = [0,0]$.

Definition 3.7. (Grey Risk Game): The grey risk game $\langle N, c' \rangle$ is the game $\langle N, c' \rangle \in \mathcal{IG}^N$ where the grey characteristic function for each $c_m \subseteq N$ is defined as

$$c'(c_m) \in [\xi(c_m, \lambda_0 = 0), \xi c_m, \lambda_0 = 1)] = [\xi_{min}(c_m), \xi_{max}(c_m)] \in G(\mathbb{R}). \quad (3.17)$$

4. Application

In this section, the multi-owner logistics network problem addressed by Baykasoğlu and Kubur Özbel (2019) is adopted as a numerical example. In the aforementioned study, a directed network structure with a single source and a single sink node, controlled by three different owners where $N = \{1,2,3\}$ is examined. As seen in Figure 1, the arc capacities in the network contain uncertainty and are represented by interval numbers.

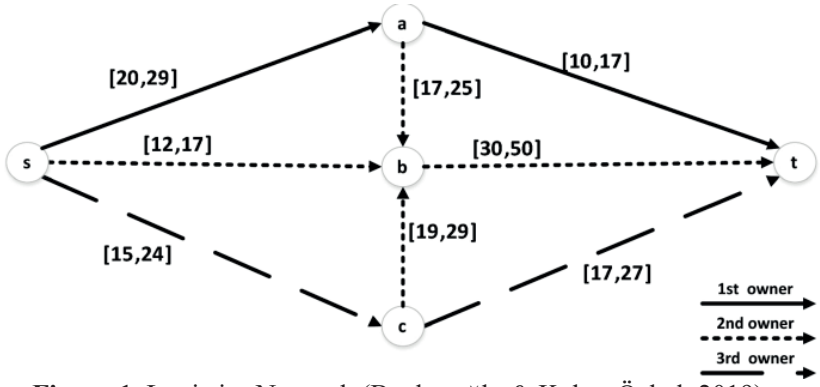

Figure 1. Logistics Network (Baykasoğlu & Kubur Özbel, 2019)

Maximum flow values for all possible coalitions are reported by Baykasoğlu and Kubur Özbel (2019). These values are taken directly to form the lower and upper bounds of the grey characteristic function and are summarized in Table 1.

Table 1. Grey maximum flow and risk values of all coalitions taken from Baykasoğlu and Kubur Özbel (2019)

$\{S\}$	$v'(\{S\})$	$c'(\{S\})$
{1}	$v'(\{1\}) \in [10,17]$	$c'(\{1\}) \in [0,0.25]$
{2}	$v'(\{2\}) \in [12,17]$	$c'(\{2\}) \in [0,0.17]$
{3}	$v'(\{3\}) \in [15,24]$	$c'(\{3\}) \in [0,0.38]$
{1,2}	$v'(\{1,2\}) \in [32,46]$	$c'(\{1,2\}) \in [0,0.47]$
{1,3}	$v'(\{1,3\}) \in [25,41]$	$c'(\{1,3\}) \in [0,0.64]$
{2,3}	$v'(\{2,3\}) \in [27,41]$	$c'(\{2,3\}) \in [0,0.40]$
{1,2,3}	$v'(\{1,2,3\}) \in [47,70]$	$c'(\{1,2,3\}) \in [0,0.79]$

4.1. Grey Banzhaf Value

For the Grey Banzhaf, the equation defined in (2.4) will be used in both flow and risk calculations.

Grey Banzhaf Value for Flow:

$$\beta_1'(v') \in \left[\underline{\beta_1'(v')}, \overline{\beta_1'(v')}\right]$$
$$= \frac{1}{4}[(v'(\{1\}) - v'(\emptyset)) + (v'(\{1,2\}) - v'(\{2\}))$$
$$+ (v'(\{1,3\}) - v'(\{3\})) + (v'(N) - v'(\{2,3\}))]$$
$$= \frac{1}{4}[[10,17] + ([32,46] - [12,17]) + ([25,41] - [15,24]) + ([47,70]$$
$$- [27,41])]$$
$$= \frac{1}{4}[[10,17] + [20,29] + [10,17] + [20,29]]$$
$$= \frac{1}{4}[60,92] = [15,23]$$

$$\beta_2'(v') \in \left[\underline{\beta_2'(v')}, \overline{\beta_2'(v')}\right]$$
$$= \frac{1}{4}[v'(\{2\}) + (v'(\{1,2\}) - v'(\{1\})) + (v'(\{2,3\})$$
$$- v'(\{3\})) + (v'(N) - v'(\{1,3\}))]$$
$$= \frac{1}{4}[[12,17] + [20,29] + [12,17] + [22,29]]$$
$$= \frac{1}{4}[66,92] = [16.5,23]$$

$$\beta_3'(v') \in \left[\underline{\beta_3'(v')}, \overline{\beta_3'(v')}\right]$$
$$= \frac{1}{4}[v'(\{3\}) + (v'(\{1,3\}) - v'(\{1\})) + (v'(\{2,3\}) - v'(\{2\})) + (v'(N) - v'(\{1,2\}))]$$
$$= \frac{1}{4}[[15,24] + [15,24] + [15,24] + [15,24]]$$
$$= \frac{1}{4}[60,96] = [15,24]$$
$$\beta_i'(v') \in ([15,23], [16.5,23], [15,24])$$

Grey Banzhaf Value for Risk:

$$\beta_1'(c') \in \left[\underline{\beta_1'(c')}, \overline{\beta_1'(c')}\right]$$
$$= \frac{1}{4}[[0,0.25] + ([0,0.47] - [0,0.17]) + ([0,0.64] - [0,0.38]) + ([0,0.79] - [0,0.40])]$$
$$= \frac{1}{4}[[0,0.25] + [0,0.30] + [0,0.26] + [0,0.39]]$$
$$= \frac{1}{4}[0,1.20] = [0,0.3]$$

$$\beta_2'(c') \in \left[\underline{\beta_2'(c')}, \overline{\beta_2'(c')}\right]$$
$$= \frac{1}{4}[[0,0.17] + ([0,0.47] - [0,0.25]) + ([0,0.40] - [0,0.38]) + ([0,0.79] - [0,0.64])]$$
$$= \frac{1}{4}[[0,0.17] + [0,0.22] + [0,0.02] + [0,0.15]]$$
$$= \frac{1}{4}[0,0.56] = [0,0.14]$$

$$\beta_3'(c') \in \left[\underline{\beta_3'(c')}, \overline{\beta_3'(c')}\right]$$
$$= \frac{1}{4}[[0,0.38] + ([0,0.64] - [0,0.25]) + ([0,0.40] - [0,0.17]) + ([0,0.79] - [0,0.47])]$$
$$= \frac{1}{4}[[0,0.38] + [0,0.39] + [0,0.23] + [0,0.32]]$$
$$= \frac{1}{4}[0,1.32] = [0,0.33]$$

4.2. Grey CIS-Value

For the Grey CIS-Value, the equation defined in (2.5) will be used in both flow and risk calculations.

Grey CIS-Value for Flow:

$$\mathcal{G}CIS'_1(v') \in \left[\underline{\mathcal{G}CIS'_1(v')}, \overline{\mathcal{G}CIS'_1(v')}\right]$$
$$= [10,17] + \frac{1}{3}\left([47,70] - ([10,17] + [12,17] + [15,24])\right)$$
$$= [10,17] + [3.33,4] = [13.33,21]$$

$$\mathcal{G}CIS'_2(v') \in \left[\underline{\mathcal{G}CIS'_2(v')}, \overline{\mathcal{G}CIS'_2(v')}\right]$$
$$= [12,17] + \frac{1}{3}\left([47,70] - ([10,17] + [12,17] + [15,24])\right)$$
$$= [10,17] + [3.33,4] = [15.33,21]$$

$$\mathcal{G}CIS'_3(v') \in \left[\underline{\mathcal{G}CIS'_3(v')}, \overline{\mathcal{G}CIS'_3(v')}\right]$$
$$= [15,24] + \frac{1}{3}\left([47,70] - ([10,17] + [12,17] + [15,24])\right)$$
$$= [15,24] + [3.33,4] = [18.33,28]$$

Grey CIS-Value for Risk:

$$\mathcal{G}CIS'_1(c') \in \left[\underline{\mathcal{G}CIS'_1(c')}, \overline{\mathcal{G}CIS'_1(c')}\right]$$
$$= [0,0.25] + \frac{1}{3}\left([0,0.79] - ([0,0.25] + [0,0.17] + [0,0.38])\right)$$
$$= [0,0.25] + [0,-0.003] = [0,0.247]$$

$$\mathcal{G}CIS'_2(c') \in \left[\underline{\mathcal{G}CIS'_2(c')}, \overline{\mathcal{G}CIS'_2(c')}\right]$$
$$= [0,0.17] + \frac{1}{3}\left([0,0.79] - ([0,0.25] + [0,0.17] + [0,0.38])\right)$$
$$= [0,0.17] + [0,-0.003] = [0,0.167]$$

$$\mathcal{G}CIS'_3(c') \in \left[\underline{\mathcal{G}CIS'_3(c')}, \overline{\mathcal{G}CIS'_3(c')}\right]$$
$$= [0,0.38] + \frac{1}{3}\left([0,0.79] - ([0,0.25] + [0,0.17] + [0,0.38])\right)$$
$$= [0,0.38] + [0,-0.003] = [0,0.377]$$

4.3. Grey ENSC-Value

For the Grey ENSC-Value, the equation defined in (2.6) will be used in both flow and risk calculations.

Grey ENSC-Value for Flow:

$$\mathcal{G}ENSC'_1(v') \in \left[\underline{\mathcal{G}ENSC'_1(v')}, \overline{\mathcal{G}ENSC'_1(v')}\right]$$
$$= \frac{1}{3}\left([47,70] + ([32,46] + [25,41] + [27,41])\right) - [27,41]$$
$$= [43.67,66] - [27,41] = [16.67,25]$$

$$\mathcal{G}ENSC'_2(v') \in \left[\underline{\mathcal{G}ENSC'_2(v')}, \overline{\mathcal{G}ENSC'_2(v')}\right]$$
$$= \frac{1}{3}\left([47,70] + ([32,46] + [25,41] + [27,41])\right) - [25,41]$$
$$= [43.67,66] - [25,41] = [18.67,25]$$

$$\mathcal{G}ENSC'_3(v') \in \left[\underline{\mathcal{G}ENSC'_3(v')}, \overline{\mathcal{G}ENSC'_3(v')}\right]$$
$$= \frac{1}{3}\left([47,70] + ([32,46] + [25,41] + [27,41])\right) - [32,46]$$
$$= [43.67,66] - [32,46] = [11.67,20]$$

Grey ENSC-Value for Risk:

$$\mathcal{G}ENSC'_1(c') \in \left[\underline{\mathcal{G}ENSC'_1(c')}, \overline{\mathcal{G}ENSC'_1(c')}\right]$$
$$= \frac{1}{3}\left([0,0.79] + ([0,0.40] + [0,0.64] + [0,0.47])\right) - [0,0.40]$$
$$= [0,0.767] - [0,0.40] = [0,0.367]$$

$$\mathcal{G}ENSC'_2(c') \in \left[\underline{\mathcal{G}ENSC'_2(c')}, \overline{\mathcal{G}ENSC'_2(c')}\right]$$
$$= \frac{1}{3}\left([0,0.79] + ([0,0.40] + [0,0.64] + [0,0.47])\right) - [0,0.64]$$
$$= [0,0.767] - [0,0.64] = [0,0.127]$$

$$\mathcal{G}ENSC'_3(c') \in \left[\underline{\mathcal{G}ENSC'_3(c')}, \overline{\mathcal{G}ENSC'_3(c')}\right]$$
$$= \frac{1}{3}\left([0,0.79] + ([0,0.40] + [0,0.64] + [0,0.47])\right) - [0,0.47]$$
$$= [0,0.767] - [0,0.47] = [0,0.297]$$

4.4. Grey ED-Value

For the Grey ED-Value, the equation defined in (2.7) will be used in both flow and risk calculations.

$$\mathcal{G}ED_i'(v') \in \left[\underline{\mathcal{G}ED_i'(v')}, \overline{\mathcal{G}ED_i'(v')}\right] = \frac{v'(N)}{|N|} = \frac{[47,70]}{3} = [15.67,23.33]$$

$$\mathcal{G}ED_i'(c') \in \left[\underline{\mathcal{G}ED_i'(c')}, \overline{\mathcal{G}ED_i'(c')}\right] = \frac{c'(N)}{|N|} = \frac{[0,0.79]}{3} = [0,0.263]$$

Following the calculation of grey Equal Surplus Sharing Approaches for flow and risk, all coalition values and results for the four Equal Surplus Sharing Solutions are obtained. A comprehensive evaluation of these results is presented below.

It has been demonstrated that the grey flow game $\langle N, v' \rangle$ is superadditive as follows:

$$v'(\{1,3\}) = [25,41] \succeq [10,17] + [15,24] = [25,41]$$
$$v'(\{1,2,3\}) = [47,70] \succeq [10,17] + [12,17] + [15,24] = [37,58].$$

This result mathematically demonstrates that the participation of each owner in the coalition yields strictly better results compared to acting alone. This feature guarantees that forming coalitions is a rational strategy in real-life applications such as logistics networks and natural gas transmission systems in the literature (Koch et al., 2015; Tran et al., 2018). Numerical results also support this finding. While the grey flow values of individual players are [10,17], [12,17] and [15,24] respectively, the value of the grand coalition increases to the level of [47,70]. This increase indicates that collaborative operations expand network utilization across complementary arcs and reduce inefficiencies stemming from fragmented ownership structures. From the perspective of application areas, this result indicates that total system output can increase significantly by either removing institutional boundaries or strengthening coordination protocols in transportation, energy transmission and supply networks are controlled by multiple operators.

The $\mathcal{G}CIS$, $\mathcal{G}ENSC$ and $\mathcal{G}ED$ values satisfy the efficiency condition:

$$\begin{aligned}\mathcal{G}CIS_1'(v') + \mathcal{G}CIS_2'(v') + \mathcal{G}CIS_3'(v') \\ \in \left[\underline{\mathcal{G}CIS_1'(v')}, \overline{\mathcal{G}CIS_1'(v')}\right] + \left[\underline{\mathcal{G}CIS_2'(v')}, \overline{\mathcal{G}CIS_2'(v')}\right] \\ + \left[\underline{\mathcal{G}CIS_3'(v')}, \overline{\mathcal{G}CIS_3'(v')}\right] = [47,70] = v'(\{1,2,3\}),\end{aligned}$$

$$\mathcal{G}ENSC'_1(v') + \mathcal{G}ENSC'_2(v') + \mathcal{G}ENSC'_3(v') \in \left[\underline{\mathcal{G}ENSC'_1(v')}, \overline{\mathcal{G}ENSC'_1(v')}\right] + \left[\underline{\mathcal{G}ENSC'_2(v')}, \overline{\mathcal{G}ENSC'_2(v')}\right] + \left[\underline{\mathcal{G}ENSC'_3(v')}, \overline{\mathcal{G}ENSC'_3(v')}\right] = [47,70] = v'(\{1,2,3\}),$$

$$\mathcal{G}ED'_1(v') + \mathcal{G}ED'_2(v') + \mathcal{G}ED'_2(v') \in \left[\underline{\mathcal{G}ED'_1(v')}, \overline{\mathcal{G}ED'_1(v')}\right] + \left[\underline{\mathcal{G}ED'_2(v')}, \overline{\mathcal{G}ED'_2(v')}\right] + \left[\underline{\mathcal{G}ED'_3(v')}, \overline{\mathcal{G}ED'_3(v')}\right] = [47,70] = v'(\{1,2,3\}).$$

The Grey Banzhaf value is obtained in a way that does not satisfy the efficiency property

$$\beta'_1(v') + \beta'_2(v') + \beta'_3(v') \in \left[\underline{\beta'_1(v')}, \overline{\beta'_1(v')}\right] + \left[\underline{\beta'_2(v')}, \overline{\beta'_2(v')}\right] + \left[\underline{\beta'_3(v')}, \overline{\beta'_3(v')}\right] = [45.5,70] \neq [47,70] = v'(\{1,2,3\})$$

This demonstrates that the known property of the Banzhaf value in deterministic games carries over to grey games (Branzei et al., 2008) and confirms that this property is preserved within the grey framework as well.

The verification of the core condition reveals a significant divergence among the solution concepts. Although the $\mathcal{G}$CIS-value satisfies individual rationality:

$$\mathcal{G}CIS'_1(v') \in \left[\underline{\mathcal{G}CIS'_1(v')}, \overline{\mathcal{G}CIS'_1(v')}\right] = [13.33,21] \geq v'(\{1\}) = [10,17],$$
$$\mathcal{G}CIS'_2(v') \in \left[\underline{\mathcal{G}CIS'_2(v')}, \overline{\mathcal{G}CIS'_2(v')}\right] = [15.33,21] \geq v'(\{2\}) = [12,17],$$
$$\mathcal{G}CIS'_3(v') \in \left[\underline{\mathcal{G}CIS'_3(v')}, \overline{\mathcal{G}CIS'_3(v')}\right] = [18.33,28] \geq v'(\{3\}) = [15,24].$$

It violates coalitional rationality:

$$\mathcal{G}CIS'_1(v') + \mathcal{G}CIS'_2(v') \in \left[\underline{\mathcal{G}CIS'_1(v')}, \overline{\mathcal{G}CIS'_1(v')}\right] + \left[\underline{\mathcal{G}CIS'_2(v')}, \overline{\mathcal{G}CIS'_2(v')}\right] = [28.66,42] \geq v'(\{1,2\}) = [32,46].$$

The inequality $28.66 < 32$ at the lower bound indicates that the two-owner coalition may have an incentive to leave the grand coalition. In contrast, the $\mathcal{G}ENSC$-value satisfies all coalitional rationality conditions.

$$\mathcal{G}ENSC'_1(v') + \mathcal{G}ENSC'_2(v') \in \left[\underline{\mathcal{G}ENSC'_1(v')}, \overline{\mathcal{G}ENSC'_1(v')}\right] + \left[\underline{\mathcal{G}ENSC'_2(v')}, \overline{\mathcal{G}ENSC'_2(v')}\right] = [35.34,50] \geq [32,46],$$

$$\mathcal{G}ENSC'_1(v') + \mathcal{G}ENSC'_3(v') \in \left[\underline{\mathcal{G}ENSC'_1(v')}, \overline{\mathcal{G}ENSC'_1(v')}\right] + \left[\underline{\mathcal{G}ENSC'_3(v')}, \overline{\mathcal{G}ENSC'_3(v')}\right] = [28.34,45] \geq [25,41],$$

$$\mathcal{G}ENSC'_2(v') + \mathcal{G}ENSC'_3(v') \in \left[\underline{\mathcal{G}ENSC'_2(v')}, \overline{\mathcal{G}ENSC'_2(v')}\right] + \left[\underline{\mathcal{G}ENSC'_3(v')}, \overline{\mathcal{G}ENSC'_3(v')}\right] = [30.34,45] \geq [27,41].$$

This finding mathematically demonstrates that the $\mathcal{G}ENSC$-value lies within the grey core and that no sub-coalition has a rational justification for leaving the grand coalition. This property, known in the literature as deterministic games (van den Brink & Funaki, 2009; Driessen & Funaki, 1991), has been demonstrated in the grey flow game in this study.

Based on this, the solutions of the egalitarian distribution methods calculated for flow and risk are presented in Table 2 and Table 3 and the whitened flow and risk values are presented in Table 4 and Table 5.

Table 2. Results of egalitarian distribution methods in the grey flow game

	ϕ_1	ϕ_2	ϕ_3	Total	Core
$\beta'_i(v')$	∈ [15,23]	∈ [16.5,23]	∈ [15,24]	∈ [46.5,70]	**Partial**
$\mathcal{G}CIS'_i(v')$	∈ [13.33,21]	∈ [15.33,21]	∈ [18.33,28]	∈ [47,70]	✗
$\mathcal{G}ENSC'_i(v')$	∈ [16.67,25]	∈ [18.67,25]	∈ [11.67,20]	∈ [47,70]	✓
$\mathcal{G}ED'_i(v')$	∈ [15.67,23.33]	∈ [15.67,23.33]	∈ [15.67,23.33]	∈ [47,70]	**Partial**

Table 3. Results of egalitarian distribution methods in the grey risk game

	ϕ_1	ϕ_2	ϕ_3	Total
$\beta'_i(c')$	∈ [0,0.300]	∈ [0,0.140]	∈ [0,0.330]	∈ [0,0.770]
$\mathcal{G}CIS'_i(c')$	∈ [0,0.247]	∈ [0,0.167]	∈ [0,0.377]	∈ [0,0.791]
$\mathcal{G}ENSC'_i(c')$	∈ [0,0.367]	∈ [0,0.127]	∈ [0,0.297]	∈ [0,0.791]
$\mathcal{G}ED'_i(c')$	∈ [0,0.263]	∈ [0,0.263]	∈ [0,0263]	∈ [0,0.789]

Crisp Comparison with Whitening ($\alpha = 0.5$)

To facilitate the interpretation of the results, whitening values with $\alpha = 1/2$ are calculated using the formula

$$\phi_i' = \frac{\underline{\phi_i'} + \overline{\phi_i'}}{2} \tag{4.1}$$

are shown in Table 4 and Table 5.

Table 4. Whitened flow distribution results

	ϕ_1	ϕ_2	ϕ_3	**Total**
$\beta_i'(v')$	19.00	19.75	19.50	58.25
$\mathcal{GCIS}_i'(v')$	17.17	18.17	23.17	58.50
$\mathcal{GENSC}_i'(v')$	20.83	21.83	15.83	58.50
$\mathcal{GED}_i'(v')$	19.50	19.50	19.50	58.50

Table 5. Whitened risk distribution results

	ϕ_1	ϕ_2	ϕ_3	**Total**
$\beta_i'(c')$	0.150	0.070	0.165	0.385
$\mathcal{GCIS}_i'(c')$	0.124	0.084	0.189	0.396
$\mathcal{GENSC}_i'(c')$	0.184	0.064	0.149	0.396
$\mathcal{GED}_i'(c')$	0.132	0.132	0.132	0.395

5. An Application

In this study, Equal Surplus Sharing Approaches for cooperative maximum flow problems defined under grey uncertainty are addressed through flow and risk allocation. A framework has been established that allows the distribution of both network performance and the risk burden arising from uncertainty within the same cooperative structure. The fundamental contribution of the study is to demonstrate that collaboration is a mechanism that not only increases the total flow but also reorganizes the uncertainty burden by coupling collaboration, which is evaluated solely based on coalitional flow capacity in classical or uncertain interval maximum flow games, with risk magnitudes expressed by grey numbers.

The theoretical foundation of the model has been established with grey arithmetic operations, the partial subtraction operator, and the solution concepts of Equal Surplus Sharing Approaches defined over the grey class. Based on the application data from the multi-owner logistics network example taken from Baykasoğlu and Kubur Özbel (2019), the Grey Banzhaf value, $\mathcal{G}CIS$-value, $\mathcal{G}ENSC$-value and $\mathcal{G}ED$-value have been calculated for both flow and risk.

This study contributes to the literature in several ways. First, the egalitarian distribution approach solutions used by Dönmez et al. (2024) in grey inventory games have been applied to maximum flow games. In doing so, the applicability of grey solutions from the egalitarian distribution approach to various cooperative network problems has been demonstrated. Second, in addition to the Shapley value approach of Baykasoğlu and Kubur Özbel (2019), both flow and risk have been allocated simultaneously under four different fairness criteria. This approach offers decision-makers a spectrum of solutions suitable to their preferences rather than imposing a single solution. Third, the coalition synergy (collaboration producing a risk lower than the sum of individual risks) that emerged in the CIS-value analysis of the grey risk game has been demonstrated within the framework of grey uncertainty.

From the perspective of various application areas, these findings offer concrete guidance to decision-makers operating multi-owner logistics networks (Frisk et al., 2010), natural gas transmission systems (Koch et al., 2015; Tran et al., 2018) and electrical transmission grids (Banez-Chicharro et al., 2017). In particular, the fact that the ENSC-value lies within the core indicates that this solution should be preferred in applications where long-term coalition stability is sought (in contexts such as multinational pipeline operations or joint logistics network management).

Several directions are suggested for future research. First and foremost, heterogeneous-aspiration-level scenarios, in which owners with different risk preferences form coalitions, can be investigated. Furthermore, flow loss can be incorporated into the model (Olgun & Aydemir, 2021), the nucleolus and the başlat denklem tau-value adapted to grey maximum flow games, and a systematic comparison can be conducted between the grey Shapley value and the egalitarian distribution approach solutions proposed in this study.

References

Alparslan Gök, S. Z., Branzei, O., & Branzei, R. (2008). Cooperative interval games arising from airport situations with interval data. *Tilburg University, CentER Discussion Paper*. https://doi.org/10.2139/ssrn.1150185

Alparslan Gök, S. Z., Branzei, R., & Tijs, S. (2009). Convex interval games. *Journal of Applied Mathematics and Decision Sciences, 2009*, 1–14. https://doi.org/10.1155/2009/342089

Alparslan Gök, S. Z., Branzei, R., & Tijs, S. (2011). Big boss interval games. *International Journal of Uncertainty, Fuzziness and Knowledge-Based Systems, 19*(1), 135–149. https://doi.org/10.1142/S0218488511006927

Alparslan Gök, S. Z., Qasim, E., Palanci, O., & Weber, G. W. (2019). Airport situations and games with grey uncertainty. *International Journal of Industrial Engineering and Operational Research, 1*(1), 51–59. https://doi.org/10.22034/ijieor.v1i1.8

Asano, T., & Asano, Y. (2000). Recent developments in maximum flow algorithms. *Journal of the Operations Research Society of Japan, 43*(2), 2–31. https://doi.org/10.15807/jorsj.43.2

Banez-Chicharro, F., Olmos, L., Ramos, A., & Latorre, J. M. (2017). Estimating the benefits of transmission expansion projects: An Aumann–Shapley approach. *Energy, 118*, 1044–1054. https://doi.org/10.1016/j.energy.2016.10.135

Baykasoğlu, A., & Kubur Özbel, B. (2019). Explicit flow-risk allocation for cooperative maximum flow problems under interval uncertainty. *Operational Research, 22*, 1165–1198. https://doi.org/10.1007/s12351-019-00500-5

Ben-Tal, A., Goryashko, A., Guslitzer, E., & Nemirovski, A. (2004). Adjustable robust solutions of uncertain linear programs. *Mathematical Programming, 99*(2), 351–376. https://doi.org/10.1007/s10107-003-0454-y

Branzei, R., Dimitrov, D., & Tijs, S. (2008). *Models in cooperative game theory*. Springer Berlin Heidelberg. https://doi.org/10.1007/978-3-540-77954-4_5

Chanas, S., & Kołodziejczyk, W. (1982). Maximum flow in a network with fuzzy arc capacities. *Fuzzy Sets and Systems, 8*(2), 165–173. https://doi.org/10.1016/0165-0114(82)90006-9

Chanas, S., & Kołodziejczyk, W. (1984). Real-valued flows in a network with fuzzy arc capacities. *Fuzzy Sets and Systems, 13*(2), 139–151. https://doi.org/10.1016/0165-0114(84)90014-9

Chanas, S., & Kolodziejczyk, W. (1986). Integer flows in network with fuzzy capacity constraints. *Networks, 16*(1), 17–31. https://doi.org/10.1002/net.3230160103

Charnes, A., & Cooper, W. W. (1959). Chance-constrained programming. *Management Science, 6*(1), 73–79. https://doi.org/10.1287/mnsc.6.1.73

Dantzig, G. B. (1955). Linear programming under uncertainty. *Management Science, 1*(3–4), 197–206. https://doi.org/10.1287/mnsc.1.3-4.197

Deng, J. L. (1982). Control problems of grey systems. *Systems & Control Letters, 1*(5), 288–294. https://doi.org/10.1016/S0167-6911(82)80025-X

Driessen, T. S. H., & Funaki, Y. (1991). Coincidence of and collinearity between game theoretic solutions. *Operations-Research-Spektrum, 13*(1), 15–30. https://doi.org/10.1007/BF01719767

Dönmez, H. İ., Olgun, M. O., & Alparslan Gök, S. Z. (2024). Equal surplus sharing in grey inventory games. *Alphanumeric Journal, 12*(3), 215–226. https://doi.org/10.17093/alphanumeric.1492875

Evans, J. R. (1976). Maximum flow in probabilistic graphs — The discrete case. *Networks, 6*(2), 161–183. https://doi.org/10.1002/net.3230060208

Fishman, G. S. (1987). The distribution of maximum flow with applications to multistate reliability systems. *Operations Research, 35*(4), 607–618. https://doi.org/10.1287/opre.35.4.607

Ford, L. R., & Fulkerson, D. R. (1956). Maximal flow through a network. *Canadian Journal of Mathematics, 8*, 399–404. https://doi.org/10.4153/CJM-1956-045-5

Frisk, M., Göthe-Lundgren, M., Jörnsten, K., & Rönnqvist, M. (2010). Cost allocation in collaborative forest transportation. *European Journal of Operational Research, 205*(2), 448–458. https://doi.org/10.1016/j.ejor.2010.01.015

Goldberg, A. V., & Tarjan, R. E. (1988). A new approach to the maximum-flow problem. *Journal of the ACM, 35*(4), 921–940. https://doi.org/10.1145/48014.61051

Hafezalkotob, A., & Makui, A. (2015). Cooperative maximum-flow problem under uncertainty in logistic networks. *Applied Mathematics and Computation, 250*, 593–604. https://doi.org/10.1016/j.amc.2014.10.080

Huang, H., Li, F., & Mishra, Y. (2015). Modeling dynamic demand response using Monte Carlo simulation and interval mathematics for boundary estimation. *IEEE Transactions on Smart Grid, 6*(6), 2704–2713. https://doi.org/10.1109/TSG.2015.2435011

Huang, Y. F., Ye, W. L., & Zhou, F. F. (2013). Research on the profit distribution of logistics company strategic alliance based on Shapley value. *Advanced Materials Research, 765–767*, 3253–3257. https://doi.org/10.4028/www.scientific.net/AMR.765-767.3253

Ji, X., Yang, L., & Shao, Z. (2006). Chance constrained maximum flow problem with fuzzy arc capacities. *Lecture Notes in Computer Science, 4114*, 11–19. https://doi.org/10.1007/978-3-540-37275-2_2

Kalai, E., & Zemel, E. (1982a). Generalized network problems yielding totally balanced games. *Operations Research, 30*(5), 998–1008. https://doi.org/10.1287/opre.30.5.998

Kalai, E., & Zemel, E. (1982b). Totally balanced games and games of flow. *Mathematics of Operations Research, 7*(3), 476–478. https://doi.org/10.1287/moor.7.3.476

Koch, T., Hiller, B., Pfetsch, M. E., & Schewe, L. (2015). *Evaluating gas network capacities*. SIAM. https://doi.org/10.1137/1.9781611973693

Liu, S., & Forrest, J. Y.-L. (2010). *Grey systems: Theory and applications*. Springer.

Minoux, M. (2009). On robust maximum flow with polyhedral uncertainty sets. *Optimization Letters, 3*(3), 367–376. https://doi.org/10.1007/s11590-009-0116-y

Minoux, M. (2010). Robust network optimization under polyhedral demand uncertainty is NP-hard. *Discrete Applied Mathematics, 158*(5), 597–603. https://doi.org/10.1016/j.dam.2009.09.025

Olgun, M. O., Alparslan Gök, S. Z., & Özdemir, G. (2016). Cooperative grey games and an application on economic order quantity model. *Kybernetes, 45*(5), 828–838. https://doi.org/10.1108/K-06-2015-0160

Olgun, M. O., Özdemir, G., & Alparslan Gök, S. Z. (2017). Gri stok modelinin işbirlikçi oyun teorisi ile maliyet dağıtımlarının incelenmesi. *Uludağ Üniversitesi Mühendislik Fakültesi Dergisi, 22*(1), 23–34. https://doi.org/10.17482/uumfd.335422

Olgun, M. O., & Aydemir, E. (2021). A new cooperative depot sharing approach for inventory routing problem. *Annals of Operations Research, 307*(1–2), 417–441. https://doi.org/10.1007/s10479-021-04122-z

Reyes, P. M. (2005). Logistics networks: A game theory application for solving the transshipment problem. *Applied Mathematics and Computation, 168*(2), 1419–1431. https://doi.org/10.1016/j.amc.2004.10.030

Shaocheng, T. (1994). Interval number and fuzzy number linear programmings. *Fuzzy Sets and Systems, 66*(3), 301–306. https://doi.org/10.1016/0165-0114(94)90097-3

Tran, T. H., French, S., Ashman, R., & Kent, E. (2018). Impact of compressor failures on gas transmission network capability. *Applied Mathematical Modelling, 55*, 741–757. https://doi.org/10.1016/j.apm.2017.11.034

Tversky, A., & Kahneman, D. (1992). Advances in prospect theory: Cumulative representation of uncertainty. *Journal of Risk and Uncertainty, 5*(4), 297–323. https://doi.org/10.1007/BF00122574

van den Brink, R., & Funaki, Y. (2009). Axiomatizations of a class of equal surplus sharing solutions for TU-games. *Theory and Decision, 67*(3), 303–340. https://doi.org/10.1007/s11238-007-9083-x

Zou, R., Liu, Y., Liu, L., & Guo, H. (2010). REILP approach for uncertainty-based decision making in civil engineering. *Journal of Computing in Civil Engineering, 24*(4), 357–364. https://doi.org/10.1061/(ASCE)CP.1943-5487.0000037

Chapter 3

Applied Mathematics in Mental Health: A Game-Theoretic Perspective on Psychological Symptoms

Çağnur Çörekli[1]

Abstract

For decades, psychological symptoms have primarily been interpreted as indicators of dysfunction and pathology. However, recent developments in evolutionary psychiatry, mathematical psychology, and computational modeling suggest that certain symptoms may also be understood as adaptive responses to environmental challenges. This chapter examines mental health through the lens of game theory and proposes that many psychological symptoms can be conceptualized as equilibrium strategies emerging from interactions between individuals and their environments. Anxiety, social anxiety, depression, obsessive-compulsive behaviors, and post-traumatic stress responses are analyzed as strategic adaptations shaped by costs, benefits, uncertainty, and risk management. Particular attention is given to Nash equilibrium as a framework for understanding the persistence of apparently maladaptive behaviors. The chapter further argues that psychotherapy and psychiatric interventions may be interpreted as processes that alter payoff structures rather than merely suppress symptoms. By integrating applied mathematics with contemporary psychological theory, the chapter offers a novel perspective on the origins, maintenance, and treatment of psychological symptoms.

1. Introduction

Mental disorders represent one of the most significant public health challenges of the twenty-first century. Depression, anxiety disorders, obsessive-compulsive symptoms, and trauma-related conditions contribute substantially to disability, reduced quality of life, and increased economic burden worldwide. According to evolutionary psychiatry, however, psychological symptoms should not always be viewed exclusively as indicators of dysfunction. Instead, some

1 Asst. Prof., Recep Tayyip Erdoğan University, ORCID ID: 0000-0002-5265-1425

https://doi.org/10.58830/ozgur.pub1361.c5493

symptoms may reflect adaptive mechanisms that evolved to help individuals cope with environmental uncertainty, social competition, and potential threats **(Nesse & Williams, 2012; Nesse, 2019)**. Traditional psychiatric models typically conceptualize symptoms as pathological deviations from normal psychological functioning. While this perspective has contributed substantially to advances in diagnosis and treatment, it often leaves unanswered a fundamental evolutionary question: why are psychological responses such as anxiety, vigilance, social sensitivity, and withdrawal so widespread across human populations? If these responses were entirely maladaptive, natural selection would be expected to reduce their prevalence over evolutionary time. The persistence of such phenomena suggests that they may have served important adaptive functions under certain environmental conditions **(Nesse, 2005)**. Recent advances in mathematical psychology, computational psychiatry, and evolutionary behavioral sciences have provided new frameworks for addressing this question. Computational models increasingly conceptualize human cognition as a predictive system that continuously evaluates environmental risks, rewards, and uncertainties **(Friston, 2010; Huys et al., 2016)**. Within these frameworks, behavior can often be interpreted as a strategic response to perceived environmental contingencies rather than merely a consequence of dysfunction. Game theory offers a particularly powerful mathematical framework for examining such strategic behavior. Originally developed by **Von Neumann and Morgenstern (1947)** and later expanded through **Nash's (1950)** equilibrium concept, game theory analyzes situations in which outcomes depend not only on an individual's decisions but also on environmental conditions and the actions of other agents. The subsequent development of evolutionary game theory by **Maynard Smith (1982)** further demonstrated how stable behavioral strategies can emerge through adaptive processes over time.

This chapter argues that many psychological symptoms can be understood as strategic responses generated by cognitive systems attempting to minimize losses, manage uncertainty, and maximize long-term outcomes. Anxiety, social anxiety, depression, obsessive-compulsive behaviors, and post-traumatic stress responses are examined as potential Nash equilibrium strategies that emerge from interactions between individuals and their environments. From this perspective, symptoms may not always reflect failures of the mind; rather, they may represent solutions to complex adaptive problems, even when those solutions produce substantial subjective distress.

2. Game Theory and Human Behavior

Game theory was originally developed to analyze strategic decision-making in economics and military conflicts **(Von Neumann & Morgenstern, 1947)**. However, its applications have expanded considerably and now encompass biology, psychology, political science, and neuroscience. At its core, game theory examines situations in which the outcomes of a decision depend upon the interaction between multiple agents, each pursuing strategies that maximize their perceived payoffs. One of the most influential concepts in game theory is the Nash equilibrium **(Nash, 1950)**. A Nash equilibrium exists when no player can improve their outcome by unilaterally changing their strategy while other players maintain theirs. Importantly, equilibrium does not necessarily imply optimality or well-being. Instead, it represents a stable state in which alternative strategies appear less advantageous given existing conditions. This distinction is particularly relevant for understanding psychological symptoms. Many forms of behavior that appear maladaptive from an external perspective may nevertheless constitute stable responses within an individual's subjective payoff structure. Evolutionary game theory further suggests that such strategies may persist if they historically provided survival or reproductive advantages under specific environmental circumstances **(Smith, 1982)**. From a psychological perspective, individuals continuously evaluate potential gains and losses associated with social interactions, threat detection, resource allocation, and decision-making. Cognitive systems evolved to operate under uncertainty, where the costs of different types of errors are often asymmetrical **(Cosmides & Tooby, 1996)**. Consequently, behavioral strategies may emerge that prioritize minimizing catastrophic losses rather than maximizing immediate comfort or happiness. Game theory therefore provides a useful framework for examining psychological symptoms not simply as pathological outcomes but as strategic adaptations shaped by environmental contingencies, risk assessment, and evolutionary trade-offs.

3. Social Anxiety as an Equilibrium Strategy

Social anxiety is traditionally defined as a persistent fear of negative evaluation, embarrassment, or rejection in social situations. Individuals experiencing social anxiety often avoid social interactions, public speaking, initiating conversations, or situations in which they may become the focus of attention. Conventional clinical models typically interpret these behaviors as maladaptive responses arising from distorted cognitions, excessive fear, or dysfunctional beliefs. While such explanations have received substantial empirical support, they do not fully explain why social anxiety remains one of the most common psychological conditions across cultures and historical

periods. An evolutionary perspective offers an alternative interpretation. According to **Gilbert (2001)**, social anxiety may be understood as a form of competitive anxiety emerging from social hierarchies. Human beings compete not only for material resources but also for social resources such as approval, prestige, support, friendship, and status. Within such competitive environments, individuals continuously evaluate their relative position and assess the potential consequences of social success or failure. When individuals perceive themselves as possessing fewer desirable attributes than others, or when they fear losing their current social standing, social interactions may become associated with significant risks. In these contexts, behaviors such as silence, withdrawal, gaze avoidance, concealment, and heightened self-monitoring may function as defensive strategies designed to reduce the likelihood of social defeat. **Gilbert (2001)** argues that many of these responses resemble evolved subordinate-defense mechanisms that historically reduced conflict with higher-status individuals and minimized the costs of social exclusion. From a game-theoretic perspective, these observations suggest that social anxiety may not simply represent dysfunctional behavior. Instead, it may emerge as a strategic response to a perceived social environment characterized by asymmetric costs and benefits.

3.1. A Simple Game-Theoretical Model of Social Anxiety

Let's construct a two-player, two-strategy Nash game between a socially anxious individual and the social environment. A more realistic formulation is:

Players

1. Player 1: Socially Anxious Individual
2. Player 2: Social Environment (group, audience, peers)

Strategies

A. Socially Anxious Individual
   1. Participate (P)
   2. Avoid (A)

B. Social Environment
   1. Accept/Respond Positively (R)
   2. Reject/Evaluate Negatively (N)

C. Subjective Payoff Matrix

The first value is the individual's payoff; the second value is the environment's payoff.

Before presenting the payoff matrix, it is important to emphasize that the numerical values are not intended to represent empirically measured utilities. Rather, they are illustrative values designed to capture the subjective evaluation of social outcomes commonly observed in individuals with social anxiety. Consistent with cognitive and evolutionary accounts of social anxiety **(Gilbert, 2001; Haselton & Buss, 2000)**, socially anxious individuals tend to overestimate the costs of social rejection while simultaneously underestimating their ability to cope with negative social outcomes. Consequently, the model assigns a relatively large negative payoff to rejection and a comparatively high positive payoff to social acceptance. The numerical values therefore serve as conceptual representations of perceived costs and benefits rather than objective measurements.

Table 1. Subjective payoff matrix for social anxiety

	Environment: Accept (R)	**Environment: Reject (N)**
Participate (P)	(8, 5)	(-20, 2)
Avoid (A)	(0, -1)	(0, 0)

Interpretation

I. (P,R): The individual participates and receives acceptance. This is highly rewarding for the individual (+8) and beneficial for the social environment (+5).

II. (P,N): The individual participates but experiences rejection. For a socially anxious person, rejection is perceived as extremely costly (-20).

III. (A,R): The environment would have been accepting, but the individual avoids interaction. The individual gains neither reward nor punishment (0), while the environment loses a potential interaction (-1).

IV. (A,N): Avoidance prevents interaction altogether. Neither side gains much (0,0).

The payoff value of +8 assigned to participation in a supportive environment reflects the substantial psychological rewards that may accompany successful social engagement, including social acceptance, belongingness, approval, increased self-confidence, and access to interpersonal support. The corresponding payoff of +5 for the social environment reflects the benefits of reciprocal interaction, group cohesion, communication, and mutual

cooperation. The payoff values associated with successful participation are intentionally asymmetric. A value of +8 is assigned to the socially anxious individual because successful social engagement may generate multiple psychological benefits simultaneously, including social acceptance, increased self-confidence, reduced uncertainty, enhanced belongingness, and positive corrective experiences. By contrast, the social environment receives a payoff of +5 because, although it benefits from interaction, communication, and group cohesion, the magnitude of these gains is typically less transformative than the benefits experienced by the individual. The asymmetry reflects the assumption that a successful interaction is psychologically more consequential for the socially anxious individual than for the surrounding social group.

By contrast, the payoff of -20 assigned to participation in a critical environment reflects the disproportionate weight that socially anxious individuals often assign to rejection, embarrassment, criticism, or perceived social failure. The value is intentionally larger in magnitude than the reward associated with acceptance, reflecting evidence that socially anxious individuals frequently perceive negative social outcomes as considerably more impactful than positive ones **(Gilbert, 2001)**. The payoff of 0 assigned to avoidance represents a neutral outcome in which the individual neither obtains social rewards nor experiences immediate social threats. Similarly, when the individual avoids participation in a critical environment, neither player experiences a meaningful change in outcome, resulting in a payoff of (0,0). The environment, however, is assigned a modest positive payoff (+2) rather than a neutral payoff. This reflects the possibility that criticism, exclusion, or negative evaluation may help maintain existing social hierarchies, reinforce group norms, or preserve the relative status of dominant individuals within the group.

Finally, the value of -1 assigned to the social environment when the individual avoids participation despite a potentially supportive context represents a small social cost. The group invests time, attention, and opportunities for interaction but receives limited reciprocal engagement in return. Although this cost is minor compared to the individual's perceived risk of rejection, it reflects the loss of potential communication, cooperation, and social exchange. his asymmetry is intentional and represents a central feature of social anxiety. For the socially anxious individual, the possibility of criticism, embarrassment, rejection, or status loss is often perceived as highly consequential. Negative social evaluation may threaten belongingness, self-esteem, social standing, and future participation opportunities. Consequently, the subjective cost associated with rejection is modeled as substantial (-20). By contrast, when the individual chooses avoidance, the social environment experiences only a modest opportunity cost (-1). Although the group loses a potential interaction,

communication opportunity, or contribution, it does not experience a loss comparable to the one perceived by the socially anxious individual. In most social settings, the consequences of one person's silence are relatively minor for the group as a whole. Therefore, the difference between -10 and -1 reflects the disproportionate psychological weight assigned to social rejection by socially anxious individuals.

For the socially anxious individual:

1. If the environment is accepting:

a) Participate = 8

b) Avoid = 0

Best response = Participate

2. If the environment is rejecting:

a) Participate = -20

b) Avoid = 0

Best response = Avoid

Now assume the individual believes there is a substantial probability of rejection. The expected payoff of participation becomes:

$U(p)=8p+(1-p)(-20)$

where p is the perceived probability of acceptance.

Participation becomes preferable only if:

$8p-20(1-p)>0$

Then, $28p>20$, so $p>0.714$. Thus, the socially anxious individual must believe that acceptance is more than 71.4% likely before participation becomes rational.

3.1.1. Social Anxiety as a Nash Equilibrium

Consider a noncooperative game involving n players, where each player i chooses a strategy Si for i=1,2,…n. A strategy profile (S1*, S2*,…, Sn*) is said to be a Nash equilibrium when each player's chosen strategy is the best response to the equilibrium strategies of all other players. In other words, once every player adopts their equilibrium strategy, no individual player can improve their own outcome by unilaterally switching to a different strategy. For example, in a two-player game, the strategy pair (S1*, S2*) constitutes a Nash equilibrium if player 1 cannot achieve a higher payoff by deviating

from S1* while player 2 continues to play S2*, and similarly, player 2 cannot improve their payoff by changing from S2* while player 1 maintains S1*. Thus, a Nash equilibrium represents a stable strategic configuration in which no player has an incentive to deviate alone **(Nash, 1950)**.

The structure of the matrix reveals two Nash equilibria. The first equilibrium occurs at (Participate, Supportive Environment) with payoffs of (8,5). If the individual were to unilaterally switch from participation to avoidance, the payoff would decrease from 8 to 0. Likewise, if the environment were to unilaterally switch from a supportive to a critical stance, its payoff would decrease from 5 to 0. Consequently, neither player has an incentive to change strategy, making this outcome a Nash equilibrium.

A second Nash equilibrium emerges at (Avoid, Critical Environment) with payoffs of (0,0). If the environment remains critical, the individual would reduce their payoff from 0 to -10 by choosing to participate. Therefore, avoidance remains the individual's best response. Similarly, if the individual remains silent, the environment would reduce its payoff from 0 to -1 by becoming supportive. As a result, the environment also lacks an incentive to change strategy unilaterally. Since neither player can improve their outcome by changing strategy alone, this outcome also satisfies the definition of a Nash equilibrium.

From a psychological perspective, the second equilibrium is particularly important. It represents a stable but socially suboptimal state in which avoidance and social disengagement become self-reinforcing. The socially anxious individual avoids participation because speaking is perceived as excessively risky, while the environment gradually reduces efforts to engage someone who consistently withdraws. Over time, this interaction pattern becomes increasingly stable, not because it maximizes well-being, but because neither player perceives an immediate benefit from changing strategy independently. Thus, social anxiety can be conceptualized as a Nash-type equilibrium maintained by a subjective payoff structure in which the perceived cost of rejection greatly exceeds the potential reward of acceptance. The individual is not necessarily behaving irrationally. Rather, avoidance represents the most advantageous strategy available within the individual's perceived social reality. The persistence of social anxiety may therefore reflect the stability of an equilibrium rather than a failure of decision-making.

Table 2. Nash equilibrium analysis of the social anxiety game

Outcome	Individual Deviation Profitable?	Environment Deviation Profitable?	Nash Equilibrium?
(Participate, Supportive) = (8,5)	No (8 ✍ 0)	No (5✍ 2)	**Yes**
(Participate, Critical) = (-20,2)	Yes (-20 ✍ 0)	Yes (2 ✍ 5)	No
(Avoid, Supportive) = (0,-1)	Yes (0 ✍ 8)	Yes (-1 ✍ 0)	No
(Avoid, Critical) = (0,0)	No (0 ✍-20)	No (0 ✍ -1)	**Yes**

The existence of two Nash equilibria suggests that social interactions involving socially anxious individuals may stabilize around either a high-engagement or a low-engagement state. The first equilibrium is socially desirable because both parties benefit from participation and support. The second equilibrium, however, is particularly relevant for understanding the persistence of social anxiety. Although neither player receives substantial benefits, neither can improve their outcome through unilateral strategy change. Consequently, avoidance and social disengagement become self-reinforcing, creating a stable but socially suboptimal equilibrium. In other words, remaining silent becomes the safer strategy for the individual, while maintaining a critical stance becomes the safer strategy for the environment. As a result, the interaction stabilizes around a state in which neither party has an incentive to change strategy unilaterally. If the individual alone shifts from avoidance to participation, the payoff decreases from 0 to -20, exposing the individual to substantial perceived social risk. Similarly, if the environment alone shifts from a critical to a supportive stance while the individual continues to avoid participation, its payoff decreases from 0 to -1 because the effort invested in encouraging interaction yields little return. Consequently, both parties maintain their current strategies, producing a stable Nash equilibrium. Over time, the environment may reduce efforts to engage the individual, reasoning that "the person is unlikely to participate anyway," thereby reinforcing the individual's avoidance and sustaining the equilibrium.

3.1.2. Therapeutic Change as Payoff Restructuring

The game-theoretic interpretation of social anxiety has important implications for understanding psychological treatment. Traditional clinical approaches often describe psychotherapy as a process that reduces symptoms, corrects distorted beliefs, or improves emotional regulation. While these explanations remain valuable, a game-theoretic perspective offers an additional interpretation: psychotherapy may function by altering the payoff structure that maintains maladaptive behavioral equilibria. In the model presented above, avoidance emerges as a rational response because the perceived cost of social rejection substantially exceeds the potential benefits of social participation. Importantly, the maintenance of social anxiety does not necessarily depend on the objective reality of social situations. Rather, it depends on how the individual subjectively evaluates potential outcomes. Consequently, therapeutic change can occur when these subjective evaluations are modified.

Cognitive-behavioral approaches provide a clear example of this process. Individuals with social anxiety frequently interpret social rejection as catastrophic, assigning disproportionately large costs to negative social outcomes. A minor conversational mistake may be interpreted as evidence of incompetence, embarrassment, or permanent social exclusion. Through cognitive restructuring, individuals gradually learn to challenge these assumptions and develop more balanced interpretations of social experiences. Exposure-based interventions operate through a similar mechanism. Repeated exposure to feared social situations often reveals that anticipated negative outcomes either do not occur or are considerably less severe than expected. Over time, the individual learns that rejection, criticism, or social awkwardness are not necessarily catastrophic events. Instead, they become manageable experiences that can provide opportunities for learning and adaptation.

As a result, the subjective payoff structure changes. Before therapy, participation in a critical environment may be perceived as producing a payoff of -20, reflecting severe anticipated psychological costs. After successful therapeutic intervention, the same outcome may be perceived differently. The individual may begin to think:

"If I participate, something positive may happen (+8). Even if the interaction is not successful, I will gain experience, learn something useful, and improve my future performance (+1)."

Failure is no longer interpreted as punishment; it becomes information.

Consequently, the payoff matrix may be transformed as follows:

Table 3. Payoff matrix after psychotherapy

	Supportive Environment	**Critical Environment**
Participate	(8,5)	(1,2)
Avoid	(0,-1)	(0,0)

The critical change occurs in the individual's evaluation of participation under potentially negative social conditions. The perceived payoff associated with rejection shifts from -20 to +1, not because rejection becomes pleasant, but because it is reinterpreted as a tolerable and potentially informative experience rather than a catastrophic social failure. This transformation has important implications for equilibrium behavior. In the original matrix, avoidance was the individual's best response when facing a critical environment because participation would reduce the payoff from 0 to -20. In the revised matrix, however, participation yields a payoff of +1 while avoidance remains at 0. Under these conditions, participation becomes the more attractive strategy.

Likewise:

$U(p)=8p+1(1-p)$

Then, $7p+1>0$ i.e. participation becomes a dominant strategy for the individual. When even negative social outcomes are reinterpreted as opportunities for learning and growth, participation becomes beneficial regardless of the social response received. In game-theoretic terms, participation may become a dominant strategy rather than merely an equilibrium response.

From a game-theoretic perspective, psychotherapy weakens the stability of the avoidance equilibrium by changing the incentives that sustain it. The previously stable equilibrium of (Avoid, Critical Environment) becomes increasingly difficult to maintain because the individual's subjective evaluation of social risk has fundamentally changed. As participation increases, opportunities for positive social experiences also increase, creating the possibility of movement toward more adaptive equilibria characterized by engagement, communication, and social support. Importantly, this framework suggests that therapeutic improvement does not necessarily require changing the individual as a decision-maker. Instead, therapy changes how outcomes are valued and interpreted. The individual's decision-making process may remain entirely rational, while the payoff structure within which decisions are made becomes different. In this sense, psychotherapy can be conceptualized not merely as symptom reduction but as payoff restructuring. By modifying perceived costs, rewards, and probabilities, therapy alters the strategic landscape

within which behavior occurs. Once the game changes, equilibrium behavior may change as well. Thus, from a game-theoretic perspective, psychological recovery may sometimes be understood not as changing the player, but as changing the game.

4. Beyond Social Anxiety: Toward a General Framework

The social anxiety model presented above may represent only one example of a broader phenomenon. Once psychological symptoms are viewed through a game-theoretic lens, similar dynamics can be observed in many areas of human behavior. In each case, individuals appear to choose strategies that minimize perceived costs and maximize perceived benefits within their subjective understanding of the situation.

A similar pattern may be observed in depression. Depressed individuals often withdraw from social interactions. They may stop calling friends, decline invitations, or spend increasing amounts of time alone. From an external perspective, such behaviors may appear counterproductive because social support is generally associated with improved psychological well-being. However, the individual's internal calculations may be very different. The potential rewards of social interaction may be perceived as small and uncertain, whereas the risks of disappointment, rejection, criticism, or emotional exhaustion may be perceived as substantial. Under these conditions, withdrawal may become the safest available strategy. Although the behavior may ultimately contribute to loneliness and reduced well-being, it can nevertheless be understood as a response to a payoff structure in which avoiding potential losses is prioritized over pursuing potential gains.

Addictive behaviors provide another example. Individuals struggling with addiction frequently choose immediate rewards despite long-term negative consequences. The temporary relief provided by a cigarette, alcoholic drink, gambling episode, or other addictive behavior is experienced immediately, whereas the associated costs often emerge gradually over months or years. As a result, short-term rewards may outweigh distant future losses in the individual's decision-making process. From a game-theoretic perspective, the repeated selection of immediate gratification can be interpreted as a strategy emerging from a payoff structure that heavily discounts future outcomes.

Perhaps some of the most interesting examples arise in close relationships. Over time, recurring interaction patterns often emerge between partners, friends, family members, or colleagues. One individual may repeatedly adopt a giving strategy, while the other becomes accustomed to receiving. In the short term, such arrangements may appear stable because both parties receive

certain benefits. However, over longer periods, resentment, frustration, and imbalance may accumulate. Game theory helps explain how these seemingly stable interaction patterns can persist for extended periods despite producing dissatisfaction for one or both parties.

Similar principles may also apply to obsessive-compulsive behaviors, post-traumatic stress responses, perfectionism, procrastination, and many other psychological phenomena. Although the specific symptoms differ, a common theme emerges: behavior often reflects attempts to manage perceived risks, uncertainties, and potential losses. What appears irrational from an outside perspective may represent a coherent strategy within the individual's subjective model of reality.

The purpose of this chapter is not to suggest that every psychological symptom can be fully explained by game theory. Human behavior is influenced by biological, developmental, cognitive, emotional, social, and cultural factors that cannot be reduced to a single framework. Nevertheless, game theory offers a useful conceptual lens for understanding why certain behaviors persist even when they appear self-defeating. In many cases, symptoms may represent stable responses to perceived environmental conditions rather than simple failures of rationality. From this perspective, psychological symptoms may sometimes be understood not merely as signs of dysfunction, but as equilibrium strategies that emerge when individuals attempt to navigate complex social and environmental challenges under conditions of uncertainty.

5. Conclusion

Psychological disorders cannot, of course, be fully explained through mathematical models alone. Human cognition, emotion, and behavior are shaped by biological, developmental, social, cultural, and experiential factors that extend far beyond the scope of any single theoretical framework. The human mind is considerably more complex than a set of equations, and no mathematical model can capture the full richness of psychological experience. Nevertheless, game theory offers a valuable perspective for understanding why certain behavioral patterns persist. One of its central insights is that individuals do not necessarily maintain behaviors because they are irrational. Rather, they often continue to employ strategies that appear reasonable within their subjective understanding of the world. What may seem maladaptive from an external perspective can represent a rational response to perceived costs, rewards, risks, and uncertainties. The concept of Nash equilibrium is particularly useful in this regard. A Nash equilibrium does not necessarily describe a situation in which all parties are satisfied or thriving. Instead, it

describes a stable state in which no individual believes that changing strategy alone will lead to a better outcome. From this perspective, some psychological symptoms may be understood as "suboptimal but stable" equilibria that emerge within the social and psychological games individuals navigate throughout their lives.

Importantly, an individual's payoff is determined not only by objective events but also by expectations, beliefs, emotions, and perceptions of how others are likely to respond. In psychological contexts, what people expect to happen may be just as influential as what actually happens. Consequently, subjective interpretations become part of the game itself. The perceived cost of rejection, failure, uncertainty, or loss may substantially shape behavior even when those outcomes are unlikely to occur. This perspective has important implications for understanding therapeutic change. If symptoms are maintained by subjective payoff structures, then psychological improvement may sometimes involve more than changing the individual. It may involve changing the way outcomes are evaluated, interpreted, and anticipated. In game-theoretic terms, therapy can be understood as a process of restructuring the payoff landscape that governs behavior. As perceptions of costs and rewards change, previously stable equilibria may weaken, allowing new and more adaptive patterns of behavior to emerge.

The aim of this chapter has not been to reduce mental health to mathematics, but rather to demonstrate how mathematical thinking can provide new conceptual tools for understanding psychological phenomena. By viewing symptoms as potential equilibrium strategies rather than merely signs of dysfunction, game theory offers a complementary perspective that may enrich existing psychological and psychiatric models. Social anxiety is presented here as an illustrative example of a broader equilibrium framework. Future work may develop formal game-theoretic models for specific psychological conditions. Perhaps the future of mental health lies not only in understanding the player, but also in understanding the game. In many cases, psychological suffering may persist because individuals remain trapped within stable patterns of perceived costs and rewards. If so, one of the most important tasks of psychological intervention may be helping individuals recognize that the rules of the game are not fixed, and that when the game changes, the equilibrium can change as well.

References

Andrews, P. W., & Thomson Jr, J. A. (2009). The bright side of being blue: depression as an adaptation for analyzing complex problems. Psychological review, 116(3), 620.

Cosmides, L., & Tooby, J. (1996). Are humans good intuitive statisticians after all? Rethinking some conclusions from the literature on judgment under uncertainty. cognition, 58(1), 1-73.

Friston, K. (2010). The free-energy principle: A unified brain theory? Nature Reviews Neuroscience, 11(2), 127–138.

Gilbert, P. (2001). Evolution and social anxiety: The role of attraction, social competition, and social hierarchies. Psychiatric Clinics, 24(4), 723-751.

Haselton, M. G., & Buss, D. M. (2000). Error management theory: a new perspective on biases in cross-sex mind reading. Journal of personality and social psychology, 78(1), 81.

Haselton, M. G., Nettle, D., & Andrews, P. W. (2015). The evolution of cognitive bias. The handbook of evolutionary psychology, 724-746.

Huys, Q. J., Maia, T. V., & Frank, M. J. (2016). Computational psychiatry as a bridge from neuroscience to clinical applications. Nature neuroscience, 19(3), 404-413.

McNally, R. J. (2006). Cognitive abnormalities in post-traumatic stress disorder. Trends in cognitive sciences, 10(6), 271-277.

Nash Jr, J. F. (1950). Equilibrium points in n-person games. Proceedings of the national academy of sciences, 36(1), 48-49.

Nesse, R. M. (2005). Natural selection and the regulation of defenses: A signal detection analysis of the smoke detector principle. Evolution and human behavior, 26(1), 88-105.

Nesse, R. M., & Williams, G. C. (2012). Why we get sick: The new science of Darwinian medicine. Vintage.

Nesse, R. M. (2019). Good Reasons for Bad Feelings: Insights from the Frontier of Evolutionary Psychiatry. Penguin Books.

Price, J., Sloman, L., Gardner Jr, R., Gilbert, P., & Rohde, P. (1994). The social competition hypothesis of depression. The British Journal of Psychiatry, 164(3), 309-315.

Smith, J. M. (1982). Evolution and the Theory of Games. In Did Darwin get it right? Essays on games, sex and evolution (pp. 202-215). Boston, MA: Springer US.

Von Neuman, J., & Morgenstern, O. (1947). Theory of Games and Economic Behavior, Princeton University Press.

Chapter 4

Extensions of Singular Fourth Order Dynamic Operators with Transmission Conditions

Hatice Bulut Demiralay[1]

Abstract

In the present paper, a singular fourth-order dynamic operator on time scales is investigated in the presence of impulsive conditions. Initially, a suitable boundary value framework adapted to the impulsive structure of the operator is constructed. Subsequently, the maximal dissipative, self-adjoint, and further appropriate extensions of the associated singular fourth-order differential operator, which acts on unbounded time scales under impulsive effects, are comprehensively characterized.

1. Introduction

The calculus of time scales provides a comprehensive framework for the unification of continuous and discrete mathematical paradigms. Since its formal conceptualization in the early 1990s (Hilger,1990), this field has emerged as a pivotal area of research, effectively bridging the theoretical gap between differential and difference equations. The resulting theory of dynamic equations offers a robust analytical toolset for modeling complex phenomena across diverse scientific domains. Notably, time scale analysis has become indispensable in simulating heat conduction, entomological population shifts, infectious disease trajectories, financial market volatility, and the computational dynamics of neural networks (Hilger,1990; Thomas et al., 2005).

Furthermore, the expansion of symmetric operators is an essential element in diverse sectors of mathematical physics, notably within quantization issues and solvable quantum mechanics paradigms. Initially established by J. von Neumann (Neumann, 1929), the theory of extensions was significantly refined by Calkin (Calkin, 1939), who characterized self-adjoint extensions through abstract boundary conditions. Subsequent advancements by Rofe-Beketov (Rofe-Beketov,1969) introduced the use of linear relations to delineate these extensions. The establishment of boundary value space theory by Bruk (Bruk, 1976) and Kochubei (Kochubei, 1975) constituted a significant breakthrough, offering a systematic framework to classify all maximal dissipative, accretive,

1 PhD Student, Burdur Mehmet Akif Ersoy University, bulut.math@hotmail.com.tr, ORCID ID: 0009-0006-3652-4350

https://doi.org/10.58830/ozgur.pub1361.c5494

and self-adjoint extensions of symmetric operators. This subject remains a focal point for mathematical research (Allahverdiev, 1995; Tuna and Allahverdiev, 2018), with exhaustive theoretical treatments available in (Gorbachuk et al., 1989)

On the other hand, impulsive problems have attracted substantial academic attention, resulting in an extensive body of both theoretical and empirical research (see (Allahverdiev et al., 2023; Allahverdiev and Tuna, 2019; Aydemir et al., 2018; Aydemir et al., 2019; Amirov et al., 2021; Güldü, 2013). These phenomena are intrinsic to numerous scientific fields characterized by abrupt transitions, such as heat and mass transfer mechanisms (Lykov and Mikhailov, 1965), geophysical modeling (Lapwood and Usami, 1981) and the intricacies of radio science (Litvinenko and Soshnikov, 1964). The comprehensive literature surrounding these issues underscores their vital role in precisely modeling systems that experience instantaneous perturbations.

The primary objective of the present study is oriented toward exploring a singular fourth-order dynamic operator on time scales, with particular consideration given to the effects of impulsive perturbations. By integrating impulsive perturbations into the time scale framework, we provide a rigorous analysis of the operator's structural properties. This includes the systematic construction of boundary value spaces and the subsequent classification of its fundamental extensions.

The structure of this paper is organized as follows: Section 2 provides a concise overview of the fundamental properties of time scales to establish a necessary theoretical background. In Section 3, we establish a boundary value space associated with singular fourth-order dynamic operators, focusing exclusively on the Limit-2 case. Within this framework, we offer a comprehensive characterization of all maximal dissipative, accretive, and self-adjoint extensions among others utilizing explicit boundary conditions. Finally, Section 4 extends this analysis to the Lim-4 case, providing an exhaustive description of all operator extensions under these conditions.

2. Preliminaries

This section briefly outlines the fundamental tenets of time scale calculus requisite for the ensuing analysis. For a comprehensive theoretical background and rigorous derivations, we refer the reader to the established literature (Bohner and Peterson, 2001; Bohner and Peterson, 2003; Atici and Guseinov, 2002; Lakshmikantham et al.,2013; Guseinov, 2005; Hilger, 1990; Huseynov, 2012).

Definition 2.1.: Consider a time scale $\mathbb{T}$. The mapping $\sigma: \mathbb{T} \to \mathbb{T}$, designated as the forward jump operator, is formulated as:

$$\sigma(r) = \inf\{w \in \mathbb{T}: w > r\},\ r \in \mathbb{T}.$$

Correspondingly, the backward jump operator $\rho: \mathbb{T} \to \mathbb{T}$ is defined by:

$$\rho(r) = \sup\{w \in \mathbb{T}: w < r\},\ r \in \mathbb{T}.$$

To quantify the step size between points, we introduce the graininess functions $\mu_\sigma(r) = \sigma(r) - r$ and $\mu_\rho(r) = \rho(r) - r$. The topological classification of any point $r \in \mathbb{T}$ is determined by these functions: r is categorized as left-scattered if $\mu_\rho(r) \neq 0$ and left-dense if $\mu_\rho(r) = 0$. Analogously, it is right-scattered if $\mu_\sigma(r) \neq 0$ and right-dense if $\mu_\sigma(r) = 0$. Furthermore, we define the restricted sets $\mathbb{T}^k$, $\mathbb{T}_k$,and $\mathbb{T}^*$ to ensure the existence of derivatives at boundary points. Specifically, $\mathbb{T}^k$ is obtained by removing the maximum element of $\mathbb{T}$ if it is left-scattered; otherwise, $\mathbb{T}^k = \mathbb{T}$. In a symmetric fashion, $\mathbb{T}_k$ excludes the minimum element if it is right-scattered. The intersection of these subsets is denoted as $\mathbb{T}^* = \mathbb{T}^k \cap \mathbb{T}_k$.

Definition 2.2.: A function f defined on $\mathbb{T}$ is considered Δ -differentiable at $r \in \mathbb{T}$ provided there exists a value $f^\Delta(r)$ satisfying the condition that for any $\varepsilon > 0$, a neighborhood U of r exists such that for all $w \in U$:

$$|f(\sigma(r)) - f(w) - f^\Delta(r)(\sigma(r) - w)| \leq \varepsilon|\sigma(r) - w|.$$

By utilizing the backward jump operator ρ, the dual concept of ∇-differentiability is defined in an analogous fashion. Furthermore, within the domain of continuously differentiable functions, the following dual relations establish the connection between these two derivative operators (Bohner and Peterson, 2001):

$$f^\Delta(r) = f^\nabla(\sigma(r)), \qquad f^\nabla(r) = f^\Delta(\rho(r)).$$

Example 2.1.: The following instances demonstrate how the Δ-differential operator generalizes classical calculus:

When $\mathbb{T} = \mathbb{R}$, the forward jump operator becomes $\sigma(r) = r$, and the Δ-derivative simplifies to the traditional derivative $f^\Delta(r) = f'(r)$.

When $\mathbb{T} = \mathbb{Z}$, we have $\sigma(r) = r + 1$, which identifies the operator with the forward difference $f^\Delta(r) = \Delta f(r) = f(r + 1) - f(r)$.

When $\mathbb{T} = q^{\mathbb{N}_0}$, the jump operator is defined as $\sigma(r) = qr$ for $q > 1$, resulting in the q-difference quotient $f^\Delta(r) = \frac{f(qr)-f(r)}{qr-r}$.

Definition 2.3.: Let f denote a function defined on the time scale $\mathbb{T}$, and suppose that $k, m \in \mathbb{T}$. We designate $F: \mathbb{T} \to \mathbb{R}$ as a Δ-antiderivative of f if the equality $F^\Delta(r) = f(r)$ is satisfied for every $r \in \mathbb{T}^k$. In this framework, the definite integral of f is determined by the fundamental relation:

$$\int_k^m f\,(r)\Delta r = F(m) - F(k)\,.$$

A parallel construction is utilized to define the ∇-antiderivative, substituting the forward difference mechanism with its backward counterpart.

The space $L^2_\Delta\,(\mathbb{T}^*)$ comprises all functions defined on $\mathbb{T}^*$ for which the following norm condition is satisfied:

$$\|f\| := \left(\int_k^l |f(r)|^2\,\Delta r\right)^{1/2} + \left(\int_l^m |f(r)|^2\,\Delta r\right)^{1/2} < \infty.$$

Assume $\mathbb{T}$ denotes a time scale which is bounded below but extends indefinitely upward, satisfying $\inf\mathbb{T} = k > -\infty$ and $\sup\mathbb{T} = \infty$. This domain shall also be denoted as $[k,l) \cup (l,\infty)_{\mathbb{T}}$.

The set $L^2_\Delta[k,l) \cup (l,\infty)_{\mathbb{T}}$ forms a Hilbert space when endowed with the inner product given by:

$$\langle f,g\rangle := \int_k^l f\,(r)\overline{g(r)}\Delta r + \int_l^\infty f\,(r)\overline{g(r)}\Delta r,\ \ f,g \in L^2_\Delta[k,l) \cup (l,\infty)_{\mathbb{T}}.$$

(see (Rynne, 2007)).

The following fourth-order dynamic equation is examined within this framework:

$$\Upsilon\varsigma(r) := (p_0\varsigma^{\Delta\nabla})^{\nabla\Delta}(r) - (p_1\varsigma^{\nabla})^{\Delta} + p_2(r)\varsigma(r) = \lambda\varsigma(r), r \in [k,l) \cup (l,\infty)_{\mathbb{T}}, \qquad (2.1)$$

the analysis assumes that the coefficients p_0, p_1 and p_2 are real-valued. Additionally, p_0^{-1}, p_1 and p_2 are required to be locally Δ-integrable on $[k,l) \cup (l,\infty)_{\mathbb{T}}$, with the further stipulation that $p_0 > 0$ holds throughout the domain $[k,l) \cup (l,\infty)_{\mathbb{T}}$.

A similar problem has also been investigated without impulsive conditions (Tuna and Bayrak, 2018; Tuna and Bulut, 2018).

To streamline the notation, the following shorthand will be employed:

$$\varsigma^{[0]} = \varsigma$$
$$\varsigma^{[1]} = \varsigma^{\Delta}$$
$$\varsigma^{[2]} = p_0\varsigma^{\Delta\nabla}$$
$$\varsigma^{[3]} = p_1\varsigma^{\nabla} - \left(\varsigma^{[2]}\right)^{\nabla}$$
$$\varsigma^{[4]} = p_2\varsigma - \left(\varsigma^{[3]}\right)^{\Delta}.$$

Subsequently, we transform the dynamic equation given in (2.1) into its equivalent Hamiltonian system representation. To this end, we introduce the following vector-valued variables:

$$X = \begin{bmatrix} \varsigma \\ \varsigma^{\Delta} \\ -\left(p_0\varsigma^{\Delta\nabla}\right)^{\Delta} + p_1\varsigma^{\Delta} \\ p_0\varsigma^{\Delta\Delta} \end{bmatrix},\ \hat{X} = \begin{bmatrix} \varsigma \\ \varsigma^{\Delta} \\ -\left(p_0\varsigma^{\Delta\nabla}\right)^{\nabla} + p_1\varsigma^{\nabla} \\ p_0\varsigma^{\Delta\nabla} \end{bmatrix}$$

which transforms (2.1) into the following form:

$$J\,\hat{X}^{\Delta} = (\lambda C + E)X, \qquad (2.2)$$

where

$$C=\begin{bmatrix}1&0&0&0\\0&0&0&0\\0&0&0&0\\0&0&0&0\end{bmatrix},\ E=\begin{bmatrix}-p_2&0&0&0\\0&-p_1&1&0\\0&1&0&0\\0&0&0&1/p_0\end{bmatrix}$$

and

$$J=\begin{bmatrix}0&0&-1&0\\0&0&0&-1\\1&0&0&0\\0&1&0&0\end{bmatrix}.$$

It should be noted that C and E possess real and symmetric properties.

The Green identity corresponding to the solutions $\varsigma(r,\lambda)$ and $z(r,\lambda)$ takes the form

$$\int_k^l (\Upsilon\varsigma)(r)\,\overline{z(r)}\Delta r+\int_l^\infty (\Upsilon\varsigma)\,(r)\overline{z(r)}\Delta r-\int_k^l \varsigma(r)\,\overline{(\Upsilon z)(r)}\Delta r-\int_l^\infty \varsigma\,(r)\overline{(\Upsilon z)(r)}\Delta r$$
$$=[\varsigma,z]_\infty-[\varsigma,z](l+)+[\varsigma,z](l-)-[\varsigma,z]_k], \tag{2.3}$$

here $[\varsigma,z]_r:=\varsigma^{[0]}(r)\overline{z}^{[3]}(r)-\varsigma^{[3]}(r)\overline{z}^{[0]}(r)+\varsigma^{[1]}(r)\overline{z}^{[2]}(r)-\varsigma^{[2]}(r)\overline{z}^{[1]}(r)$ and $[\varsigma,z]_\infty:=\lim_{r\to\infty}[\varsigma,z]_r$ (see (Anderson et al., 2006). It follows that the limit $[\varsigma,z]_\infty$ exists and remains finite. Denoting by $X(r,\lambda)$ and $Z(r,\lambda)$ the associated vector functions introduced in (2.2), one obtains

$$X^TJZ(r)=[\varsigma,z]_r.$$

Let $\tau_i, 1\le i\le 4$, represent the solutions of Eq. (2.1) determined under the normalization requirement

$$p_0^2(r)W(\tau_1,\tau_2,\tau_3,\tau_4)=1$$

and

$$\begin{bmatrix}[\tau_1,\tau_1]&[\tau_2,\tau_1]&[\tau_3,\tau_1]&[\tau_4,\tau_1]\\[\tau_1,\tau_2]&[\tau_2,\tau_2]&[\tau_3,\tau_2]&[\tau_4,\tau_2]\\[\tau_1,\tau_3]&[\tau_2,\tau_3]&[\tau_3,\tau_3]&[\tau_4,\tau_3]\\[\tau_1,\tau_4]&[\tau_2,\tau_4]&[\tau_3,\tau_4]&[\tau_4,\tau_4]\end{bmatrix}=\begin{bmatrix}0&0&-1&0\\0&0&0&-1\\1&0&0&0\\0&1&0&0\end{bmatrix},$$

where the Wronskian corresponding to τ_1,τ_2,τ_3 and τ_4 is given by (see (Anderson et al., 2006)

$$W(\tau_1,\tau_2,\tau_3,\tau_4)=\begin{vmatrix}\tau_1&\tau_2&\tau_3&\tau_4\\\tau_1^{[1]}&\tau_2^{[1]}&\tau_3^{[1]}&\tau_4^{[1]}\\\tau_1^{[2]}&\tau_2^{[2]}&\tau_3^{[2]}&\tau_4^{[2]}\\\tau_1^{[3]}&\tau_2^{[3]}&\tau_3^{[3]}&\tau_4^{[3]}\end{vmatrix}.$$

Lemma 2.1.: For arbitrary $f, g \in L^2_\Delta[k,l) \cup (l,\infty)_{\mathbb{T}}$, the following Plücker relation holds:

$$[f,g]_r = \begin{vmatrix} [\tau_2,g]_r & [g,\tau_4]_r \\ [\tau_2,f]_r & [f,\tau_4]_r \end{vmatrix} + \begin{vmatrix} [\tau_1,g]_r & [g,\tau_3]_r \\ [\tau_1,f]_r & [f,\tau_3]_r \end{vmatrix}. \tag{2.4}$$

Proof. The argument proceeds analogously to the proof of Lemma 1 in (Fulton, 1989); therefore, the details are omitted.

We denote by

$$D_{max} = \left\{ \tau \in L^2_\Delta[k,l) \cup (l,\infty)_{\mathbb{T}} \middle| \begin{matrix} the\ first\ three\ \Delta\ derivatives\ are \\ locally\ \Delta - absolutely\ continuous \\ in\ [k,l) \cup (l,\infty)_{\mathbb{T}}, Z(l+) = UZ(l-) \\ and\ \Upsilon\tau \in L^2_\Delta[k,l) \cup (l,\infty)_{\mathbb{T}}. \end{matrix} \right\},$$

where

$$Z = \begin{pmatrix} \varsigma^{(0)} \\ \varsigma^{(1)} \\ \varsigma^{(3)} \\ \varsigma^{(2)} \end{pmatrix}, U = \begin{pmatrix} m & 0 & 0 & 0 \\ 0 & n & 0 & 0 \\ 0 & 0 & \frac{1}{m} & 0 \\ 0 & 0 & 0 & \frac{1}{n} \end{pmatrix},$$

and $m, n \in \mathbb{R},\ m, n \neq 0$.

Through the relation $\Gamma_{\max}\tau = \Upsilon\tau$, we characterize the maximal operator $\Gamma_{\max}$ on D_{max} .
The linear manifold D_{min} is designated to consist of all functions $\varsigma \in D_{max}$ that satisfy

$$\varsigma^{[0]}(\mathrm{k}) = \varsigma^{[1]}(\mathrm{k}) = \varsigma^{[2]}(\mathrm{k}) = \varsigma^{[3]}(\mathrm{k}) = 0, = [\varsigma, z]_\infty = 0, \forall z \in D_{max}. \tag{2.5}$$

Restricting the operator operator $\Gamma_{\max}$ to the domain D_{min} yields the minimal operator $\Gamma_{\min}$.

We then have the adjoint relation $\Gamma^*_{\min} = \Gamma_{\max}$. Furthermore, we note that $\Gamma_{\min}$ is a closed symmetric operator characterized by deficiency indices (2,2), (3,3) or (4,4) (see, (Naimark, 1968; Fulton, 1989)).

We now recall the following result.

Definition 2.4.: A linear operator V with dense domain $D(V)$ in a Hilbert space H is said to be dissipative (respectively, accumulative) if $\mathrm{Im}(Vf,f) \geq 0$, (respectively, $\mathrm{Im}(Vf,f) \leq 0$) for every $f \in D(V)$.It is termed maximal dissipative (respectively, maximal accumulative) provided that it admits no proper dissipative (accumulative) extension (see, (Maksudov and Allahverdiev, 1993; Allahverdiev, 2016; Canoğlu and Allahverdiev, 2003)).

Definition 2.5.: Let V be a closed symmetric operator in a Hilbert space H with equal deficiency indices. Then, a triplet $(\mathbb{H}, \gamma_1, \gamma_2)$ is classified as a

boundary value space for V, under the condition that γ_1 and γ_2 constitute linear mappings from $D(V^*)$ into H that satisfy the following criteria:

i) For all $f, g \in D(V^*)$ the following relation holds:

$$\langle V^* f, g\rangle_H - \langle f, V^* g\rangle_H = \langle \gamma_1 f, \gamma_2 g\rangle_{\mathbb{H}} - \langle \gamma_2 f, \gamma_1 g\rangle_{\mathbb{H}};$$

ii) Given arbitrary $F_1, F_2 \in H$ there exists an element $f \in D(V^*)$ satisfying $\gamma_1 f = F_1$ and $\gamma_2 f = F_2$ (see (Gorbachuk and Gorbachuk, 1984)).

3. Lim-2 Case

The primary objective of this section is to analyze singular fourth-order dynamic operators under the framework of the Limit-2 case. Within the context of boundary value space theory, we provide a complete characterization of maximal dissipative, accretive, self-adjoint, and other admissible extensions by specifying the corresponding boundary conditions.

Suppose the symmetric operator $\Gamma_{\min}$ is characterized by deficiency indices (2,2), which corresponds to the Limit-2 case. In this situation, the boundary form satisfies $[\tau, z]_\infty = 0$ for every z (see (Naimark, 1968)). Moreover, the domain D_{min} of $\Gamma_{\min}$ is exactly the set of all vectors $\varsigma \in D_{min}$ for which the boundary conditions $\varsigma^{[0]}(k) = \varsigma^{[1]}(k) = \varsigma^{[2]}(k) = \varsigma^{[3]}(k) = 0$ are fulfilled.

We introduce the linear operators S_1 and S_2 mapping D_{max} into $\mathbb{C}^2$ by

$$S_1 f = \begin{pmatrix} -\varsigma^{[0]}(k) \\ \varsigma^{[1]}(k) \end{pmatrix},\ S_2 f = \begin{pmatrix} \varsigma^{[3]}(k) \\ \varsigma^{[2]}(k) \end{pmatrix}, \tag{3.1}$$

where the components are given in terms of the boundary values at k. We proceed by formulating and establishing several auxiliary lemmas.

Lemma 3.1.: For any $\tau, z \in D_{max}$, the following identity holds:

$$\langle \Gamma_{\max}\varsigma, z\rangle_{L^2_\Delta} - \langle \varsigma, \Gamma_{\max} z\rangle_{L^2_\Delta} = \langle S_1\varsigma, S_2 z\rangle_{\mathbb{C}^2} - \langle S_2\varsigma, S_1 z\rangle_{\mathbb{C}^2}. \tag{3.2}$$

Proof. For all $\varsigma, z \in D_{max}$ Green's identity takes the form

$$\langle \Gamma_{\max}\varsigma, z\rangle_{L^2_\Delta} - \langle \varsigma, \Gamma_{\max} z\rangle_{L^2_\Delta} = -[\varsigma, z]_k. \tag{3.3}$$

Hence, we obtain

$$\begin{aligned} \langle S_1\varsigma, S_2 z\rangle_{\mathbb{C}^2} - \langle S_2\varsigma, S_1 z\rangle_{\mathbb{C}^2} &= -\varsigma^{[0]}(k)\bar{z}^{[3]}(k) - \varsigma^{[1]}(k)\bar{z}^{[2]}(k) \\ &\quad +\varsigma^{[3]}(k)\bar{z}^{[0]}(k) + \varsigma^{[2]}(k)\bar{z}^{[1]}(k) \\ &= -[\varsigma, z]_k\ . \end{aligned}$$

By applying relation (3.3), identity (3.2) follows immediately.

Lemma 3.2.: For arbitrary complex numbers $\alpha_1, \alpha_2, \alpha_3, \alpha_4$ there exists a function $\varsigma \in D_{max}$ such that

$$\varsigma^{[0]}(k) = \alpha_1, \varsigma^{[1]}(k) = \alpha_2, \varsigma^{[2]}(k) = \alpha_3, \varsigma^{[3]}(k) = \alpha_4.$$

Proof. Let $u = \begin{pmatrix} u_1 \\ u_2 \end{pmatrix}$, and $v = \begin{pmatrix} v_1 \\ v_2 \end{pmatrix}$ be arbitrary elements of $\in \mathbb{C}^2$. Define the vector-valued function

$$\varsigma(r) = \alpha_1(r)u_1 + \alpha_2(r)v_1 + \alpha_3(r)u_2 + \alpha_4(r)v_2,$$

where $\alpha_i(r) \in L^2_\Delta[k,l) \cup (l,\infty)_{\mathbb{T}}$ $(i = 1,\ldots,4)$, and the functions α_i satisfy the boundary requirements

$$\begin{array}{llll} \alpha_1^{[0]}(k) = 1 & \alpha_1^{[1]}(k) = 0 & \alpha_1^{[2]}(k) = 0 & \alpha_1^{[3]}(k) = 0 \\ \alpha_2^{[0]}(k) = 0 & \alpha_2^{[1]}(k) = 0 & \alpha_2^{[2]}(k) = 0 & \alpha_2^{[3]}(k) = 1 \\ \alpha_3^{[0]}(k) = 0 & \alpha_3^{[1]}(k) = -1 & \alpha_3^{[2]}(k) = 0 & \alpha_3^{[3]}(k) = 0 \\ \alpha_4^{[0]}(k) = 0 & \alpha_4^{[1]}(k) = 0 & \alpha_4^{[2]}(k) = 1 & \alpha_4^{[3]}(k) = 0 \end{array}.$$

Then $\varsigma \in D_{max}$ and the boundary mappings satisfy $S_1\varsigma = u,\ S_2\varsigma = v$.

Therefore, the following statements are valid.

Theorem 3.1.: As formulated in (3.1), the triplet $\langle \mathbb{C}^2, S_1, S_2 \rangle$, constitutes a boundary value space corresponding to the operator $\Gamma_{\min}$.

Corollary 3.1.: Assume that M is a contraction acting in $\mathbb{C}^2$. Consider the operator obtained by restricting $\Gamma_{\min}$ to the class of functions $\varsigma \in D_{max}$ for which either

$$(M - I)S_1\varsigma + i(M + I)S_2\varsigma = 0 \tag{3.4}$$

or

$$(M - I)S_1\varsigma - i(M + I)S_2\varsigma = 0 \tag{3.5}$$

holds. Enforcing these criteria results, respectively, in the maximal dissipative extension and the maximal accretive extension of the operator $\Gamma_{\min}$. On the other hand, any maximal dissipative (respectively, maximal accretive) extension of $\Gamma_{\min}$ can be realized as the restriction of $\Gamma_{\max}$ to the collection of functions $\varsigma \in D_{max}$ that satisfy condition (3.4) (respectively, (3.5)), and this extension uniquely specifies the contraction M. Moreover, when M is an isometry, conditions (3.4)–(3.5) characterize the maximal symmetric extensions of $\Gamma_{\min}$ in $L^2_\Delta[k,l) \cup (l,\infty)_{\mathbb{T}}$. If, in addition, M is a unitary operator, then these criteria determine the self-adjoint extensions.

In this context, we consider the following boundary conditions

$$\varsigma^{[3]}(k) - h_1\varsigma^{[0]}(k) = 0,$$
$$\varsigma^{[1]}(k) - h_2\varsigma^{[2]}(k) = 0,$$

for $\mathrm{Im}h_1 \geq 0$ or $h_1 = \infty$ and $\mathrm{Im}h_2 \geq 0$ or $h_2 = \infty$, the above separated boundary conditions generate maximal dissipative extensions of $\Gamma_{\min}$; if $\mathrm{Im}h_1 = 0$ or $\mathrm{Im}h_2 = 0$, (or $h_1, h_2 = \infty$), they yield self-adjoint extensions.

4. Lim-4 Case

The aim of this part of the study is to analyze singular fourth-order dynamic operators within the framework of the Limit-4 case. Through the formulation of proper boundary conditions, a comprehensive classification of their maximal dissipative, maximal accretive, self-adjoint, and further allowable extensions is presented.

Suppose that the operator $\Gamma_{\min}$ is characterized by deficiency indices (4,4). Consequently, the functions τ_i lie in the domain D_{max} and satisfy $\tau_i \in L^2_\Delta[k,l) \cup (l,\infty)_{\mathbb{T}}$ for every $i \in \{12,3,4\}$.

Theorem 4.1.: Definition domain D_{min} associated with the operator $\Gamma_{\min}$ comprises exactly those functions $\varsigma \in D_{max}$ for which the following requirements are fulfilled:

$$\begin{gathered}\varsigma^{[0]}(\mathrm{k}) = \varsigma^{[1]}(\mathrm{k}) = \varsigma^{[2]}(\mathrm{k}) = \varsigma^{[3]}(\mathrm{k}) = 0, \\ [\varsigma,\tau_1]_\infty = [\varsigma,\tau_2]_\infty = [\varsigma,\tau_3]_\infty = [\varsigma,\tau_4]_\infty = 0\end{gathered} \tag{4.1}$$

Proof. The required conclusion follows directly from relations ([23]) and ([p]).

Define the linear operator Ω_1 and Ω_2 from D_{max} into $\mathbb{C}^4$ by

$$\Omega_1\varsigma = \begin{pmatrix} -\varsigma^{[0]}(k) \\ -\varsigma^{[1]}(k) \\ [\varsigma,\tau_2]_\infty \\ [\varsigma,\tau_1]_\infty \end{pmatrix}, \Omega_2\tau = \begin{pmatrix} \varsigma^{[3]}(k) \\ \varsigma^{[2]}(k) \\ [\varsigma,\tau_4]_\infty \\ [\varsigma,\tau_3]_\infty \end{pmatrix}. \tag{4.2}$$

Afterward, the following are obtained.

Theorem 4.2.: For the operator $\Gamma_{\min}$, we establish that the triple $\langle \mathbb{C}^4, \Omega_1, \Omega_2 \rangle$ given in (4.2) constitutes a boundary value space.

Proof. Given any $\varsigma, z \in D_{max}$, it follows that

$$\begin{aligned}\langle\Omega_1\varsigma,\Omega_2 z\rangle-(\langle\Omega_2\varsigma,\Omega_1 z\rangle &= -\varsigma^{[0]}(k)\bar{z}^{[3]}(k)-\varsigma^{[1]}(k)\bar{z}^{[2]}(k)\\ &\quad+[\varsigma,\tau_2]_\infty[z,\tau_4]_\infty+[\varsigma,\tau_1]_\infty[z,\tau_3]_\infty\\ &\quad+\varsigma^{[3]}(k)\bar{z}^{[0]}(k)+\varsigma^{[2]}(k)\bar{z}^{[1]}(k)\\ &\quad-[\varsigma,\tau_4]_\infty[z,\tau_2]_\infty-[\varsigma,\tau_3]_\infty[z,\tau_1]_\infty\\ &= -\varsigma^{[0]}(k)\bar{z}^{[3]}(k)-\varsigma^{[1]}(k)\bar{z}^{[2]}(k)\\ &\quad+\varsigma^{[3]}(k)\bar{z}^{[0]}(k)+\varsigma^{[2]}(k)\bar{z}^{[1]}(k)\\ &\quad+[\varsigma,\tau_4]_\infty[\tau_2,z]_\infty-[\varsigma,\tau_2]_\infty[\tau_4,z]_\infty\\ &\quad+[\varsigma,\tau_3]_\infty[\tau_1,z]_\infty-[\tau_1,\varsigma]_\infty[z,\tau_3]_\infty.\end{aligned}$$

By the Plücker identity (2.4), we obtain

$$\langle\Omega_1\varsigma,\Omega_2 z\rangle-(\langle\Omega_2\varsigma,\Omega_1 z\rangle=[\varsigma,z]_\infty-[\varsigma,z]_k.$$

Using Green's formula (2.3), we obtain

$$\langle\Omega_1\varsigma,\Omega_2 z\rangle-(\langle\Omega_2\varsigma,\Omega_1 z\rangle=\langle\Gamma_{\max}\varsigma,z\rangle_{L^2_\Delta}-\langle\varsigma,\Gamma_{\max}z\rangle_{L^2_\Delta},$$

which shows that the first requirement in the definition of a boundary value space is satisfied.

The verification of the second condition is provided by the lemma stated below.

Lemma 4.1.: For any complex numbers $\alpha_0,\alpha_1,\alpha_2,\alpha_3,\beta_0,\beta_1,\beta_2$,and β_3 there is a function $\varsigma\in D_{max}$ satisfying

$$\begin{aligned}\varsigma^{[0]}(k) &= \alpha_0,\ \varsigma^{[1]}(k)=\alpha_1,\ \varsigma^{[2]}(k)=\alpha_2,\ \varsigma^{[3]}(k)=\alpha_3\\ [\varsigma,\tau_1]_\infty &= \beta_0,\ [\varsigma,\tau_2]_\infty=\beta_1,\ [\varsigma,\tau_3]_\infty=\beta_2,\ [\varsigma,\tau_4]_\infty=\beta_3\ .\end{aligned}$$

Proof. Let f be any function belonging to $L^2_\Delta[k,l)\cup(l,\infty)_{\mathbb{T}}$ such that

$$\begin{aligned}\langle f,\tau_1\rangle_{L^2_\Delta}&=\beta_0+\alpha_3,\langle f,\tau_2\rangle_{L^2_\Delta}=\beta_1-\alpha_1\\ \langle f,\tau_3\rangle_{L^2_\Delta}&=\beta_2-\alpha_0,\langle f,\tau_4\rangle_{L^2_\Delta}=\beta_3+\alpha_2.\end{aligned}\tag{4.3}$$

Such a function f exists, and it can be chosen as a linear combination of τ_1,τ_2,τ_3 and τ_4. In fact, let

$$f=c_1\tau_1+c_2\tau_2+c_3\tau_3+c_4\tau_4.$$

Then the relations in (4.3) form a linear system for the coefficients c_1,c_2,c_3,c_4. The determinant of this system coincides with the Gram determinant associated with linearly independent functions $\tau_1,\tau_2,\tau_3\ \tau_4$, and hence it is nonzero.

Denote by $\varsigma(r)$ a function satisfying the equation $\Upsilon(\varsigma) = f$ which fulfills the initial conditions

$$\varsigma^{[0]}(k) = \alpha_0,\ \varsigma^{[1]}(k) = \alpha_1,\ \varsigma^{[2]}(k) = \alpha_2,\ \varsigma^{[3]}(k) = \alpha_3.$$

Suppose that $\varsigma(r)$ represents the required element. Applying Green's formula (2.3) to the pair $\varsigma(r)$ and τ_j, we obtain

$$\langle f, \tau_j\rangle_{L^2_\triangle} = \langle \Upsilon(\varsigma), \tau_j\rangle_{L^2_\triangle} = [\varsigma, \tau_j]_\infty - [\varsigma, \tau_j]_0,\ j = 1,\ldots,4.$$

Since $\Upsilon(\tau_j) = 0$ for $(j = 1,2,3,4)$ and the initial data $\varsigma^{[0]}(k) = \alpha_0,\ \varsigma^{[1]}(k) = \alpha_1,\ \varsigma^{[2]}(k) = \alpha_2,\ \varsigma^{[3]}(k) = \alpha_3$, hold, it follows that

$$[\varsigma, \tau_j]_k = \begin{cases} -\alpha_3, & \text{when } j = 1 \\ \alpha_1, & \text{when } j = 2 \\ \alpha_0, & \text{when } j = 3 \\ -\alpha_2, & \text{when } j = 4 \end{cases}.$$

Thus we get

$$\begin{aligned} \langle f, \tau_1\rangle_{L^2_\triangle} &= [\varsigma, \tau_1]_\infty - [\varsigma, \tau_1]_k \\ &= [\varsigma, \tau_1]_\infty + \alpha_3, \\ \langle f, \tau_2\rangle_{L^2_\triangle} &= [\varsigma, \tau_2]_\infty - [\varsigma, \tau_2]_k \\ &= [\varsigma, \tau_2]_\infty - \alpha_1, \\ \langle f, \tau_3\rangle_{L^2_\triangle} &= [\varsigma, \tau_3]_\infty - [\varsigma, \tau_3]_k \\ &= [\varsigma, \tau_3]_\infty - \alpha_0, \\ \langle f, \tau_4\rangle_{L^2_\triangle} &= [\varsigma, \tau_4]_\infty - [\varsigma, \tau_4]_k \\ &= [\varsigma, \tau_4]_\infty + \alpha_2. \end{aligned}$$

According to (4.3), we have

$$[\varsigma, \tau_1]_\infty = \beta_0,\ [\varsigma, \tau_2]_\infty = \beta_1,\ [\varsigma, \tau_3]_\infty = \beta_2,\ [\varsigma, \tau_4]_\infty = \beta_3.$$

Corollary 4.1.: Let M be a contraction operator on $\mathbb{C}^4$. We consider the operator defined by restricting $\Gamma_{\min}$ to the class of functions $\varsigma \in D_{max}$ that satisfy either the boundary condition

$$(M - I)\Omega_1\varsigma + i(M + I)\Omega_2\varsigma = 0 \tag{4.4}$$

or

$$(M - I)\Omega_1\varsigma - i(M + I)\Omega_2\varsigma = 0. \tag{4.5}$$

Accordingly, these operators represent the maximal dissipative and maximal accretive extensions of $\Gamma_{\min}$, respectively. Conversely, any maximal dissipative (respectively, accretive) expansion of $\Gamma_{\min}$ is achievable through the restriction

of $\Gamma_{\max}$ to those functions $\varsigma \in D_{max}$ satisfying condition (4.4) (respectively, (4.5)), with this expansion uniquely fixing the contraction M.

Moreover, when M is an isometric operator, conditions (4.4) and (4.5) characterize the maximal symmetric extensions of $\Gamma_{\min}$ in $L^2_{\Delta}[k,l) \cup (l,\infty)_{\mathbb{T}}$. In the case where M is unitary property , these boundary conditions correspond to self-adjoint extensions.

In this connection, we take into account the following boundary conditions:

$$\varsigma^{[3]}(k) - h_1\varsigma^{[0]}(k) = 0$$

$$\varsigma^{[2]}(k) - h_2\,\varsigma^{[1]}(k) = 0,$$

$$[\varsigma,\tau_4]_{\infty} - h_3[\varsigma,\tau_2]_{\infty} = 0,$$

$$[\varsigma,\tau_3]_{\infty} - h_4[\varsigma,\tau_1]_{\infty} = 0,$$

under separated boundary conditions, the maximal dissipative (self-adjoint) extensions of the operator $\Gamma_{\min}$are uniquely determined by the constraints $\mathrm{Im}h_i \geq 0$ or $h_i = \infty$ (specifically $\mathrm{Im}h_i = 0$ or $h_i = \infty$) for each index $i \in \{1,2,3,4\}$. These parameters define the precise domain boundaries required for the validity of such extensions.

References

Allahverdiev, B. P. (1995). Extensions of symmetric Schrodinger operators with matrix potentials. *Izvestiya Rossiiskoi Akademii Nauk. Seriya Matematicheskaya*, *59*(1), 49-64.

Allahverdiev, B. P. (2013). Extensions of symmetric second-order difference operators with matrix coefficients. *Journal of Difference Equations and Applications*, 19(5), 839–849.

Allahverdiev, B. P. (2016). Extensions of symmetric singular second-order dynamic operators on time scales. *Filomat*, 30(6), 1475–1484.

Allahverdiev, B. P., & Tuna, H. (2019). Nonlinear singular Sturm–Liouville problems with impulsive conditions. *Facta Universitatis*, 34(3), 439–457.

Allahverdiev, B. P., Tuna, H., & Isayev, H. A. (2023). Existence results for impulsive dynamic singular nonlinear Sturm–Liouville equations on infinite intervals. *Turkish Journal of Mathematics*, 47, 176–1777.

Amirov, R. K., Ergun, A., & Durak, S. (2021). Half-inverse problems for the quadratic pencil of the Sturm–Liouville equations with impulse. *Numerical Methods for Partial Differential Equations*, 37(1), 915–924.

Anderson, D. R., Guseinov, G. Sh., & Hoffacker, J. (2006). Higher-order self-adjoint boundary-value problems on time scales. *Journal of Computational and Applied Mathematics*, 194(2), 309–342.

Atici, F. M., & Guseinov, G. Sh. (2002). On Green's functions and positive solutions for boundary value problems on time scales. *Journal of Computational and Applied Mathematics*, 141(1–2), 75–99.

Aydemir, K., Olğar, H., & Mukhtarov, O. Sh. (2019). The principal eigenvalue and the principal eigenfunction of a boundary-value transmission problem. *Turkish Journal of Mathematics and Computer Science*, 11(2), 97–100.

Aydemir, K., Olgar, H., Mukhtarov, O. Sh., & Muhtarov, F. (2018). Differential operator equations with interface conditions in modified direct sum spaces. *Filomat*, 32(3), 921–931.

Bohner, M., & Peterson, A. (2001). Dynamic equations on time scales. Birkhäuser.

Bohner, M., & Peterson, A. (Eds.). (2003). Advances in dynamic equations on time scales. Birkhäuser.

Bruk, V. M. (1976). On a class of boundary value problems with spectral parameter in the boundary condition. *Mathematics of the USSR-Sbornik*, *29*(2), 186-192.

Calkin, J. W. (1939). Abstract symmetric boundary conditions. *Transactions of the American Mathematical Society*, *45*(3), 369-442.

Canoğlu, A., & Allahverdiev, B. P. (2003). Selfadjoint and dissipative extensions of a symmetric Schrödinger operator. *Mathematica Balkanica*, 17(1–2), 113–120.

Fulton, C. T. (1989). The Bessel-squared equation in the lim-2, lim-3, lim,4 cases. *The Quarterly Journal of Mathematics*, *40*(4), 423-456.

Guseinov, G. Sh. (2005). Self-adjoint boundary value problems on time scales and symmetric Green's functions. *Turkish Journal of Mathematics*, 29(4), 365–380.

.Gorbachuk, M. L., & Gorbachuk, V. I. (1984). Boundary Value Problems for Operator Differential Equations. Naukova Dumka. (English translation, 1991, Birkhäuser Verlag).

Gorbachuk, V. I., Gorbachuk, M. L., & Kochubei, A. N. (1989). Extension theory for symmetric operators and boundary value problems for differential equations. *Ukrainian Mathematical Journal*, *41*(10), 1117-1129.

Güldü, Y. (2013). Half-inverse problem for impulsive Dirac operator with discontinuous coefficient. *Abstract and Applied Analysis*, 2013, 181809.

Hilger, S. (1990). Analysis on measure chains—a unified approach to continuous and discrete calculus. *Results in mathematics*, *18*(1), 18-56.

Huseynov, A. (2012). Weyl's limit point and limit circle for a dynamic system. *In Dynamical systems and methods* (pp. 215–225). Springer.

Kochubei, A. N. (1975). Extensions of symmetric operators and symmetric binary relations. *Mathematical notes of the Academy of Sciences of the USSR*, *17*(1), 25-28.

Lakshmikantham, V., Sivasundaram, S., & Kaymakçalan, B. (2013). *Dynamic systems on measure chains* (Vol. 370). Springer Science & Business Media.

Lapwood, E. R., & Usami, T. (1981). *Free oscillations of the Earth*. Cambridge, UK: Cambridge University Press.

Lykov, A. V., & Mikhailov, Y. A. (1965). *The theory of heat and mass transfer*. Jerusalem, Israel: Israel Program for Scientific Translations.

Litvinenko, O. N., & Soshnikov, V. I. (1964). The theory of heterogeneous lines and their applications in radio engineering. *Radio, Moscow*.

Maksudov, F. G. O., & Allahverdiev, B. P. (1993). On extensions of symmetric Schrödinger operators with matrix potentials. In *Doklady Akademii Nauk* (Vol. 332, No. 1, pp. 18-20). Russian Academy of Sciences.

Naĭmark, M. A. (1969). Linear differential operators 2nd ed.(" Nauka", Moscow) Google Scholar MA Naĭmark 1967, 1968. *Linear differential operators I & II*.

von Neumann, J. (1929). Mathematische Begründung der Quantenmechanik. Göttinger Nachrichten 1927, 1-57. Wahrscheinlichkeitstheoretischer Aufbau der Quantenmechanik. Göttinger Nachrichten 1927, 245-272. Allgemeine Eigenwerttheorie Hermitescher Funktionaloperatoren. *Mathematische Annalen*, *102*, 49-131.

Rofe-Beketov, F. S. (1969). Selfadjoint extensions of differential operators in a space of vector-valued functions. In *Doklady Akademii Nauk* (Vol. 184, No. 5, pp. 1034-1037). Russian Academy of Sciences.

Rynne, B. P. (2007). L2 spaces and boundary value problems on time scales. *Journal of Mathematical Analysis and Applications*, 328, 1217–1236.

Spedding, V. (2003). Taming nature's numbers. *New Scientist*, 179, 28–31.

Thomas, D. M., Vandemuelebroeke, L., & Yamaguchi, K. (2005). A mathematical evolution model for phytoremediation. *Discrete and Continuous Dynamical Systems B*, 5(2), 411–422.

Tuna, H., & Allahverdiev, B. P. (2018). Dissipative extensions of fourth-order differential operators. *Thai Journal of Mathematics* , 16(1), 275–285.

Tuna, H., & Bayrak, S. (2018). On extensions of singular fourth-order dynamic operators on time scales. *Filomat*, 32(11), 3843–3851.

Tuna, H., & Bulut, H. (2018). Transverse vibration of non uniform Euler–Bernoulli beams on bounded time scales. *Fundamental Journal of Mathematics and Applications*, 1(1), 77–81.

Chapter 5

Embeddability Degree of Finite Groups and Approximate Embeddings

Mehmet Uc[1]

Abstract

This study introduces the *embeddability degree*, a new probabilistic invariant for finite groups motivated by the idea of measuring how closely one group can be embedded into another when an exact embedding does not exist. This proposed invariant provides a quantitative way to evaluate injective maps according to how frequently they preserve the group operation. We establish several fundamental properties of this notion, including a characterization of the case where the embeddability degree is equal to one, a criterion for its vanishing, a symmetry result for groups of equal order, and a composition-type inequality involving three finite groups. We also compute the invariant explicitly for several small cyclic groups, showing that even in elementary cases it reflects meaningful arithmetic and structural features. These initial results suggest that the embeddability degree offers a natural quantitative perspective on classical embedding problems in finite group theory.

1. Introduction

In finite group theory, structural questions have traditionally been studied in an exact algebraic framework. A group is either abelian or nonabelian, a map either preserves the group operation, or it does not, and one group either embeds into another or fails to do so. This classical viewpoint remains central to algebra. However, over the past several decades, probabilistic and quantitative perspectives have introduced a complementary methodology for studying algebraic structures. Rather than treating structural properties as purely binary phenomena, one may ask how frequently a given property occurs or to what extent a function approximates a prescribed algebraic behavior. This perspective has generated a rich body of numerical invariants that provide meaningful structural information about finite groups.

1 Asst. Prof. Dr., Department of Mathematics, Burdur Mehmet Akif Ersoy University, mehmetuc@mehmetakif.edu.tr, ORCID ID: 0000-0003-3680-9103

https://doi.org/10.58830/ozgur.pub1361.c5495

One of the earliest and most influential examples of this philosophy is the commutativity degree of a finite group, which measures the probability that two randomly selected elements commute. Foundational contributions by Gallagher (1970), Gustafson (1973), and Rusin (1979) demonstrated that probabilistic quantities can encode significant algebraic information regarding finite groups. Later developments by Lescot (1995, 2001) deepened this theory by connecting commutativity probabilities with structural classifications and central extensions. These studies established that probabilistic invariants are not merely numerical curiosities, but rather effective tools for detecting structural properties.

The concept was subsequently generalized in several directions. The relative commutativity degree, introduced and studied in detail by Erfanian et al. (2007) and further examined by Rezaei and Erfanian (2014), provides a refined measure of commutative behavior between a subgroup and the ambient group. Additional extensions include subgroup commutativity measures (Tarnauceanu, 2009), generalized commutativity degrees (Nath & Das, 2011), lower bound analyses (Nath & Das, 2010), and structural classifications involving prescribed commutativity values (Barzegar et al., 2013). More recently, probabilistic commutativity concepts have been extended beyond classical groups. For example, analogous invariants have been studied for semigroups (Ghaneei & Azadi, 2021), higher-order commutativity settings (Hashemi & Pirzadeh, 2022), while crossed module actions (Cetin \& Gurdal, 2024) provide a natural setting for similar quantitative extensions. These developments illustrate the remarkable flexibility of probabilistic algebraic methods.

A related direction concerns algebraic structures arising from operator theory and associated algebraic systems. Although seemingly distinct from finite group theory, quantitative algebraic viewpoints have also appeared in operator-theoretic contexts. For example, Gurdal (2009a, 2009b) investigated structural properties of extended eigenvalues and eigenvectors for classical operators on Wiener-type algebras. Likewise, Chashiani and Rezaei (2021) studied commutativity degree in the setting of group algebras, thereby explicitly linking probabilistic group-theoretic invariants with algebraic operator frameworks. Such interactions suggest that quantitative algebraic concepts often transcend their original settings and admit broader mathematical interpretations.

Motivated by this growing probabilistic perspective, one may naturally shift attention from algebraic properties of groups themselves to the behavior of functions between groups. Classical group theory primarily emphasizes homomorphisms, since these preserve multiplication exactly. Nevertheless, from a quantitative viewpoint, exact preservation may be unnecessarily restrictive. A function may fail to be a homomorphism globally while still behaving homomorphically on a substantial proportion of ordered pairs. This idea motivates the notion of homomorphism degree, which measures the proportion of pairs satisfying the homomorphic identity. Such a concept provides a quantitative measure of approximate algebraic compatibility.

Similarly, surjectivity can also be quantified. Rather than asking whether a homomorphism is surjective in strict sense, one may measure the relative size of its image within the codomain. This leads naturally to a surjectivity degree, offering another numerical invariant describing structural efficiency. Recent work by Uc (2025) investigated quantitative relationships between commutativity, homomorphic behavior, and surjectivity in finite groups, demonstrating that these probabilistic invariants are not isolated notions but rather parts of a coherent quantitative framework.

These observations suggest a broader guiding principle: classical structural properties may often admit meaningful quantitative analogues. The present chapter develops this philosophy in the context of group embeddings.

Recall that a finite group G embeds into a finite group H if there exists an injective group homomorphism $\varphi: G \to H$. From the classical viewpoint, embeddability is a purely binary notion: either such a map exists or it does not. However, this strict dichotomy conceals potentially informative intermediate behavior. Even when no genuine embedding exists, there may still be injective functions from G into H that preserve multiplication on a substantial subset of ordered pairs. Such maps are not homomorphisms in the classical sense, yet they may exhibit significant algebraic compatibility.

This observation motivates the introduction of a new probabilistic invariant, called the *embeddability degree*. Informally, these invariant measures the maximal homomorphic behavior achievable among injective maps between two finite groups. Thus, it combines two distinct structural requirements: injectivity, reflecting the classical embedding condition, and approximate homomorphic preservation, reflecting the probabilistic philosophy of modern quantitative group theory.

The embeddability degree naturally interpolates between exact and approximate structural compatibility. If its value is equal to one, then an actual embedding exists and the classical notion is recovered. At the opposite extreme, if the source group has strictly larger order than the target group, injective maps cannot exist at all, forcing the invariant to vanish. Intermediate values quantify varying levels of approximate compatibility. Consequently, the invariant does not merely indicate whether an embedding exists, but also measures how closely such an embedding can be approximated when exact realization is impossible.

This perspective is conceptually consistent with the broader development of probabilistic methods in algebra, where exact structural properties are complemented by quantitative measurements reflecting partial or approximate behavior. In the setting of finite groups, such approaches have proved particularly fruitful in the study of commutativity-related invariants and their generalizations. In this sense, the embeddability degree may be viewed as a natural continuation of this quantitative line of investigation.

Another appealing aspect of the embeddability degree is its connection with classical structural invariants. Since its definition is built upon approximate

homomorphic behavior, it is closely related to homomorphism-based probabilistic measures. At the same time, because injectivity is imposed as an essential condition, the invariant remains fundamentally tied to subgroup structure, group order, and classical embedding constraints. In this sense, it occupies an intermediate position between probabilistic group theory and classical structural algebra.

Even elementary examples suggest that the invariant captures genuinely nontrivial information. For cyclic groups, the interaction between arithmetic divisibility, injectivity constraints, and approximate homomorphic preservation leads to subtle behavior. This indicates that the invariant is sensitive not only to cardinality considerations but also to deeper algebraic structure.

Although the present work focuses primarily on foundational theory, the notion appears sufficiently flexible to admit broader generalizations. One might envision analogous invariants for algebraic systems beyond groups, including semigroup actions, module-theoretic structures, or operator-induced algebraic frameworks. The flexibility of probabilistic and quantitative viewpoints suggests that similar methodological ideas may find applications in broader algebraic settings beyond the finite groups considered here. Therefore, the applicability of quantitative perspectives across diverse mathematical settings, from probabilistic group theory to algebraic operator systems and even fractal-inspired frameworks (Gurdal et al., 2025; Allahverdiev et al., 2026), suggests that the underlying methodology may have substantial conceptual reach.

The main purpose of this chapter is to establish the initial theory of the embeddability degree for finite groups. After recalling the necessary preliminaries, we formally introduce the invariant and investigate its first fundamental properties. In particular, we characterize the extremal case in which the invariant attains the value one, establish vanishing criteria, derive structural symmetry results under equal-order assumptions, and prove composition-type inequalities governing interactions among multiple finite groups. Several explicit computations are also presented for finite cyclic groups in order to illustrate the behavior of the invariant concretely.

We hope that this quantitative viewpoint enriches the classical theory of embeddings by introducing a flexible framework capable of measuring approximate structural compatibility between finite groups.

2. Preliminaries

Throughout this chapter, all groups are assumed to be finite unless otherwise stated. In this section, we recall the basic notions and probabilistic invariants that will be used in the subsequent development.

Let G be a finite group. The identity element of G will be denoted by e_G, or simply by e whenever no ambiguity arises. The center of G is defined by

$$Z(G) := \{x \in G : xg = gx \text{ for all } g \in G\},$$

and for any element $x \in G$, its centralizer is given by

$$C_G(x) := \{g \in G : gx = xg\}.$$

For finite groups G and H, an embedding of G into H means an injective group homomorphism $\varphi: G \to H$.

One of the most classical probabilistic invariants in finite group theory is the commutativity degree, which measures the likelihood that two randomly selected group elements commute.

Definition 2.1.: Let G be a finite group. The *commutativity degree* of G is defined by

$$d(G) := \frac{|\{(x,y) \in G \times G : xy = yx\}|}{|G|^2}. \tag{2.1}$$

This invariant admits an equivalent and often useful formulation in terms of centralizers. Indeed, for each fixed element $x \in G$, the number of elements commuting with x is exactly $|C_G(x)|$. Hence,

$$d(G) = \frac{1}{|G|^2} \sum_{x \in G} |C_G(x)|. \tag{2.2}$$

The commutativity degree satisfies $0 < d(G) \leq 1$; and $d(G) = 1$ if and only if G is abelian.

A natural extension of this notion is the relative commutativity degree, which measures the interaction between a subgroup and the ambient group.

Definition 2.2.: Let G be a finite group and let $H \leq G$. The *relative commutativity degree* of H in G is defined by

$$d(H,G) := \frac{|\{(h,g) \in H \times G : hg = gh\}|}{|H| \cdot |G|}. \tag{2.3}$$

Equivalently, by counting commuting partners via centralizers, we obtain

$$d(H,G) = \frac{1}{|H||G|} \sum_{h \in H} |C_G(h)|. \tag{2.4}$$

These invariant measures the probability that a randomly chosen element of H commutes with a randomly chosen element of G. In particular, $d(G,G) = d(G)$.

To quantify how closely an arbitrary function behaves like a group homomorphism, the homomorphism degree was introduced.

Definition 2.3.: Let G and H be finite groups, and let $f: G \to H$ be an arbitrary function. The *homomorphism degree* of f is defined by

$$\chi(f) := \frac{|\{(a,b) \in G \times G : f(ab) = f(a)f(b)\}|}{|G|^2}. \tag{2.5}$$

Thus, $\chi(f)$ measures the proportion of ordered pairs for which the homomorphism identity holds. Clearly, $0 \leq \chi(f) \leq 1$. Moreover, $\chi(f) = 1$ if and only if f is a group homomorphism.

Another probabilistic invariant relevant to mappings between finite groups is the surjectivity degree.

Definition 2.4.: Let $\varphi: G \to H$ be a group homomorphism between finite groups. The *surjectivity degree* of φ is defined by $\sigma(\varphi) := \frac{|\mathrm{Im}\varphi|}{|H|}$.

This invariant quantifies how much of the codomain is covered by the homomorphism. It satisfies $0 < \sigma(\varphi) \leq 1$, and $\sigma(\varphi) = 1$ if and only if φ is surjective.

These probabilistic invariants capture different structural aspects of finite groups and mappings between them. The commutativity degree reflects internal commutative behavior, the relative commutativity degree measures subgroup-group interaction, the homomorphism degree quantifies approximate multiplicativity of arbitrary maps, and the surjectivity degree measures the extent to which a homomorphism covers its codomain.

Motivated by these quantitative perspectives, especially the homomorphism degree, it is natural to ask how effectively one finite group can be embedded into another by injective maps that preserve the group operation on as many ordered pairs as possible. This leads to the notion of the embeddability degree, which will be introduced and studied in the next section.

3. The Embeddability Degree

This section introduces our new probabilistic invariant for finite groups, called the embeddability degree, and investigates some of its basic properties. Throughout this section, all groups are assumed to be finite. We first recall the homomorphism degree of an arbitrary function between finite groups.

Definition 3.1.: Let G and H be finite groups. The *embeddability degree* of G into H is defined by

$$\eta(G, H) := \max\{\chi(f): f: G \to H \text{ is injective}\}. \tag{3.1}$$

provided that at least one injective function from G to H exists. If no such injective function exists, we define $\eta(G, H) := 0$. Since G and H are finite groups, the set of injective functions $f: G \to H$ is finite. Hence, the supremum is actually attained, and we may use maximum instead of supremum.

The invariant $\eta(G, H)$ measures how closely G can be embedded into H by an injective function which behaves like a homomorphism on as many ordered pairs as possible.

Although the following two propositions are straightforward, we include their proof since they illustrate the method of computing the embeddability degree and clarify the role of the defining condition in a simple but fundamental case.

Proposition 3.2. Let G and H be finite groups. Then, $\eta(G,H)=1$ if and only if G embeds into H, that is, if and only if there exists an injective group homomorphism from G to H.

Proof. Suppose first that G embeds into H. Then, there exists an injective group homomorphism $f: G \to H$. Since f is a homomorphism, we have $f(ab)=f(a)f(b)$ for all $a,b \in G$. Therefore, every ordered pair $(a,b) \in G^2$ satisfies the homomorphism identity. Hence, $\chi(f)=\frac{|G|^2}{|G|^2}=1$. Thus, $\eta(G,H)=1$.

Conversely, suppose that $\eta(G,H)=1$. Then, there exists an injective function $f: G \to H$ such that $\chi(f)=1$. This means that

$$|\{(a,b) \in G^2 : f(ab)=f(a)f(b)\}| = |G|^2.$$

Hence every pair $(a,b) \in G^2$ satisfies $f(ab)=f(a)f(b)$. Therefore, f is a group homomorphism. Since f is injective by definition of $\eta(G,H)$, f is an embedding of G into H. □

Proposition 3.3.: Let G and H be finite groups. Then, $\eta(G,H)=0$ if and only if $|G|>|H|$.

Proof. If $|G|>|H|$, then there is no injective function from G to H. Therefore, by definition, $\eta(G,H)=0$.

Conversely, suppose that $|G| \le |H|$. Then, there exists at least one injective function $f: G \to H$. Choose such a function with $f(e_G)=e_H$. Then, for the pair (e_G,e_G), we have

$$f(e_G e_G)=f(e_G)=e_H$$

and

$$f(e_G)f(e_G)=e_H e_H=e_H.$$

Thus, the pair (e_G,e_G) satisfies the homomorphism identity. Hence, $\chi(f) \ge \frac{1}{|G|^2}$. Therefore, $\eta(G,H) \ge \frac{1}{|G|^2} > 0$. So, $\eta(G,H)=0$ cannot occur when $|G| \le |H|$. This proves the equivalence. □

Corollary 3.4.: If $|G| \le |H|$, then $\eta(G,H) \ge \frac{1}{|G|^2}$.

The following proposition shows that when the two groups have the same cardinality, the embeddability degree becomes symmetric, reflecting a natural reciprocity between the two groups.

Proposition 3.5.: Let G and H be finite groups such that $|G|=|H|$. Then, $\eta(G,H)=\eta(H,G)$.

Proof. Since $|G|=|H|$, every injective function $f: G \to H$ is bijective. Let $f: G \to H$ be a bijection. We show that $\chi(f)=\chi(f^{-1})$. Let $(a,b) \in G^2$, and set $x=f(a)$, $y=f(b)$. Then, $(x,y) \in H^2$. Now $f(ab)=f(a)f(b)$ if and only if $f(ab)=xy$.

Applying f^{-1} to both sides gives $ab = f^{-1}(xy)$. Since $a = f^{-1}(x)$ and $b = f^{-1}(y)$, this is equivalent to

$$f^{-1}(xy) = f^{-1}(x)f^{-1}(y).$$

Thus, the pair (a, b) is a homomorphic pair for f if and only if the pair $(x, y) = (f(a), f(b))$ is a homomorphic pair for f^{-1}.

Since the map

$$G^2 \to H^2, \qquad (a, b) \mapsto (f(a), f(b))$$

is a bijection, the number of successful pairs for f equals the number of successful pairs for f^{-1}. Therefore, $\chi(f) = \chi(f^{-1})$. Taking the maximum over all bijections $f: G \to H$, we obtain

$\eta(G, H) = \eta(H, G)$. □

The following theorem establishes a fundamental composition inequality for the embeddability degree, relating the embeddability behavior across three finite groups through the interaction of optimal injective maps.

Theorem 3.6.: Let G, H, K be finite groups. Then,

$$\eta(G, K) \geq \max\left\{0, \eta(G, H) + (\eta(H, K) - 1)\frac{|H|^2}{|G|^2}\right\}. \tag{3.2}$$

Proof. If either $\eta(G, H) = 0$ or $\eta(H, K) = 0$, then the asserted inequality is trivial whenever the right-hand side is non-positive. Hence, we may assume that

$$\eta(G, H) > 0 \qquad \text{and} \qquad \eta(H, K) > 0.$$

Then, there exist injective functions $f: G \to H$, $g: H \to K$ such that

$$\chi(f) = \eta(G, H) \qquad \text{and} \qquad \chi(g) = \eta(H, K).$$

Since f and g are injective, the composition $g \circ f: G \to K$ is also injective.

Define $S_f := \{(a, b) \in G^2 : f(ab) = f(a)f(b)\}$. Then, $|S_f| = \chi(f)|G|^2$. Consider the map

$$G^2 \to H^2, \qquad (a, b) \mapsto (f(a), f(b)).$$

Since f is injective, this map is also injective. Therefore, the set

$$T_f := \{(f(a), f(b)) : (a, b) \in S_f\} \subseteq H^2$$

has cardinality $|T_f| = |S_f| = \chi(f)|G|^2$. Now define

$$S_g := \{(x, y) \in H^2 : g(xy) = g(x)g(y)\}.$$

Then, $|S_g| = \chi(g)|H|^2$. Both T_f and S_g are subsets of H^2. Hence, $|T_f \cap S_g| \geq |T_f| + |S_g| - |H|^2$. Therefore, $|T_f \cap S_g| \geq \chi(f)|G|^2 + \chi(g)|H|^2 - |H|^2$.

Now take $(a,b) \in G^2$ such that $(f(a),f(b)) \in T_f \cap S_g$. Since $(f(a),f(b)) \in T_f$, we have $f(ab) = f(a)f(b)$. Since $(f(a),f(b)) \in S_g$, we have $g(f(a)f(b)) = g(f(a))g(f(b))$.

Combining these two equalities gives

$$(g \circ f)(ab) = g(f(ab)) = g(f(a)f(b)) = g(f(a))g(f(b)) = (g \circ f)(a)(g \circ f)(b).$$

Thus, every element of $T_f \cap S_g$ gives a successful homomorphic pair for $g \circ f$.

Consequently,

$$\chi(g \circ f) \geq \frac{\chi(f)|G|^2 + \chi(g)|H|^2 - |H|^2}{|G|^2}.$$

Hence,

$$\chi(g \circ f) \geq \chi(f) + (\chi(g) - 1)\frac{|H|^2}{|G|^2}.$$

Substituting $\chi(f) = \eta(G,H)$, $\chi(g) = \eta(H,K)$, we obtain

$$\chi(g \circ f) \geq \eta(G,H) + (\eta(H,K) - 1)\frac{|H|^2}{|G|^2}.$$

Since $g \circ f$ is injective, we have $\eta(G,K) \geq \chi(g \circ f)$. Thus,

$$\eta(G,K) \geq \eta(G,H) + (\eta(H,K) - 1)\frac{|H|^2}{|G|^2}.$$

If the right-hand side is negative, the trivial bound $\eta(G,K) \geq 0$ gives the stated maximum form. □

4. Explicit computations for small cyclic groups

The following examples illustrate the computation of the embeddability degree for several small cyclic groups. Throughout this subsection, cyclic groups are written additively.

Example 4.1.: We compute $\eta(\mathbb{Z}_2, \mathbb{Z}_3)$. Let $\mathbb{Z}_2 = \{0,1\}$, $\mathbb{Z}_3 = \{0,1,2\}$. There are exactly six injective functions from $\mathbb{Z}_2$ to $\mathbb{Z}_3$. We list them and compute $\chi(f)$ for each.

Let $f(0) = a$, $f(1) = b$, where $a,b \in \mathbb{Z}_3$ and $a \neq b$. The homomorphism condition is $f(x+y) = f(x) + f(y)$. The four ordered pairs in $\mathbb{Z}_2^2$ are $(0,0)$, $(0,1)$, $(1,0)$, $(1,1)$.

For these pairs, the corresponding conditions are: $(0,0)$: $f(0) = f(0) + f(0)$, that is $a = 2a$. In $\mathbb{Z}_3$, this is equivalent to $a = 0$.

For $(0,1)$, we get $f(1) = f(0) + f(1)$, that is $b = a + b$, again equivalent to $a = 0$.

For $(1,0)$, we get $f(1) = f(1) + f(0)$, that is $b = b + a$, again equivalent to $a = 0$.

For $(1,1)$, since $1 + 1 = 0$ in $\mathbb{Z}_2$, we get $f(0) = f(1) + f(1)$, that is $a = 2b$.

Now we compute all injective functions. Table 1 below summarizes the computation of $\chi(f)$ for all injective functions $f: \mathbb{Z}_2 \to \mathbb{Z}_3$.

Table 1. Homomorphism degrees of all injective functions from $\mathbb{Z}_2$ to $\mathbb{Z}_3$

f(0)	f(1)	successful pairs	$\chi(f)$
0	1	(0,0), (0,1), (1,0)	$\frac{3}{4}$
0	2	(0,0), (0,1), (1,0)	$\frac{3}{4}$
1	0	none	0
1	2	(1,1)	$\frac{1}{4}$
2	0	none	0
2	1	(1,1)	$\frac{1}{4}$

Therefore, the maximum value is $\frac{3}{4}$. Hence $\eta(\mathbb{Z}_2, \mathbb{Z}_3) = \frac{3}{4}$.

Example 4.2.: We compute $\eta(\mathbb{Z}_2, \mathbb{Z}_5)$. Let $\mathbb{Z}_2 = \{0,1\}, \mathbb{Z}_5 = \{0,1,2,3,4\}$. Let $f: \mathbb{Z}_2 \to \mathbb{Z}_5$ be injective and write $f(0) = a,\ f(1) = b$, with $a \neq b$.

As in the previous example, the first three pairs $(0,0), (0,1), (1,0)$ are successful if and only if $a = 0$. The last pair $(1,1)$ is successful if and only if $a = 2b$ in $\mathbb{Z}_5$.

If $a = 0$, then the first three pairs are successful. Since $b \neq 0$ and $2b = 0$ has no nonzero solution in $\mathbb{Z}_5$, the pair $(1,1)$ is not successful. Therefore, $\chi(f) = \frac{3}{4}$ for every injective f with $f(0) = 0$.

If $a \neq 0$, then the first three pairs are not successful. At most the pair $(1,1)$ can be successful. Hence, $\chi(f) \leq \frac{1}{4}$. Thus the maximum value is $\frac{3}{4}$. Therefore $\eta(\mathbb{Z}_2, \mathbb{Z}_5) = \frac{3}{4}$.

Theorem 4.3.: Let $n \geq 2$. Then, $\eta(\mathbb{Z}_2, \mathbb{Z}_n) = \begin{cases} 1, & 2 \mid n, \\ \frac{3}{4}, & 2 \nmid n. \end{cases}$

Proof. Let $f: \mathbb{Z}_2 \to \mathbb{Z}_n$ be injective, and write $f(0) = a,\ f(1) = b$, with $a \neq b$. The four ordered pairs in $\mathbb{Z}_2^2$ yield the following conditions:

$$(0,0): \quad a = 2a,$$
$$(0,1): \quad b = a + b,$$
$$(1,0): \quad b = b + a,$$
$$(1,1): \quad a = 2b.$$

The first three conditions are all equivalent to $a = 0$.

If $2 \mid n$, then $\mathbb{Z}_n$ contains an element of order 2, namely $n/2$. Define $f(0) = 0$, $f(1) = \frac{n}{2}$.

Then, $2f(1) = 2 \cdot \frac{n}{2} = n = 0$ in $\mathbb{Z}_n$. Hence,

$$f(1 + 1) = f(0) = 0 = 2f(1) = f(1) + f(1).$$

The other three conditions are also satisfied because $f(0) = 0$. Therefore, f is an injective homomorphism, and $\eta(\mathbb{Z}_2, \mathbb{Z}_n) = 1$.

Now suppose that $2 \nmid n$. If $a = 0$, then the first three pairs are successful. Since $b \neq 0$, the equation $2b = 0$ has no nonzero solution in $\mathbb{Z}_n$, because 2 is invertible modulo n. Therefore, the pair $(1,1)$ is not successful, and $\chi(f) = \frac{3}{4}$.

If $a \neq 0$, then the first three conditions fail. Only the last condition $a = 2b$ may hold, and therefore $\chi(f) \leq \frac{1}{4}$. Thus, the maximum value is $\frac{3}{4}$. Consequently, $(\mathbb{Z}_2, \mathbb{Z}_n) = \frac{3}{4}$ whenever n is odd. □

Example 4.4.: We compute $\eta(\mathbb{Z}_3, \mathbb{Z}_4)$. Let $\mathbb{Z}_3 = \{0,1,2\}$, $\mathbb{Z}_4 = \{0,1,2,3\}$. Let $f: \mathbb{Z}_3 \to \mathbb{Z}_4$ be injective and write $f(0) = a$, $f(1) = b$, $f(2) = c$, where a, b, c are distinct elements of $\mathbb{Z}_4$.

There are nine ordered pairs in $\mathbb{Z}_3^2$: $(0,0), (0,1), (0,2), (1,0), (1,1), (1,2), (2,0), (2,1), (2,2)$.

We compute the homomorphism condition for each pair.

For $(0,0)$: $f(0 + 0) = f(0) = a$, while $f(0) + f(0) = a + a = 2a$. Thus, $(0,0)$ is successful if and only if $a = 2a$, equivalently $a = 0$.

For $(0,1)$: $f(0 + 1) = f(1) = b$, while $f(0) + f(1) = a + b$. Thus, $(0,1)$ is successful if and only if $b = a + b$, equivalently $a = 0$.

For $(1,0)$, similarly, $f(1 + 0) = f(1) = b$, and $f(1) + f(0) = b + a$. Thus, $(1,0)$ is successful if and only if $a = 0$.

For $(0,2)$ and $(2,0)$, the same argument gives again the condition $a = 0$.

Therefore, the five pairs $(0,0), (0,1), (1,0), (0,2), (2,0)$ are successful if and only if $a = 0$.

Now consider the remaining four pairs.

For $(1,1)$, since $1+1=2$ in $\mathbb{Z}_3$, we get $f(1+1)=f(2)=c$, while $f(1)+f(1)=b+b=2b$. Thus $(1,1)$ is successful if and only if $c=2b$.

For $(1,2)$, since $1+2=0$ in $\mathbb{Z}_3$, we get $f(1+2)=f(0)=a$, while $f(1)+f(2)=b+c$. Thus $(1,2)$ is successful if and only if $a=b+c$.

For $(2,1)$, the same condition appears: $a=c+b$. Since $\mathbb{Z}_4$ is abelian, this is equivalent to $a=b+c$.

For $(2,2)$, since $2+2=1$ in $\mathbb{Z}_3$, we get $f(2+2)=f(1)=b$, while $f(2)+f(2)=c+c=2c$. Thus, $(2,2)$ is successful if and only if $b=2c$.

To obtain many successful pairs, we choose $a=0$. Then, the first five pairs are automatically successful. We need to maximize the number of successful pairs among the remaining four.

Choose $f(0)=0$, $f(1)=1$, $f(2)=3$. Then, $a=0$, $b=1$, and $c=3$. We check the remaining four pairs:

$(1,1)$: $c=3, 2b=2$. So, $(1,1)$ is not successful.

$(1,2)$: $a=0,\ b+c=1+3=4=0$ in $\mathbb{Z}_4$. Hence, $(1,2)$ is successful.

$(2,1)$: $a=0,\ c+b=3+1=4=0$. Hence, $(2,1)$ is successful.

$(2,2)$: $b=1,\ 2c=2\cdot 3=6=2$ in $\mathbb{Z}_4$. Hence, $(2,2)$ is not successful.

Thus, exactly seven pairs are successful: $(0,0), (0,1), (1,0), (0,2), (2,0), (1,2), (2,1)$. Therefore, $\chi(f)=\frac{7}{9}$. So, $\eta(\mathbb{Z}_3,\mathbb{Z}_4)\geq\frac{7}{9}$.

We now show that no injective function can give a larger value. If $a\neq 0$, then the first five pairs fail. Hence, at most four pairs can be successful, so $\chi(f)\leq\frac{4}{9}<\frac{7}{9}$. Thus, a maximizing function must satisfy $a=0$.

Assume $a=0$. Then b, c are distinct nonzero elements of $\mathbb{Z}_4$. The remaining conditions are $c=2b$, $b+c=0$, $b=2c$. The middle condition $b+c=0$ gives two successful pairs, namely $(1,2)$ and $(2,1)$. The other two conditions give at most one successful pair each.

We claim that when $a=0$, at most two of the remaining four pairs can be successful. Indeed, if $c=2b$ and $b+c=0$ hold simultaneously, then $b+2b=0$, so $3b=0$. In $\mathbb{Z}_4$, this implies $b=0$, because 3 is invertible modulo 4, contradicting $b\neq 0$. Similarly, the simultaneous validity of $b=2c$ and $b+c=0$ would imply $3c=0$, hence $c=0$, a contradiction. Finally, if $c=2b$ and $b=2c$ hold simultaneously, then $b=2(2b)=4b=0$, again a contradiction because $b\neq 0$.

Thus, among the last four pairs, at most the two middle pairs $(1,2)$ and $(2,1)$ can be simultaneously successful. Therefore, the total number of successful pairs is at most $5+2=7$. Hence, $\eta(\mathbb{Z}_3,\mathbb{Z}_4)=\frac{7}{9}$.

Example 4.5: We compute $\eta(\mathbb{Z}_3, \mathbb{Z}_5)$. Let $\mathbb{Z}_3 = \{0,1,2\}$, $\mathbb{Z}_5 = \{0,1,2,3,4\}$. Let $f(0) = a, f(1) = b,\ f(2) = c$, with a, b, c distinct.

As in the previous example, the first five pairs $(0,0), (0,1), (1,0), (0,2), (2,0)$ are successful if and only if $a = 0$. The remaining four pairs give the conditions $(1,1)$: $c = 2b$, $(1,2)$: $a = b + c$, $(2,1)$: $a = b + c$, $(2,2)$: $b = 2c$

Choose $f(0) = 0,\ f(1) = 1,\ f(2) = 4$. Then, $a = 0$, $b = 1$, and $c = 4$. The first five pairs are successful.

For the remaining four pairs:

$(1,1)$: $c = 4$, $2b = 2$. So $(1,1)$ is not successful.

$(1,2)$: $a = 0$, $b + c = 1 + 4 = 5 = 0$. So $(1,2)$ is successful.

$(2,1)$: $a = 0$, $c + b = 4 + 1 = 5 = 0$. So $(2,1)$ is successful.

$(2,2)$: $b = 1$, $2c = 2 \cdot 4 = 8 = 3$ in $\mathbb{Z}_5$. Thus $(2,2)$ is not successful.

Hence, exactly seven pairs are successful, and $\chi(f) = \frac{7}{9}$. Therefore, $\eta(\mathbb{Z}_3, \mathbb{Z}_5) \geq \frac{7}{9}$.

We now prove maximality. If $a \neq 0$, then the first five pairs fail, so at most four pairs are successful. Thus, $\chi(f) \leq \frac{4}{9} < \frac{7}{9}$. Hence, any maximizing function must satisfy $a = 0$.

Assume $a = 0$. Then b, c are distinct nonzero elements of $\mathbb{Z}_5$. The remaining conditions are $c = 2b$, $b + c = 0$, $b = 2c$. The condition $b + c = 0$ gives two successful pairs, namely $(1,2)$ and $(2,1)$.

We show that no other remaining condition can hold simultaneously with it. If $c = 2b$ and $b + c = 0$, then $b + 2b = 0$, so $3b = 0$. Since 3 is invertible modulo 5, this gives $b = 0$, contradicting injectivity because $a = 0$ and $b \neq a$.

Similarly, if $b = 2c$ and $b + c = 0$, then $2c + c = 0$, so $3c = 0$, which implies $c = 0$, again impossible.

Finally, if $c = 2b$ and $b = 2c$, then $b = 2(2b) = 4b$, so $3b = 0$. Again $b = 0$, contradiction.

Therefore, at most two of the last four pairs can be successful. Hence, the total number of successful pairs is at most $5 + 2 = 7$. Thus $\eta(\mathbb{Z}_3, \mathbb{Z}_5) = \frac{7}{9}$.

Theorem 4.6.: Let $n \geq 3$. Then $\eta(\mathbb{Z}_3, \mathbb{Z}_n) = \begin{cases} 1, & 3 \mid n, \\ \frac{7}{9}, & 3 \nmid n. \end{cases}$

Proof. Let $f: \mathbb{Z}_3 \to \mathbb{Z}_n$ be injective and write

$$f(0) = a, \qquad f(1) = b, \qquad f(2) = c,$$

where a, b, c are distinct elements of $\mathbb{Z}_n$.

As computed above, the five pairs $(0,0), (0,1), (1,0), (0,2), (2,0)$ are successful if and only if $a = 0$. The remaining four pairs give the conditions

$$(1,1): \quad c = 2b,$$
$$(1,2): \quad a = b + c,$$
$$(2,1): \quad a = b + c,$$
$$(2,2): \quad b = 2c.$$

If $3 \mid n$, then $\mathbb{Z}_n$ contains an element of order 3, namely $n/3$. Define

$$f(0) = 0, \qquad f(1) = \frac{n}{3}, \qquad f(2) = \frac{2n}{3}.$$

Then, f is an injective group homomorphism from $\mathbb{Z}_3$ into $\mathbb{Z}_n$. Hence, $\eta(\mathbb{Z}_3, \mathbb{Z}_n) = 1$.

Now suppose that $3 \nmid n$. We show that $\eta(\mathbb{Z}_3, \mathbb{Z}_n) = \frac{7}{9}$.

First choose any nonzero $b \in \mathbb{Z}_n$ such that $2b \neq 0$, and define $a = 0,\ c = -b$.

For example, one may take $b = 1$ whenever $n \geq 4$. Then,

$$f(0) = 0, \qquad f(1) = b, \qquad f(2) = -b$$

is injective, because $b \neq 0$ and $b \neq -b$. The latter inequality follows from

$$b = -b \Longrightarrow 2b = 0,$$

which would force $b = 0$ when n is odd, and can be avoided by choosing b appropriately when n is even and $3 \nmid n$. With this choice, the first five pairs are successful, and the two pairs $(1,2)$ and $(2,1)$ are also successful because $b + c = b + (-b) = 0 = a$.

Thus, at least seven pairs are successful, so $\eta(\mathbb{Z}_3, \mathbb{Z}_n) \geq \frac{7}{9}$.

We now prove that more than seven successful pairs are impossible. If $a \neq 0$, then the first five pairs fail. Therefore, at most four pairs can be successful, and hence $\chi(f) \leq \frac{4}{9} < \frac{7}{9}$.

Thus, any maximizing function must have $a = 0$.

Assume $a = 0$. Then b, c are distinct nonzero elements of $\mathbb{Z}_n$. The remaining conditions are

$$c = 2b, \qquad b + c = 0, \qquad b = 2c.$$

If both $c = 2b$ and $b + c = 0$ hold, then $b + 2b = 0$, so $3b = 0$. Since $3 \nmid n$, multiplication by 3 is injective on $\mathbb{Z}_n$. Therefore $b = 0$, a contradiction.

Similarly, if both $b = 2c$, and $b + c = 0$ hold, then $3c = 0$, and $c = 0$, a contradiction.

Finally, if both $c = 2b$, and $b = 2c$ hold, then $b = 2c = 2(2b) = 4b$, so $3b = 0$. Again $b = 0$, a contradiction. Therefore, at most one of the single-pair conditions

$$c = 2b, \qquad b = 2c$$

can hold, and neither can hold together with the two-pair condition $b + c = 0$.

The best possibility is the condition $b + c = 0$, which gives exactly two successful pairs among the last four. Hence, the maximum number of successful pairs is $5 + 2 = 7$.

Therefore, $\eta(\mathbb{Z}_3, \mathbb{Z}_n) = \frac{7}{9}$. □

Example 4.7.: We illustrate the composition inequality using $G = \mathbb{Z}_2$, $H = \mathbb{Z}_3$, $K = \mathbb{Z}_5$. From the computations above, $\eta(\mathbb{Z}_2, \mathbb{Z}_3) = \frac{3}{4}$, $\eta(\mathbb{Z}_3, \mathbb{Z}_5) = \frac{7}{9}$, and $\eta(\mathbb{Z}_2, \mathbb{Z}_5) = \frac{3}{4}$. The composition inequality gives $\eta(\mathbb{Z}_2, \mathbb{Z}_5) \geq \eta(\mathbb{Z}_2, \mathbb{Z}_3) + (\eta(\mathbb{Z}_3, \mathbb{Z}_5) - 1)\frac{|\mathbb{Z}_3|^2}{|\mathbb{Z}_2|^2}$. Substituting the values gives $\eta(\mathbb{Z}_2, \mathbb{Z}_5) \geq \frac{3}{4} + \left(\frac{7}{9} - 1\right)\frac{9}{4}$. Since $\frac{7}{9} - 1 = -\frac{2}{9}$, we get $\left(\frac{7}{9} - 1\right)\frac{9}{4} = -\frac{2}{9} \cdot \frac{9}{4} = -\frac{1}{2}$. Therefore, $\eta(\mathbb{Z}_2, \mathbb{Z}_5) \geq \frac{3}{4} - \frac{1}{2} = \frac{1}{4}$. Indeed, $\eta(\mathbb{Z}_2, \mathbb{Z}_5) = \frac{3}{4} \geq \frac{1}{4}$. Thus, the composition inequality is valid in this example, although it gives a non-sharp lower bound.

5. Conclusion

In this chapter, we introduced the embeddability degree as a new probabilistic invariant associated with pairs of finite groups. The main motivation was to move beyond the classical all-or-nothing notion of group embedding and to consider a quantitative measure of how closely one finite group can be represented inside another through injective maps that preserve the group operation as frequently as possible.

After establishing the necessary probabilistic background, we developed the basic framework of this invariant and examined several of its first structural properties. In particular, we showed that the embeddability degree recovers the classical notion of embedding in the extremal case, vanishes precisely when injective maps cannot exist for cardinality reasons, and exhibits a natural symmetry when the groups involved have the same order. We also obtained a composition-type inequality that connects the embeddability behavior of three finite groups.

The explicit computations for small cyclic groups show that even in elementary cases, the invariant is capable of reflecting nontrivial algebraic behavior. These examples suggest that the arithmetic structure of the groups involved plays an important role in determining the embeddability degree, and that concrete calculations may reveal broader patterns worthy of further study.

The results presented here should be viewed as a first step rather than a complete theory. Several natural questions remain open. For instance, it would be

interesting to determine exact values of the embeddability degree for wider classes of finite groups, to understand how the invariant behaves under standard group-theoretic constructions, and to investigate possible connections with other probabilistic invariants already studied in the literature.

More broadly, the embeddability degree offers a way to examine approximate structural compatibility between finite groups from a quantitative perspective. It is our hope that this notion may provide a useful framework for further work at the intersection of probabilistic group theory and the study of group embeddings.

References

Allahverdiev, B. P., Tuna, H., & Kocabıyık, M. (2026). Sampling Theory Associated with Fractal Sturm–Liouville Equations. *Mathematical Methods in the Applied Sciences*, 1-18.

Arvasi, Z., Çağlayan, E. I., & Odabaş, A. (2022). Commutativity degree of crossed modules. *Turkish Journal of Mathematics*, 46(1), 242–256.

Barzegar, R., Erfanian, A., & Farrokhi, M. D. G. (2013). Finite groups with three relative commutativity degrees. *Bulletin of the Iranian Mathematical Society*, 39(2), 271–280.

Chashiani, A., & Rezaei, R. (2021). On the commutativity degree of a group algebra. *Afrika Matematika*, 32(5), 1137–1145.

Çetin, S., & Gürdal, U. (2024). Crossed modules with action. *Ukrainian Mathematical Journal*, 76(4), 649–668.

Erfanian, A., Rezaei, R., & Lescot, P. (2007). On the relative commutativity degree of a subgroup of a finite group. *Communications in Algebra*, 35(12), 4183–4197.

Gallagher, P. X. (1970). The number of conjugacy classes in a finite group. *Mathematische Zeitschrift*, 118, 175–179.

Ghaneei, M., & Azadi, M. (2021). The nth commutativity degree of semigroups. *Journal of Linear and Topological Algebra*, 10(3), 225–233.

Gürdal, M. (2009a). Description of extended eigenvalues and extended eigenvectors of integration operators on the Wiener algebra. *Expositiones Mathematicae*, 27(2), 153–160.

Gürdal, M. (2009b). On the extended eigenvalues and extended eigenvectors of shift operator on the Wiener algebra. *Applied Mathematics Letters*, 22(11), 1727–1729.

Gürdal, U., Oğur, Ö., & Çetin, S. (2025). Unima on [0, 1]. *Fuzzy Sets and Systems*, 516, 109439.

Gustafson, W. H. (1973). What is the probability that two group elements commute? *The American Mathematical Monthly*, 80(9), 1031–1034.

Hashemi, M., & Pirzadeh, M. (2022). A generalization of the nth-commutativity degree in finite groups. *Computational Sciences and Engineering*, 2(1), 33–40.

Lescot, P. (1995). Isoclinism classes and commutativity degrees of finite groups. *Journal of Algebra*, 177(3), 847–869.

Lescot, P. (2001). Central extensions and commutativity degree. *Communications in Algebra*, 29, 4451–4460.

Nath, R. K., & Das, A. K. (2010). On a lower bound of commutativity degree. *Rendiconti del Circolo Matematico di Palermo*, 59, 137–142.

Nath, R. K., & Das, A. K. (2011). On generalized commutativity degree of a finite group. *Rocky Mountain Journal of Mathematics*, 41(6), 1987–2000.

Rezaei, R., & Erfanian, A. (2014). A note on the relative commutativity degree of finite groups. *Asian-European Journal of Mathematics*, 7(1), 1450017.

Rusin, D. (1979). What is the probability that two elements of a finite group commute? *Pacific Journal of Mathematics*, 82(1), 237–247.

Tărnăuceanu, M. (2009). Subgroup commutativity degrees of finite groups. *Journal of Algebra*, 321(9), 2508–2520.

Uc, M. (2025). Quantitative relations between commutativity, surjectivity, and homomorphism degrees in finite groups. *Süleyman Demirel Üniversitesi Fen Bilimleri Enstitüsü Dergisi*, 29(3), 705–715.

Chapter 6

A Szász-Durrmeyer Type Approximation Operator Based On Gauss-Appell Polynomials

Fatih Rıza Çelik[1]

Abstract

This chapter introduces a Szász-Durrmeyer type approximation operator generated by Gauss-Appell polynomials. The construction is motivated by the link between Gauss hypergeometric functions, umbral calculus, and Appell polynomial families. After fixing the auxiliary variable as a parameter, the generating function of the Gauss-Appell polynomials is used to define a positive linear operator on the semi-infinite interval. The basic algebraic structure of the operator is examined through its first moments and central moments. These identities make it possible to establish the main approximation properties in a weighted setting. In particular, a Korovkin-type convergence theorem is obtained, showing that the operators approximate continuous functions uniformly on compact subsets. Quantitative estimates are then derived by means of the usual modulus of continuity, Peetre's K-functional, and the second-order modulus of smoothness. A Voronovskaya type asymptotic formula is also proved, which describes the limiting behaviour of the approximation error and clarifies the role of the first two central moments. Finally, a numerical example supported by graphs and pointwise error tables illustrates the convergence behaviour of the proposed operators. The results show that increasing the main parameter improves the approximation, while the additional parameters provide useful local control over the accuracy.

1. INTRODUCTION

In recent decades, hypergeometric functions have attracted renewed attention due to their deep connections with several areas of mathematics, such as algebraic geometry, representation theory, number theory, combinatorics, and related fields. Among these functions, the Gauss hypergeometric function, denoted by ${}_2\mathcal{H}_1(\alpha,\beta;\gamma;u)$, occupies a central place as a classical special function with important applications in complex analysis, differential equations and mathematical physics. It is well known that the Gauss hypergeometric

1 Dr., Haydar Aliyev Fen Lisesi, fatihrizacelik@gmail.com, https://orcid.org/0000-0001-9482-1018

https://doi.org/10.58830/ozgur.pub1361.c5496

function ${}_2\mathcal{H}_1(\alpha,\beta;\gamma;u)$ is a solution of the hypergeometric differential equation [1]

$$u(u-1)y''(u)+(\gamma-(\alpha+\beta+1)u)y'(u)-\alpha\beta y(u)=0, |u|<1, \quad (1)$$

where α,β and γ may be real or complex parameters with $\gamma \notin \{\dots,-2,-1,0\}$. This differential equation is a member of the Fuchsian class on the complex projective line and possesses three regular singular points, namely $u=0,1$ and ∞.

The Gauss hypergeometric function ${}_2\mathcal{H}_1(\alpha,\beta;\gamma;u)$ is represented by the following power series:

$${}_2\mathcal{H}_1(\alpha,\beta;\gamma;u)=\sum_{m=0}^{\infty}\frac{(\alpha)_m(\beta)_m}{(\gamma)_m}\frac{u^m}{m!}, \qquad |u|<1. \quad (2)$$

The Pochhammer symbol is defined by

$$\begin{cases}(\beta)_m=\beta(\beta+1)\dots(\beta+m-1) & ;m\geq 1\\ (\beta)_0=1 & ;m=0\end{cases}.$$

The umbral approach is a well established symbolic method that provides an effective framework for dealing with a wide variety of problems in science and engineering, especially those related to special functions. By using formal symbolic rules and algebraic type operations, this technique helps reveal underlying structures, reduce the complexity of lengthy computations and offer a clearer interpretation of mathematical relations that may be difficult to handle by classical methods. In this respect, the umbral method is particularly useful in the study of special functions, since it facilitates the construction of new forms, the analysis of their operational properties, and the extension of known families. Therefore, it has become an important tool in several applied areas, including physics, fluid mechanics, and dynamical systems.

In a recent study [2], the hypergeometric function was expressed within the framework of umbral calculus by means of an exponential type representation. Appell polynomials have attracted considerable attention in recent years because of their broad range of applications [3]. Various studies have examined their characterization, generalizations and connections with special functions through algebraic and operational methods [4]. Further research has also investigated noncommutative extensions, generating functions, combinatorial structures and applications in mathematical physics [5,6]. In addition, confluent Appell polynomials and their main properties have been introduced and studied in [7].

An Appell sequence $\{T_m(u)\}_{m\geq 0}$ is commonly defined by means of an exponential generating function of the form [8]:

$$\mathbb{A}(t)e^{ut}=\sum_{k=0}^{\infty}T_k(u)\frac{t^k}{k!}, \quad (3)$$

where the function $\mathbb{A}(t)$ is given by

$$\mathbb{A}(t) = \sum_{k=0}^{\infty} a_k \frac{t^k}{k!}, a_0 \neq 0. \tag{4}$$

Using umbral methods, the authors in [9] established a connection between hypergeometric functions and the Appell family. In this way, they derived the generating function for the hypergeometric Appell polynomials in the following form:

$$\sum_{m=0}^{\infty} {}_2\mathcal{H}_1 T_m^{(\alpha,\beta;\gamma)}(u) \frac{t^m}{m!} = \mathbb{A}(t)\ {}_2\mathcal{H}_1(\alpha,\beta;\gamma;ut). \tag{5}$$

They also discussed the main properties of this broad class of special polynomials.

In addition, the authors of [9] extended their study by defining the two variable hypergeometric Appell polynomials through umbral techniques as follows:

$$\sum_{m=0}^{\infty} T_m^{(\alpha,\beta;\gamma)}(u,v) \frac{t^m}{m!} = \mathbb{A}(t)e^{ut}\ {}_2\mathcal{H}_1(\alpha,\beta;\gamma;vt^2), \qquad |ut^2| < 1 \tag{6}$$

where $\alpha, \beta, \gamma \in \mathbb{C}$ and $\gamma \notin \{\dots, -2, -1, 0\}$.

In recent years, special functions arising in mathematical physics have been widely developed in both generalized and multivariable settings. In particular, special polynomials involving two variables have provided useful analytical tools for studying various classes of partial differential equations that appear in physical models [10]. Many such special functions and their extensions have been motivated by problems originating from physical phenomena.

One of the main contributions of the present study is the construction of approximation operators based on the Gauss Appell polynomials. These operators are proved to approximate functions defined on a semi infinite interval in a suitable weighted function space. Their convergence behavior is further illustrated by a numerical example and the study ends with concluding remarks.

2. MAIN RESULTS

In this section, we construct a family of positive linear Szász-Durrmeyer type operators generated by the Gauss-Appell polynomials. To this end, we fix the auxiliary variable v as a parameter h. Then the generating function of the Gauss Appell polynomials $T_m^{(\alpha,\beta;\gamma)}(u,h)$ is given by

$$\sum_{k=0}^{\infty} T_k^{(\alpha,\beta;\gamma)}(u,h) \frac{t^k}{k!} = \mathbb{A}(t)e^{ut}\ {}_2\mathcal{H}_1(\alpha,\beta;\gamma;ht^2), \qquad |ht^2| < 1 \tag{7}$$

Since the coefficients of the generating function are non-negative under the assumptions and $\gamma > \beta > \alpha > 0$, $0 < h < 1$, $T_k^{(\alpha,\beta;\gamma)}(mu,h) > 0$ and $\mathbb{A}(t)$ has non negative coefficients with $\mathbb{A}(1) > 0$, the operator defined below is positive and linear:

$$\wp_m(g;u) = \frac{me^{-mu}}{\mathbb{A}(1)\ {}_2\mathcal{H}_1(\alpha,\beta;\gamma;h)} \sum_{k=0}^{\infty} \frac{T_k^{(\alpha,\beta;\gamma)}(mu,h)}{k!} \int_0^{\infty} e^{-mt} \frac{(mt)^k}{k!} g(t)dt. \quad (8)$$

First, we evaluate several moments and central moments of the family of operators defined in (8).

Lemma 2.1. The first few moments of the operators $\wp_m$ are given as follows:

$\wp_m(1;u) = 1,$

$\wp_m(t;u) = u + \dfrac{\Delta_1 + 1}{m},$

$\wp_m(t^2;u) = u^2 + \dfrac{(2\Delta_1 + 4)u}{m} + \dfrac{\Delta_2 + 4\Delta_1 + 2}{m^2}$

for any $u \in [0,\infty)$.

Here,

$$\mathcal{H}_j := {}_2\mathcal{H}_1(\alpha + j, \beta + j; \gamma + j; h), j = 0,1,2,$$

$$\Delta_1 := \frac{\mathbb{A}'(1)}{\mathbb{A}(1)} + 2h\frac{(\alpha)_1(\beta)_1}{(\gamma)_1}\frac{\mathcal{H}_1}{\mathcal{H}_0},$$

$$\Delta_2 := \frac{\mathbb{A}''(1)}{\mathbb{A}(1)} + 2h\frac{(\alpha)_1(\beta)_1}{(\gamma)_1}\frac{\mathcal{H}_1}{\mathcal{H}_0} + 4h^2\frac{(\alpha)_2(\beta)_2}{(\gamma)_2}\frac{\mathcal{H}_2}{\mathcal{H}_0} + 4h\frac{(\alpha)_1(\beta)_1}{(\gamma)_1}\frac{\mathbb{A}'(1)}{\mathbb{A}(1)}\frac{\mathcal{H}_1}{\mathcal{H}_0}.$$

Proof.

Differentiating the generating function in (7) with respect to t once and twice, respectively, we obtain the following identities;

$$\sum_{k=0}^{\infty} \frac{T_k^{(\alpha,\beta;\gamma)}(mu)}{k!} = \mathbb{A}(t)e^{ut}\ {}_2\mathcal{H}_1(\alpha,\beta;\gamma;ht^2),$$

$$\sum_{k=0}^{\infty} \frac{T_{k+1}^{(\alpha,\beta;\gamma)}(mu)}{k!} = e^{ut}\big(\mathbb{A}'(t) + u\mathbb{A}(t)\big)\ {}_2\mathcal{H}_1(\alpha,\beta;\gamma;ht^2)$$

$$+e^{ut}\frac{2ht(\alpha)_1(\beta)_1}{(\gamma)_1}\mathbb{A}(t)\ {}_2\mathcal{H}_1(\alpha+1,\beta+1;\gamma+1;ht^2)$$

$$\sum_{k=0}^{\infty} \frac{T_{k+2}^{(\alpha,\beta;\gamma)}(mu)}{k!} = e^{ut}\left(\mathbb{A}''(t) + 2u\mathbb{A}'(t) + u^2\mathbb{A}(t)\right) {}_2\mathcal{H}_1(\alpha,\beta;\gamma;ht^2)$$

$$+e^{ut}\left(\frac{4ht(\alpha)_1(\beta)_1}{(\gamma)_1}\left(\mathbb{A}'(t) + u\mathbb{A}(t)\right) + \frac{2h(\alpha)_1(\beta)_1}{(\gamma)_1}\mathbb{A}(t)\right) {}_2\mathcal{H}_1(\alpha+1,\beta+1;\gamma+1;ht^2)$$

$$+e^{ut}\frac{4h^2t^2(\alpha)_2(\beta)_2}{(\gamma)_2}\mathbb{A}(t)\ {}_2\mathcal{H}_1(\alpha+2,\beta+2;\gamma+2;ht^2).$$

Putting $t = 1$ and replacing u by mu in the above identities, and then applying the operator defined in (8), we obtain the required moment identities.

Lemma 2.2. For the operators $\wp_m$, the following central moments hold:

$$\wp_m\,(t-u;u) = \frac{\Delta_1 + 1}{m},$$

$$\wp_m\,((t-u)^2;u) = \frac{2u}{m} + \frac{\Delta_2 + 4\Delta_1 + 2}{m^2}.$$

Proof. By using Lemma 2.1, the desired result is obtained.

Remark 2.3. The results are as follows

$$\lim_{m\to\infty} m\wp_m(t-u;u) = \Delta_1 + 1,$$

$$\lim_{m\to\infty} m\wp_m((t-u)^2;u) = 2u$$

for $u > 0$. Moreover, for the fourth central moment, we have

$$\wp_m((t-u)^2;u) = O\left(\frac{1}{m}\right)$$

or equivalently,

$$m^2\wp_m((t-u)^4;u) = O(1).$$

Theorem 2.4. For every $g \in H$, we have

$$\lim_{m\to\infty} \wp_m(g;u) = g(u),$$

and the convergence is uniform on each compact subset of $[0,\infty)$ and

$$H = \left\{g: g \in C[0,\infty),\ \ \frac{g(u)}{1+u^2} \text{ has a finite limit as } u \longrightarrow \infty\right\}.$$

Proof. From Lemma 2.1, it follows directly that the operators $\wp_m$ reproduce the test functions 1, t and t^2 asymptotically; that is,

$$\lim_{m\to\infty} \wp_m\left(t^j,u\right) = u^j, j = 0,1,2, \tag{9}$$

and this convergence is uniform on each compact subset of [0,∞). Hence, by Korovkin-type theorem of Altomare and Campiti [11], the asserted convergence result is obtained. This completes the proof.

Theorem 2.5. Let $g \in C_B[0,\infty)$ be uniformly continuous on [0,∞). Then, for every $u \in [0,\infty)$, the following estimate holds:

$$|\wp_m(g;u) - g(u)| \le 2\omega\left(g;\sqrt{\wp_m((t-u)^2;u)}\right)$$

where $\omega(g;\cdot)$ denotes the usual modulus of continuity of g.

Proof.

$$|\wp_m(g;u) - g(u)| \le \frac{me^{-mu}}{\mathbb{A}(1)\mathcal{H}_0}\sum_{k=0}^{\infty}\frac{T_k^{(\alpha,\beta;\gamma)}(mu,h)}{k!}\int_0^{\infty} e^{-mt}\frac{(mt)^k}{k!}|g(t) - g(u)|dt$$

$$\le \frac{me^{-mu}}{\mathbb{A}(1)\mathcal{H}_0}\sum_{k=0}^{\infty}\frac{T_k^{(\alpha,\beta;\gamma)}(mu,h)}{k!}\int_0^{\infty} e^{-mt}\frac{(mt)^k}{k!}\left(1+\frac{|t-u|}{\delta}\right)\omega(g;\delta)dt$$

$$\le \left\{1 + \frac{me^{-mu}}{\mathbb{A}(1)\mathcal{H}_0}\frac{1}{\delta}\sum_{k=0}^{\infty}\frac{T_k^{(\alpha,\beta;\gamma)}(mu,h)}{k!}\int_0^{\infty} e^{-mt}\frac{(mt)^k}{k!}|t-u|dt\right\}\omega(g;\delta).$$

Estimating the integral term by the Cauchy Schwarz inequality, we obtain

$$|\wp_m(g;u) - g(u)| \le \left\{\left(1+\frac{me^{-mu}}{\mathbb{A}(1)\mathcal{H}_0}\right)\frac{1}{\delta}\sum_{k=0}^{\infty}\frac{T_k^{(\alpha,\beta;\gamma)}(mu,h)}{k!}\left(\int_0^{\infty} e^{-mt}\frac{(mt)^k}{k!}dt\right)^{\frac{1}{2}}\right.$$

$$\left.\times\left(\int_0^{\infty} e^{-mt}\frac{(mt)^k}{k!}(t-u)^2dt\right)^{\frac{1}{2}}\right\}\omega(g;\delta).$$

Applying the Cauchy Schwarz inequality once more to the summation gives

$$|\wp_m(g;u) - g(u)| \le \left\{1 + \frac{1}{\delta}\left(\frac{me^{-mu}}{\mathbb{A}(1)\mathcal{H}_0}\sum_{k=0}^{\infty}\frac{T_k^{(\alpha,\beta;\gamma)}(mu,h)}{k!}\int_0^{\infty} e^{-mt}\frac{(mt)^k}{k!}dt\right)^{\frac{1}{2}}\right.$$

$$\left.\left(\frac{me^{-mu}}{\mathbb{A}(1)\mathcal{H}_0}\sum_{k=0}^{\infty}\frac{T_k^{(\alpha,\beta;\gamma)}(mu,h)}{k!}\int_0^{\infty} e^{-mt}\frac{(mt)^k}{k!}(t-u)^2dt\right)^{\frac{1}{2}}\right\}\times\omega(g;\delta)$$

$$= \left\{1 + \frac{1}{\delta}\left(\wp_m(t;u)\right)^{\frac{1}{2}}\left(\wp_m((t-u)^2;u)\right)^{\frac{1}{2}}\right\}\omega(g;\delta)$$

$$= \left\{1 + \frac{1}{\delta}\left(\wp_m((t-u)^2;u)\right)^{\frac{1}{2}}\right\}\omega(g;\delta)$$

If we choose $\delta = \sqrt{\wp_m((t-u)^2;u)}$, this completes the proof.

Lemma 2.6. For each $u \in [0,\infty)$ and $g \in C_B[0,\infty)$, we have

$$|\wp_m(g;u)| \le \|g\|.$$

Proof. Let $\|g\| := \sup_{t\ge 0}|g(t)|$. From the definition of $\wp_m$, we obtain

$$\begin{aligned}|\wp_m(g;u)| &\le \left|\frac{me^{-mu}}{\mathbb{A}(1)\mathcal{H}_0}\sum_{k=0}^{\infty}\frac{T_k^{(\alpha,\beta;\gamma)}(mu,h)}{k!}\int_0^{\infty}e^{-mt}\frac{(mt)^k}{k!}g(t)dt\right| \\ &\le \frac{me^{-mu}}{\mathbb{A}(1)\mathcal{H}_0}\sum_{k=0}^{\infty}\frac{T_k^{(\alpha,\beta;\gamma)}(mu,h)}{k!}\int_0^{\infty}e^{-mt}\frac{(mt)^k}{k!}|g(t)|dt \\ &\le \|g\|\frac{me^{-mu}}{\mathbb{A}(1)\mathcal{H}_0}\sum_{k=0}^{\infty}\frac{T_k^{(\alpha,\beta;\gamma)}(mu,h)}{k!}\int_0^{\infty}e^{-mt}\frac{(mt)^k}{k!}dt\end{aligned}$$

Then, $|\wp_m(g;u)| \le \|g\|\wp_m(1;u) = \|g\|$.

Now let $C_B[0,\infty)$ be the space of all bounded continuous functions on $[0,\infty)$, equipped with the supremum norm

$$\|g\|_{C_B[0,\infty)} := \sup_{u\in[0,\infty)}|g(u)|, \quad g \in C_B[0,\infty).$$

For $\mu > 0$, Peetre's K-functional is given by

$$\mathcal{K}(g;\mu) := \inf_{\tau\in C_B^2[0,\infty)}\left\{\|g-\tau\|_{C_B[0,\infty)} + \mu\|\tau\|_{C_B^2[0,\infty)}\right\}.$$

Here, $C_B^2[0,\infty)$ denotes the class of all functions $\tau \in C_B[0,\infty)$ whose first and second derivatives also belong to $C_B[0,\infty)$ and it is equipped with the norm

$$\|\tau\|_{C_B^2[0,\infty)} := \|\tau\|_{C_B[0,\infty)} + \|\tau'\|_{C_B[0,\infty)} + \|\tau''\|_{C_B[0,\infty)}$$

[12].

Theorem 2.7. Let $g \in C_B[0,\infty)$. Then, for every $m \in \mathbb{N}$ and $u \in [0,\infty)$, we have

$$|\wp_m(g;u) - g(u)| \le 2\,\mathcal{K}\big(g;\mu_m(u)\big),$$

where $\mathcal{K}(g;\cdot)$ denotes Peetre's K-functional and

$$\mu_m(u) = |\wp_m(t-u;u)| + \frac{1}{2}\wp_m((t-u)^2;u).$$

Proof. Let $\tau \in C_B^2[0,\infty)$ be fixed. For $t \ge 0$, Taylor's formula yields

$$\tau(t) = \tau(u) + (t-u)\tau'(u) + \int_u^t (t-s)\,\tau''(s)ds\,. \qquad (10)$$

Applying the operator $\wp_m(\cdot\,;u)$ to (10), we obtain

$$
\begin{aligned}
|\wp_m(\tau;u)-\tau(u)| &\le \left|\wp_m\big((t-u)\tau'(u);u\big)+\wp_m\left(\int_u^t (t-s)\,\tau''(s)ds;u\right)\right| \\
&\le |\tau'(u)||\wp_m(t-u;u)|+\wp_m\left(\left|\int_u^t (t-s)\,\tau''(s)ds\right|;u\right) \\
&\le \|\tau'\|_{C_B[0,\infty)}|\wp_m(t-u;u)| \\
&+ \|\tau''\|_{C_B[0,\infty)}\wp_m\left(\int_u^t |t-s|\,ds;u\right) \\
&\le \|\tau'\|_{C_B[0,\infty)}|\wp_m(t-u;u)| \\
&+ \frac{1}{2}\|\tau''\|_{C_B[0,\infty)}\wp_m((t-u)^2;u).
\end{aligned}
$$

Consequently,

$$|\wp_m(\tau;u)-\tau(u)| \le \mu_m(u)\|\tau\|_{C_B^2[0,\infty)}.$$

Using the preceding estimate together with Lemma 2.6, for any $h \in C_B^2[0,\infty)$ we obtain

$$
\begin{aligned}
&|\wp_m(g;u)-g(u)| \\
&\quad= |\wp_m(g;u)-g(u)+\wp_m(\tau;u)-\wp_m(\tau;u)+\tau(u) \\
&\quad- \tau(u)| \\
&\quad\le |\wp_m(g-\tau;u)|+|g(u)-\tau(u)|+|\wp_m(\tau;u)-\tau(u)| \\
&\quad\le \|g-\tau\|_{C_B[0,\infty)}\wp_m(t;u)+\|g-\tau\|_{C_B[0,\infty)} \\
&\quad+ \mu_m(u)\|\tau\|_{C_B^2[0,\infty)} \\
&\quad\le 2\left(\|g-\tau\|_{C_B[0,\infty)}+\mu_m(u)\|\tau\|_{C_B^2[0,\infty)}\right).
\end{aligned}
$$

Taking the infimum over all $\tau \in C_B^2[0,\infty)$ yields

$$|\wp_m(g;u)-g(u)| \le 2\,\mathcal{K}\big(g;\mu_m(u)\big). \tag{11}$$

Hence the proof is complete.

For a function $g \in C_B[0,\infty)$, the second order modulus of continuity is defined by

$$\omega_2(g;\delta) := \sup_{0<t\le\delta}\|g(\cdot+2t)-2g(\cdot+t)+g(\cdot)\|_{C_B[0,\infty)}.$$

Moreover, Peetre's K-functional and ω_2 are connected through the estimate

$$\mathcal{K}(g;\delta) \le N\big(\omega_2\big(g;\sqrt{\delta}\big)+min\{1,\delta\}\|g\|_{C_B[0,\infty)}\big), \tag{12}$$

where $N>0$ is a constant independent of f and δ. Combining (11) and (12), we obtain

$$|\wp_m(g;u)-g(u)| \le N\left(\omega_2\left(g;\sqrt{\mu_n(u)}\right)+min\{1,\mu_m(u)\}\|g\|_{C_B[0,\infty)}\right).$$

Theorem 2.8. Let $g, g', g'' \in H$. Then, for every $u>0$,

$$\lim_{m\to\infty} m(\wp_m(g;u) - g(u)) = (\Delta_1 + 1)g'(u) + u \cdot g''(u).$$

Moreover, the convergence is uniform on each compact subset of $[0,\infty)$.

Proof. By Taylor's formula, expanding g at the point u, we

$$g(t) = g(u) + g'(u)(t-u) + \frac{g''(u)}{2}(t-u)^2 + (t-u)^2\zeta(t,u), \qquad (13)$$

where $\chi(t,u) \to 0$ as $t \to u$. Applying the operator $\wp_m$ to both sides of (13), we obtain

$$\wp_m(g;u) = g(u) + g'(u)\wp_m(t-u;u) + \frac{g''(u)}{2}\wp_m((t-u)^2;u) + \wp_m(\chi(t,u)(t-u)^2;u).$$

Consequently,

$$m\big(\wp_m(g;u) - g(u)\big) = mg'(u)\wp_m(t-u;u) + m\frac{g''(u)}{2}\wp_m((t-u)^2;u) + m\wp_m(\chi(t,u)(t-u)^2;u).$$

It remains to estimate the remainder term. By the Cauchy Schwarz inequality, we have

$$m\big(\wp_m(\chi(t,u)(t-u)^2;u)\big) \le \sqrt{\wp_m(\chi^2(t,u);u)}\sqrt{m^2\wp_m((t-u)^4;u)}.$$

Since $\chi(t,u) \to 0$ as $t \to u$ and by the convergence property of the operators $\wp_m$, we get

$$\lim_{m\to\infty} \wp_m(\chi^2(t,u);u) = \zeta^2(u,u) = 0. \qquad (14)$$

Moreover,

$$m^2\wp_m((t-u)^4;u) = O(1),$$

as $m \to \infty$. Hence,

$$\lim_{m\to\infty} m^2\wp_m((t-u)^4;u) = 0.$$

Combining this observation with Remark 2.3 and (14) completes the proof.

3. ILLUSTRATIVE EXAMPLE

To illustrate the approximation behaviour of the proposed Gauss-Appell Szász-Durrmeyer type operators, we consider the test function $g(u) = e^{-u}\sin(3u) + 2$, $x \in [0,2]$. This function is continuous, bounded and oscillatory on the considered interval. Therefore, it is suitable for testing the approximation performance of the operator. In the numerical computations, the auxiliary function is chosen as $\mathbb{A}(t) = e^t$. With this choice, the corresponding

Gauss-Appell polynomials are generated consistently by the generating function used in the construction of the operator.

1- The first graph shows the approximation behaviour of the operator for $m = 5, 20, 50, 100$. It is clearly observed that the approximation improves as m increases. For $m = 5$, the approximation curve is relatively far from the original function, especially near the peak region of the function. However, as nnn becomes larger, the operator follows the oscillatory shape of the function more accurately. The error table supports this visual observation. For example, at $u = 0$, the error decreases from 3.74785×10^{-1} for $m = 5$ to 6.1732×10^{-2} for $m = 100$. These results confirm that the proposed operator has a clear convergence tendency with respect to increasing n. The best numerical performance among the tested values is obtained for $m = 100$.

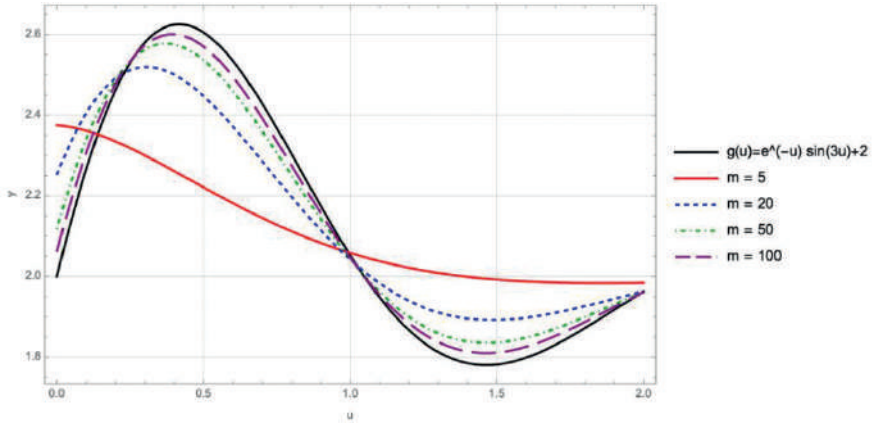

Figure 1. Approximation of $g(u) = e^{-u}\sin(3u) + 2$ by the Gauss-Appell Szász-Durrmeyer type operator for different values of m.

Table 1. Pointwise absolute errors for different values of m.

u	m = 5	m = 20	m = 50	m = 100
0.00	3.74785×10^{-1}	2.51578×10^{-1}	1.18015×10^{-1}	6.1732×10^{-2}
0.25	2.12562×10^{-1}	1.89648×10^{-2}	2.79981×10^{-3}	3.61542×10^{-3}
0.50	3.84127×10^{-1}	1.57665×10^{-1}	6.85793×10^{-2}	3.50561×10^{-2}
0.75	2.39553×10^{-1}	1.26539×10^{-1}	6.19262×10^{-2}	3.3208×10^{-2}
1.00	6.39449×10^{-3}	1.01739×10^{-2}	8.61782×10^{-3}	5.43876×10^{-3}
1.25	1.78437×10^{-1}	8.70334×10^{-2}	4.06492×10^{-2}	2.13641×10^{-2}
1.50	2.10476×10^{-1}	1.1028×10^{-1}	5.46772×10^{-2}	2.95573×10^{-2}
1.75	1.33668×10^{-1}	6.72024×10^{-2}	3.39208×10^{-2}	1.85634×10^{-2}
2.00	2.23362×10^{-2}	7.63995×10^{-4}	4.86117×10^{-4}	1.14479×10^{-3}

2- In the second graph, the influence of the parameter α is investigated. The considered values are $\alpha = 0.20, 1.50, 2.90$. The numerical curves show that

changing α has a visible but moderate effect on the approximation. Around the maximum point of the function, the approximation curves remain below the exact function. However, the general shape of the function is preserved for all selected values of α.

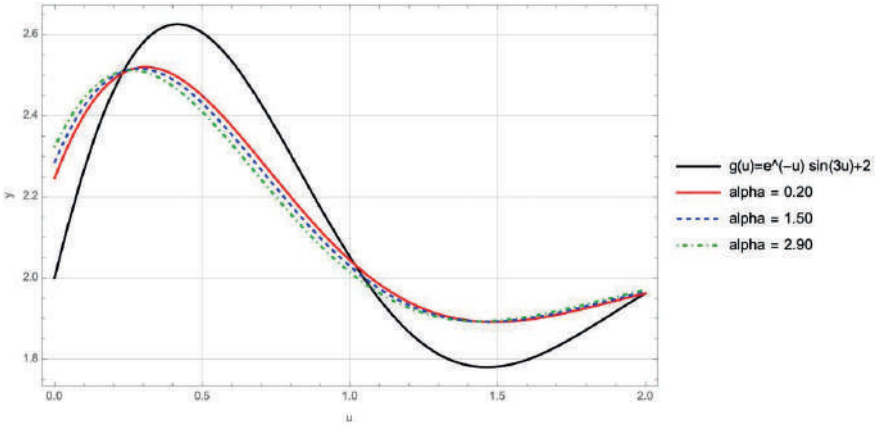

Figure 2. Approximation of $g(u) = e^{-u}\sin(3u) + 2$ for different values of α, while the remaining parameters are fixed.

The error table indicates that the smallest error is not always obtained for the same value of α. For instance, at $u = 0.5$, the errors are $1.55203 \times 10^{-1}, 1.73565 \times 10^{-1}, 1.94723 \times 10^{-1}$, corresponding to $\alpha = 0.20, 1.50, 2.90.$, respectively. Hence, at this point, the smallest error occurs for $\alpha = 0.20$. On the other hand, at $u = 1.25$, the smallest error is obtained for $\alpha = 2.90$. This shows that the parameter α affects the local behaviour of the operator. Therefore, suitable choices of α may improve the approximation quality on particular subintervals.

Table 2. Pointwise absolute errors for different values of α.

u	alpha = 0.20	alpha = 1.50	alpha = 2.90
0.00	2.4596×10^{-1}	2.84682×10^{-1}	3.2242×10^{-1}
0.25	1.93396×10^{-2}	1.79908×10^{-2}	1.95739×10^{-2}
0.50	1.55203×10^{-1}	1.73565×10^{-1}	1.94723×10^{-1}
0.75	1.23574×10^{-1}	1.44946×10^{-1}	1.67962×10^{-1}
1.00	8.09814×10^{-3}	2.27407×10^{-2}	3.7799×10^{-2}
1.25	8.78486×10^{-2}	8.23306×10^{-2}	7.71884×10^{-2}
1.50	1.10132×10^{-1}	1.11435×10^{-1}	1.13375×10^{-1}
1.75	6.66175×10^{-2}	7.09183×10^{-2}	7.57432×10^{-2}
2.00	1.81144×10^{-4}	4.35568×10^{-3}	8.7936×10^{-3}

3- The third graph presents the effect of the parameter β. The selected values are $\beta = 0.90, 1.30, 2.80$. The approximation curves are very close to each other. This indicates that, for the chosen parameter set, the effect of β on the graphical approximation is weaker than the effect of n. Although the curves are not exactly identical, their differences are relatively small.

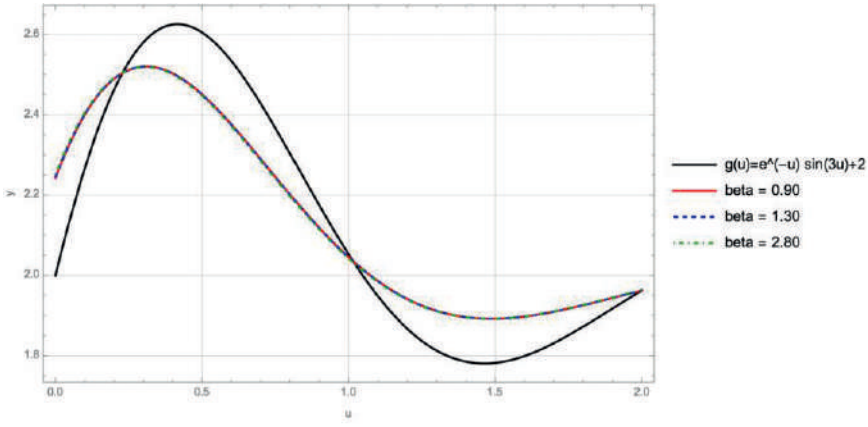

Figure 3. Approximation of $g(u) = e^{-u}\sin(3u) + 2$ for different values of β, while the remaining parameters are fixed.

This conclusion is also supported by the error table. For example, at $u = 1.5$, the errors are $1.10051 \times 10^{-1}, 1.1009 \times 10^{-1}, 1.10259 \times 10^{-1}$. These values are almost the same. Similarly, at $u = 2.0$, the errors remain very small for all tested β values. Therefore, the parameter β has only a limited numerical influence in

this example. Nevertheless, small variations are still visible in the table. This means that β can fine tune the approximation, but it does not dominate the convergence behaviour of the operator.

Table 3. Pointwise absolute errors for different values of β.

u	beta = 0.90	beta = 1.30	beta = 2.80
0.00	2.43215×10^{-1}	2.44821×10^{-1}	2.51089×10^{-1}
0.25	1.94855×10^{-2}	1.93606×10^{-2}	1.89635×10^{-2}
0.50	1.53958×10^{-1}	1.54642×10^{-1}	1.57413×10^{-1}
0.75	1.22097×10^{-1}	1.22931×10^{-1}	1.26256×10^{-1}
1.00	7.07402×10^{-3}	7.66245×10^{-3}	9.98417×10^{-3}
1.25	8.82438×10^{-2}	8.80093×10^{-2}	8.71016×10^{-2}
1.50	1.10051×10^{-1}	1.1009×10^{-1}	1.10259×10^{-1}
1.75	6.63237×10^{-2}	6.6487×10^{-2}	6.71441×10^{-2}
2.00	1.08314×10^{-4}	5.60007×10^{-5}	7.08979×10^{-4}

4- The fourth graph investigates the role of the parameter γ. The selected values are $\gamma = 2.10, 3.80, 4.50$. As in the case of the parameter β, the approximation curves corresponding to different γ values are quite close to each other. This suggests that the parameter γ has a relatively mild effect on the approximation for the present test function and interval. The error table confirms this behaviour. At $u = 0.5$, the errors are $1.58789 \times 10^{-1}, 1.55728 \times 10^{-1}, 1.5176 \times 10^{-1}$. Thus, increasing γ slightly improves the approximation at this point. At $u = 2.0$, the error decreases from 1.02214×10^{-3} for $\gamma = 2.10$ to 1.83198×10^{-4} for $\gamma = 4.50$. This shows that larger values of γ may provide better local accuracy near the right endpoint of the interval. Overall, the parameter γ has a stabilizing effect on the approximation, although its influence is not as strong as the influence of m.

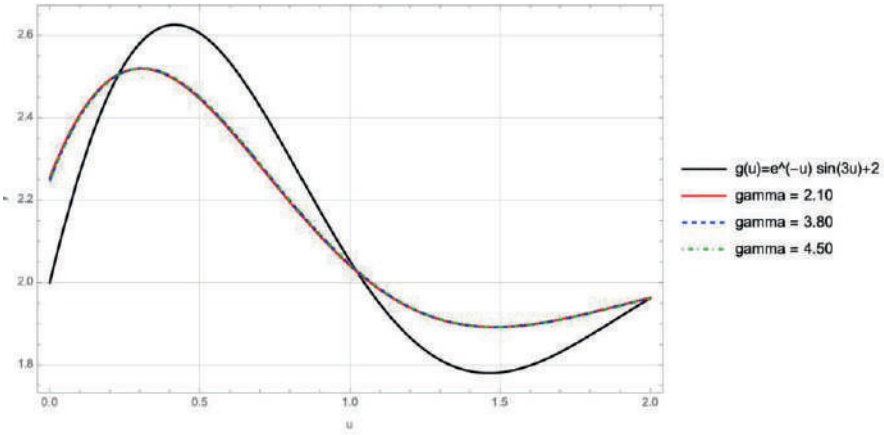

Figure 4. Approximation of $g(u) = e^{-u}\sin(3u) + 2$ for different values of γ, while the remaining parameters are fixed.

Table 4. Pointwise absolute errors for different values of γ.

u	gamma = 2.10	gamma = 3.80	gamma = 4.50
0.00	2.53998×10^{-1}	2.47303×10^{-1}	2.46054×10^{-1}
0.25	1.88593×10^{-2}	1.91937×10^{-2}	1.92729×10^{-2}
0.50	1.58789×10^{-1}	1.55728×10^{-1}	1.55176×10^{-1}
0.75	1.27859×10^{-1}	1.2424×10^{-1}	1.23578×10^{-1}
1.00	1.10831×10^{-2}	8.57915×10^{-3}	8.11646×10^{-3}
1.25	8.66869×10^{-2}	8.76491×10^{-2}	8.783×10^{-2}
1.50	1.10356×10^{-1}	1.10155×10^{-1}	1.10121×10^{-1}
1.75	6.74665×10^{-2}	6.6745×10^{-2}	6.66141×10^{-2}
2.00	1.02214×10^{-3}	3.13327×10^{-4}	1.83198×10^{-4}

4- CONCLUSION

In this chapter, a new Szász-Durrmeyer type approximation operator based on Gauss-Appell polynomials has been constructed and studied. The proposed operator combines the structural properties of Gauss hypergeometric functions with the flexibility of Appell-type polynomial families. This connection provides a useful framework for defining positive linear operators on the semi infinite interval. The fundamental moments and central moments of the operator were obtained explicitly. These results played a central role in the analysis, since they allowed us to investigate the approximation behaviour of the operator in a systematic way. By using these moment identities, a Korovkin type convergence theorem was established. Thus, it was shown that the proposed operators

converge to the considered function uniformly on compact subsets of the interval. In addition to the qualitative convergence result, quantitative estimates were obtained by means of the usual modulus of continuity, Peetre's K-functional, and the second order modulus of smoothness. These estimates describe how the approximation error depends on the smoothness of the function and on the central moments of the operator. Furthermore, a Voronovskaya type theorem was proved, giving a more precise asymptotic description of the approximation error. The illustrative example confirmed the theoretical results. The graphs and pointwise error tables showed that the approximation becomes better as the parameter m increases. The numerical results also indicated that the parameters α, β and γ influence the local behaviour of the operator. Among them, some parameters have a stronger effect on the accuracy, while others mainly provide small corrections or stabilization. Overall, the results show that the Gauss-Appell based Szász-Durrmeyer type operators form a meaningful and effective class of positive linear approximation operators. The construction may also be extended in future studies to different polynomial families, weighted spaces, or higher dimensional settings.

REFERENCES

1. Srivastava, H. M., & Manocha, H. L. (1984). *A treatise on generating functions*. Halsted Press.
2. Dattoli, G., Khan, S., Haneef, M., & Licciardi, S. (2024). Unveiling new perspectives of hypergeometric functions using umbral techniques. *Boletín de la Sociedad Matemática Mexicana, 30*, 1–21.
3. Küçükoğlu, İ., & Şimşek, Y. (2024). Unified presentations of the generating functions for a comprehensive class of numbers and polynomials. *Montes Taurus Journal of Pure and Applied Mathematics, 6*(1), 40–63.
4. Asensi, A. G., & Varona, J. L. (2024). A general method to find special functions that interpolate Appell polynomials, with examples. *Journal of Mathematical Analysis and Applications, 531*, 127825.
5. Anshelevich, M. (2004). Appell polynomials and their relatives. *International Mathematics Research Notices, 2004*(65), 3469–3531.
6. Dattoli, G., Lorenzutta, S., Mancho, A.M., & Torre, A. (1999). Generalized polynomials and associated operational identities. *Journal of Computational and Applied Mathematics, 108*(1–2), 209–218.
7. Özarslan, M. A., & Çekim, B. (2023). Confluent Appell polynomials. *Journal of Computational and Applied Mathematics, 424*, 114984.
8. Appell, P. (1880). Sur une classe de polynômes. *Annales Scientifiques de l'École Normale Supérieure, 9*(2), 119–144.
9. Khan, S., Ahmad, U., & Haneef, M. (2025). Construction of hypergeometric-Appell polynomials family via umbral calculus framework. arXiv preprint arXiv:2504.05737.
10. Costabile, F. A., Gualtieri, M. I., & Napoli, A. (2021). General bivariate Appell polynomials via matrix calculus and related interpolation hints. *Mathematics, 9*(4), 964.
11. Altomare, F., & Campiti, M. (1994). *Korovkin-type approximation theory and its applications*. Walter de Gruyter.
12. DeVore, R. A., & Lorentz, G. G. (1993). *Constructive approximation*. Springer.

Chapter 7

Lobatto Methods: A Study of Their Stability Characteristics

Mevlüde Yakit Ongun[1]

Ceren Uysal[2]

Abstract

This chapter presents an overview of Lobatto-type Runge-Kutta schemes derived from Gauss–Lobatto quadrature formulas.Since the collocation nodes include both endpoints of the integration interval, these methods possess several advantageous stability and geometric properties.. Their key feature is that both endpoints of each integration step serve as collocation nodes. Throughout the chapter, the formulation processes, Butcher tableaus, and stability properties of five primary sub-classes (Lobatto IIIA, IIIB, IIIC, IIIC*, and Generalized Lobatto, Lobatto IIID) are detailed.

Linear stability is first examined via A-stability and L-stability. In this context, it is demonstrated that the corresponding stability functions reduce to specific Padé approximations of the exponential function. For non-linear dynamics, B-stability is analyzed. Through this analysis, The analysis reveals that: among the variants considered, only Lobatto IIIC is algebraically stable, which implies B-stability.

Furthermore, geometric integration aspects, such as symplecticity, P-stability, and energy behavior on the imaginary axis, are explored. It is established that a highly effective symplectic integrator is generated when Lobatto IIIA and IIIB methods are coupled into a partitioned system. To consolidate these theoretical derivations, visual plots of the stability regions and a comprehensive comparison table are provided at the end of the chapter.

1 Prof. Dr., Suleyman Demirel University, mevludeyakit@sdu.edu.tr, ORCID ID: 0000-0003-2363-9395

2 Stud. MSc, Graduate School of Natural and Applied Sciences, Suleyman Demirel University, yl2530110008@ogr.sdu.edu.tr, ORCID ID:0009-0007-1640-4180

https://doi.org/10.58830/ozgur.pub1361.c5497

1. Introduction

The historical foundations of modern numerical integration methods can be traced to the work of Runge at the end of the nineteenth century. Subsequent contributions by Heun, Kutta and later researchers gradually led to the development of the Runge-Kutta framework used today. By extending Euler's method, Runge derived a two-stage, second-order scheme that laid the foundation for what would later become a major class of numerical integrators. In the early 20th century, researchers such as Heun and Kutta significantly advanced these ideas, leading to the systematic construction of higher-order methods. Building on Runge's framework, Kutta's contributions were particularly influential and ultimately gave rise to what are now known as Runge-Kutta (RK) methods. During this formative period, Heun proposed a three-stage, third-order method, while Kutta introduced both a four-stage fourth-order method and a six-stage fifth-order scheme. The pursuit of improved accuracy motivated the construction of methods with increasing stage numbers, and numerous researchers contributed to this development throughout the twentieth century, with notable contributions from Nyström (in 1925), Huta (in 1956), and Butcher (in 1964), who developed seven-stage sixth-order methods. By the late 1970s, Curtis and Hairer further extended explicit Runge-Kutta constructions to as many as 18 stages.

In parallel with the development of explicit schemes, the challenge of stiff differential equations motivated the study of implicit methods. Butcher's work in 1964 provided a unifying framework for implicit Runge–Kutta schemes, forming the basis of modern solvers for stiff systems. In the 1970s, he further introduced a graph-theoretic approach based on rooted trees, which enabled a systematic characterization of order conditions and greatly simplified the construction of higher-order methods. This perspective was refined by Burrage (1978a, 1978b), who investigated stability properties and developed criteria for predicting the performance of implicit schemes under varying dynamical regimes. Later, Hairer and Wanner (1993) extended these tree-based techniques to Hamiltonian systems, opening the way for geometric numerical integration (Griepentrog,1978;Brugnano et al., 2012; Brugnano et al.,2014)

More recent investigations have extended Runge-Kutta techniques to a wide variety of applications, including differential-algebraic systems and high-order collocation methods for complex engineering models. Brugnano and Magherini (2007) applied Runge–Kutta techniques to second-order differential-algebraic equations (DAEs), while Martín-Vaquero (2010) constructed 17th-order Radau IIA methods, highlighting their effectiveness in complex mechanical systems.

Within this context, Lobatto methods represent a natural progression from classical quadrature rules to structure-preserving integrators. Originally introduced by Lobatto in the context of quadrature formulas incorporating endpoint evaluations, these methods were not fully integrated into time-stepping

frameworks until the systematic development of Runge–Kutta theory in the mid-20th century. A key milestone was the introduction of the Butcher tableau by Butcher (1964), which provided an algebraic structure for analyzing such methods. In the same period, Dahlquist (1978) introduced the concept of A-stability, which became fundamental in the analysis of stiff differential equations.

During the 1970s, attention shifted toward deeper stability properties. Ehle(1973) used Padé approximation techniques to define L-stability, offering a theoretical explanation for the stiffly accurate behavior of Lobatto IIIC methods. Subsequent work by Hairer, Lubich, and Roche (1989) established the relevance of these methods for differential-algebraic equations. This line of research culminated in the comprehensive treatment by Hairer and Wanner (1996), who formalized concepts such as B-stability and algebraic stability. More recently, Hairer, Lubich, and Wanner (2006) developed the framework of geometric numerical integration, showing that Lobatto IIIA and IIIB methods form a symplectic pair capable of preserving geometric properties such as energy behavior in Hamiltonian systems.

Overall, the evolution of Lobatto methods reflects their transformation from classical quadrature-based constructions into a powerful family of structure-preserving integrators. Today, they play a central role in the numerical treatment of stiff ODEs, differential-algebraic systems, and long-time simulations in areas such as celestial mechanics and Hamiltonian dynamics. (Boscarino,2007; Boscarino,2009)

2. Preliminaries

In many scientific and engineering applications, when the integrand is complex or known only at discrete points, analytical integration becomes impractical. Consequently, Numerical methods have therefore been developed to approximate integrals to within error tolerance (Burden & Faires, 2011).

The following standard quadrature rules provide background for the structural and stability analysis of Lobatto methods in later sections.

For equal subinterval $\Delta x = (b-a)/n$

Rectangle Rule:

$$I = \int_a^b f(x)dx \cong \Delta x \sum_{j=1}^{n} f(x_j)$$

Trapezoidal Rule:

$$I = \int_a^b f(x)dx \cong \frac{\Delta x}{2}\left[f(a) + f(b) + 2\sum_{j=1}^{n-1} f(a + j\Delta x)\right]$$

Simpson's 1/3 Rule:

$$I = \int_a^b f(x)dx \cong \frac{\Delta x}{3}\left[f(a) + f(b) + 4\sum_{\substack{j=1 \\ j=Tek}}^{n-1} f(a + j\Delta x) + 2\sum_{\substack{j=2 \\ j=Çift}}^{n-2} f(a + j\Delta x)\right]$$

Simpson's 3/8 Rule:

$$I = \int_a^b f(x)dx \cong \frac{3}{8}\Delta x\left[f(a) + f(b) + 3\sum_{\substack{j=1 \\ j=1,2,4,5,7,8,..}}^{n-1} f(a + j\Delta x) + 2\sum_{\substack{j=3 \\ j=3,6,9,..}}^{n-3} f(a + j\Delta x)\right]$$

Gauss–Legendre Quadrature:

$$I = \int_{-1}^{1} f(x)dx \cong \sum_{i=1}^{n} f(x_i)\, w_i$$

where the nodes x_i are the roots of the Legendre polynomials and w_i are the corresponding weight coefficients (Bulirsch et al, 2000;Süli, Mayers, 2003; Atkinson et.al, 2008,2009; Ranocha et al, 2020).

2.1 High-order Implicit Runge-Kutta(IRK) Methods and Butcher Tableau

Implicit Runge-Kutta schemes constitute one of the most powerful approaches for solving ordinary differential equations when stability requirements are dominant.. The coefficients defining an (s)-stage Runge-Kutta method are conveniently summarized by the Butcher tableau, which serves as a standard tool for the formulation and analysis of these methods. Different choices of nodes and coefficients give rise to various subclasses of implicit Runge-Kutta schemes. Among these subclasses, Lobatto methods form an important family based on Gauss–Lobatto quadrature formulas and are characterized by the inclusion of both endpoints of the integration interval as collocation points. (Hairer, Nørsett & Wanner (1993); Iserles (2009); (Kahaner, 1989))

$$\text{Let } \; y \in \mathbb{R}^d, f: \mathbb{R} \times \mathbb{R}^d \to \mathbb{R}^d, \; y' = f\big(x, y(x)\big), \; y(x_0) = y_0 \; for \; x \geq x_0 \quad (2.1)$$

initial value problem for a first-order ordinary differential equation. For the numerical solution of this initial value problem , some commonly utilized implicit Runge-Kutta methods are: Backward Euler Method, Implicit Midpoint Method, Crank-Nicolson Method, Gauss-Legendre Method, Diagonally Implicit

Runge-Kutta (DIRK) Methods, Lobatto IIIB Method, Lobatto IIIC Method, Lobatto IIIC* Method, Generalized Lobatto Method (Burden&Faires,2011).

The s-stage Runge-Kutta method $y_{n+1} \approx y(t_n + h)$ from $y_n \approx y(t_n)$ using the following formulas

$$k_i = y_n + h\sum_{j=1}^{s} a_{ij}\, f\big(t_n + c_j h, k_j\big), \quad (1 \le i \le s)$$

$$y_{n+1} = y_n + h\sum_{i=1}^{s} b_i f(t_n + c_i h, k_i)$$

where s, denotes the number of stages, a_{ij} represent the internal stage coefficients, b_i denote the weights, and c_i denote the abscissae (Butcher, 1964;Prince,Dormand,1981; Pareschi, Russo,2001; Iserles, 2009; Liu,Sun, 2005).

Figure 1: The Butcher tableau for the Runge-Kutta methods (Butcher, 1964)

0					
c_2	a_{21}				
c_3	a_{31}	a_{32}			
$\vdots$	$\vdots$				
c_s	a_{s1}	a_{s2}	$\cdots$	a_{ss-1}	
	b_1	b_2	$\cdots$	b_{s-1}	b_s

The significance of these simplifying assumptions can be traced back to a result obtained by Butcher. The coefficients a_{ij}, c_j and b_j by which the s-stage Runge-Kutta methods are defined, are presented in the Butcher tableau as shown below.

$$\begin{array}{c|c} \boldsymbol{c} & \boldsymbol{A} \\ \hline & \boldsymbol{b}^{\mathrm{T}} \end{array} = \begin{array}{c|ccc} c_1 & a_{11} & \cdots & a_{1s} \\ \vdots & \vdots & \ddots & \vdots \\ c_s & a_{s1} & \cdots & a_{ss} \\ \hline & b_1 & \cdots & b_s \end{array}$$

Figure 2: The Butcher Tableau for s-stage Runge-Kutta method (Butcher, 1964;Liu & Sun,2005)

For consistency, the row-sum condition $c_i = \sum_{j=1}^{s} a_{ij}$ is usually imposed. If $a_{ij} = 0$ for all $j \geq i$, the method is explicit; otherwise it is implicit**.**

3. Lobatto Methods

Among the family of Runge-Kutta algorithms, Lobatto methods represent a particularly important subclass in the numerical treatment of differential equations. These schemes are also commonly known as Gauss-Lobatto formulas (Boscarino et al., 2015). A key feature of Lobatto methods is that the two ends of the interval serve as collocation points; this arrangement makes it possible to achieve high-order accuracy without sacrificing robust stability. This balance of accuracy and stability has made Lobatto methods widely used in engineering, physics, and applied mathematics. The literature recognizes several distinct subfamilies Lobatto IIIA, IIIB, IIIC, and IIIC*-each offering its own set of numerical characteristics, and all of them are classified as implicit Runge-Kutta methods.

Gauss–Lobatto formulas: The approximation employed for the solution of the problem (2.1) can be expressed by means of a standard quadrature formula in the form

$$\int_{t_n}^{t_n+h} f(t)dt \approx h_n \left(\sum_{i=1}^{s} b_i f(t_n + c_i h_n) \right).$$

where the step size is denoted by h_n , the weight coefficients by $b_1, \dots, b_s$ and the node coefficients by $c_1, \dots, c_s$.

Lobatto quadrature formulas (Gauss-Lobatto formulas) are defined for $s \geq 2$ by a construction that meets a prescribed set of node and weight conditions. The nodes c_i are taken as the roots of the polynomial

$$\frac{d^{s-2}}{dt^{s-2}}(t^{s-1}(1-t)^{s-1}).$$

and they are ordered so that the condition $c_1 = 0 < c_2 < \cdots < c_s = 1$ is satisfied. The weights and nodes together fulfill the requirement:

$$B(p): \sum_{i=1}^{s} b_i c_i^{k-1} = \frac{1}{k}, \qquad k = 1, \dots, p$$

Lobatto quadrature formulas possess a symmetric structure, i.e.,

$b_{s+1-j} = b_j, \quad c_{s+1-j} = 1 - c_j$ (Jay, 1996; Jay,2015).

3.1 The Lobatto Subfamilies

For a fixed number of stages s, nodes c_j and the weights b_j of the associated Lobatto quadrature formula are shared across the various Lobatto families. Consequently, these families are distinguished exclusively by their internal stage coefficients a_{ij}. While several equivalent definitions of these families exist in

the literature, their coefficients a_{ij} can be explicitly specified through simplifying assumptions in a linearly implicit form:

$$C(q): \sum_{j=1}^{s} a_{ij} c_j^{k-1} = \frac{c_i^k}{k}$$

$$D(r): \sum_{i=1}^{s} b_i c_i^{k-1} a_{ij} = \frac{b_j}{k}\left(1 - c_j^k\right)$$

Lobatto IIIA:

The Lobatto IIIA method is a three-stage Lobatto method. By this method, the values of the function are estimated at three points within the interval, with the endpoints of the interval also being included. The Lobatto IIIA method is symmetric, and its order is $2s - 2$.

$$Y_{n2} = \frac{1}{2}(y_n + y_{n+1}) + \frac{h_n}{8}(f(t_n, y_n) - f(t_{n+1}, y_{n+1}))$$

$$y_{n+1} = y_n + \frac{h_n}{6}(f(t_n, y_n) + 4f(t_{n+1}, Y_{n2}) + f(t_{n+1}, y_{n+1}))$$

where $t_{n+1/2} = t_n + h_{n/2}$.

Figure 3: The Butcher Tableau for s = 2,3,4,5 (Jay,2015)

$$\begin{array}{c|cc} 0 & 0 & 0 \\ 1 & \frac{1}{2} & \frac{1}{2} \\ \hline A_{s=2} & \frac{1}{2} & \frac{1}{2} \end{array} \qquad \begin{array}{c|ccc} 0 & 0 & 0 & 0 \\ \frac{1}{2} & \frac{5}{24} & \frac{1}{3} & -\frac{1}{24} \\ 1 & \frac{1}{6} & \frac{2}{3} & \frac{1}{6} \\ \hline A_{s=3} & \frac{1}{6} & \frac{2}{3} & \frac{1}{6} \end{array}$$

$$\begin{array}{c|cccc} 0 & 0 & 0 & 0 & 0 \\ \frac{1}{2}-\frac{\sqrt{5}}{10} & \frac{11+\sqrt{5}}{120} & \frac{25-\sqrt{5}}{120} & \frac{25-13\sqrt{5}}{120} & \frac{-1+\sqrt{5}}{120} \\ \frac{1}{2}+\frac{\sqrt{5}}{10} & \frac{11-\sqrt{5}}{120} & \frac{25+13\sqrt{5}}{120} & \frac{25+\sqrt{5}}{120} & \frac{-1-\sqrt{5}}{120} \\ 1 & \frac{1}{12} & \frac{5}{12} & \frac{5}{12} & \frac{1}{12} \\ \hline A_{s=4} & \frac{1}{12} & \frac{5}{12} & \frac{5}{12} & \frac{1}{12} \end{array}$$

$$\begin{array}{c|ccccc} 0 & 0 & 0 & 0 & 0 & 0 \\ \frac{1}{2}-\frac{\sqrt{21}}{14} & \frac{119+3\sqrt{21}}{1960} & \frac{343-9\sqrt{21}}{2520} & \frac{392-96\sqrt{21}}{2205} & \frac{343-69\sqrt{21}}{2520} & \frac{-21+3\sqrt{21}}{1960} \\ \frac{1}{2} & \frac{13}{320} & \frac{392+105\sqrt{21}}{2880} & \frac{8}{45} & \frac{392-105\sqrt{21}}{2880} & \frac{3}{320} \\ \frac{1}{2}+\frac{\sqrt{21}}{14} & \frac{119-3\sqrt{21}}{1960} & \frac{343+69\sqrt{21}}{2520} & \frac{392+96\sqrt{21}}{2205} & \frac{343+9\sqrt{21}}{2520} & \frac{-21-3\sqrt{21}}{1960} \\ 1 & \frac{1}{20} & \frac{49}{180} & \frac{16}{45} & \frac{49}{180} & \frac{1}{20} \\ \hline A_{s=5} & \frac{1}{20} & \frac{49}{180} & \frac{16}{45} & \frac{49}{180} & \frac{1}{20} \end{array}$$

Lobatto IIIB

The coefficients of the Lobatto IIIB, a_{ij}^B are defined through the simplifying assumption $D(r)$. These methods are required to satisfy the condition $C(q-2), a_{i1}^B = b_1, a_{is}^B = 0$. They are symmetric, and their order is $2s - 2$. The

coefficients of the method can also be derived from the coefficients of Lobatto IIIA by means of the following relations:

$$a_{ij}^{B} b_i + a_{ji}^{A} b_j - b_j b_i = 0$$

or

$$a_{ij}^{B} = b_j - a_{s+1-i,s+1-j}^{A}$$

Figure 4: The Butcher Tableau for s = 2,3,4,5 (Jay,2015)

$$\begin{array}{c|cc} 0 & \frac{1}{2} & 0 \\ 1 & \frac{1}{2} & 0 \\ \hline B_{s=2} & \frac{1}{2} & \frac{1}{2} \end{array} \qquad \begin{array}{c|ccc} 0 & \frac{1}{6} & -\frac{1}{6} & 0 \\ \frac{1}{2} & \frac{1}{6} & \frac{1}{3} & 0 \\ 1 & \frac{1}{6} & \frac{5}{6} & 0 \\ \hline B_{s=3} & \frac{1}{6} & \frac{2}{3} & \frac{1}{6} \end{array}$$

$$\begin{array}{c|cccc} 0 & \frac{1}{12} & \frac{-1-\sqrt{5}}{24} & \frac{-1+\sqrt{5}}{24} & 0 \\ \frac{1}{2}-\frac{\sqrt{5}}{10} & \frac{1}{12} & \frac{25+\sqrt{5}}{120} & \frac{25-13\sqrt{5}}{120} & 0 \\ \frac{1}{2}+\frac{\sqrt{5}}{10} & \frac{1}{12} & \frac{25+13\sqrt{5}}{120} & \frac{25-\sqrt{5}}{120} & 0 \\ 1 & \frac{1}{12} & \frac{11-\sqrt{5}}{24} & \frac{11+\sqrt{5}}{24} & 0 \\ \hline B_{s=4} & \frac{1}{12} & \frac{5}{12} & \frac{5}{12} & \frac{1}{12} \end{array}$$

$$\begin{array}{c|ccccc} 0 & \frac{1}{20} & \frac{-7-\sqrt{21}}{120} & \frac{1}{15} & \frac{-7+\sqrt{21}}{120} & 0 \\ \frac{1}{2}-\frac{\sqrt{21}}{14} & \frac{1}{20} & \frac{343+9\sqrt{21}}{2520} & \frac{56-15\sqrt{21}}{315} & \frac{343-69\sqrt{21}}{2520} & 0 \\ \frac{1}{2} & \frac{1}{20} & \frac{49+12\sqrt{21}}{360} & \frac{8}{45} & \frac{49-12\sqrt{21}}{360} & 0 \\ \frac{1}{2}+\frac{\sqrt{21}}{14} & \frac{1}{20} & \frac{343+69\sqrt{21}}{2520} & \frac{56+15\sqrt{21}}{315} & \frac{343-9\sqrt{21}}{2520} & 0 \\ 1 & \frac{1}{20} & \frac{119-3\sqrt{21}}{360} & \frac{13}{45} & \frac{119+3\sqrt{21}}{360} & 0 \\ \hline B_{s=5} & \frac{1}{20} & \frac{49}{180} & \frac{16}{45} & \frac{49}{180} & \frac{1}{20} \end{array}$$

Lobatto IIIC

The coefficients of the Lobatto IIIC satisfy the conditions

$$a_{i1}^{C} = b_1, \;\; C(q-1), \qquad D(r-1), \qquad a_{sj}^{C} = b_j$$

The order of this method is $2s-2$. It is not symmetric. The formula for Lobatto IIIC methods is expressed as follows:

$$y_{n+1} = y_n + h \sum_{i=1}^{s} b_i k_i$$

$$k_i = f(t_n + c_i h, y_n + h \sum_{j=1}^{s} a_{ij} k_j)$$

Figure 5: The Butcher Tableau for s = 2,3,4,5 için Butcher tablosu (Jay,2015)

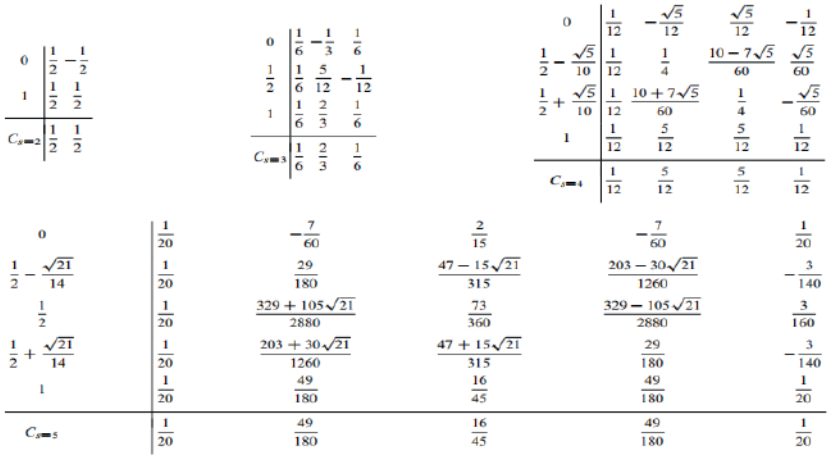

Lobatto IIIC*

The coefficients of the Lobatto IIIC* can be defined in the form a_{ij}^{C*}. The simplifying condition . $C(q-1)$ is satisfied by these methods. The order of this method is $2s-2$. It is not symmetric. The formula for the Lobatto IIIC* methods is expressed as follows:

$$a_{ij}^{C^*} b_i + a_{ji}^{C} b_j - b_j b_i = 0$$

or

$$a_{ij}^{C^*} = b_j - a_{s+1-i,s+1-j}^{C}, \;\; i,j = 1,2,\dots,s$$

Figure 6: The Butcher Tableau for s = 2,3,4,5 için Butcher tablosu (Jay,2015)

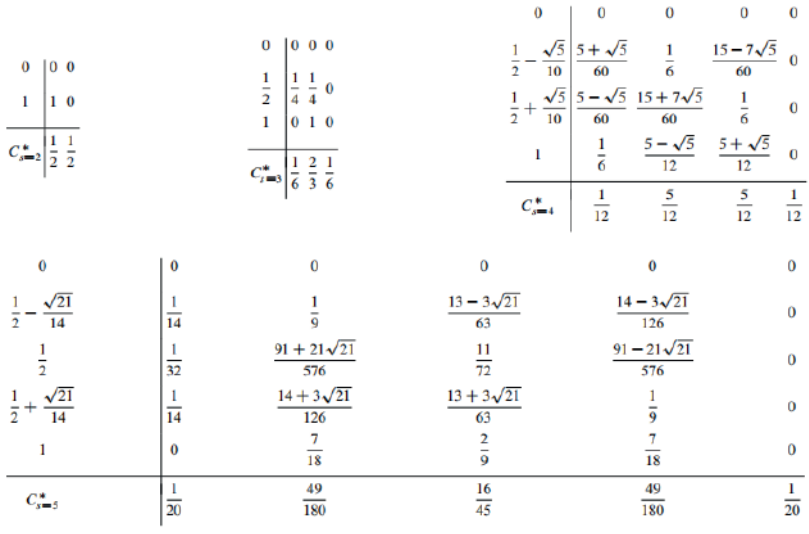

Generalized Lobatto:

Generalized Lobatto methods constitute a consistent and efficient class of methods that can be applied to numerical solution problems. The formula of the generalized Lobatto methods is expressed as follows:

$$a_{ij}^{S}\left(\frac{1}{2}\right) = \frac{1}{2}\left(a_{ij}^{A} + a_{ij}^{B}\right) \qquad i,j = 1,\dots,s$$

For particular parameter selections, generalized Lobatto methods reduce to well-known classical Lobatto schemes such as Lobatto IIID

$$a_{ij}^{D} = a_{ij}^{S}(1) = \frac{1}{2}\left(a_{ij}^{C} + a_{ij}^{C^*}\right) \quad i,j = 1,\dots,s$$

Figure 7: The coefficients of Lobatto III-NW for s = 2, 3 (Butcher, 1964)

$$\begin{array}{c|cc} 0 & \frac{1}{2} & \frac{1}{2} \\ 1 & -\frac{1}{2} & \frac{1}{2} \\ \hline & \frac{1}{2} & \frac{1}{2} \end{array} \qquad \begin{array}{c|ccc} 0 & \frac{1}{6} & 0 & -\frac{1}{6} \\ \frac{1}{2} & \frac{1}{12} & \frac{5}{12} & 0 \\ 1 & \frac{1}{2} & \frac{1}{3} & \frac{1}{6} \\ \hline & \frac{1}{6} & \frac{2}{3} & \frac{1}{6} \end{array}$$

3.2 Stability properties

Lobatto methods belong to the class of high-order implicit Runge-Kutta methods, and among their most critical attributes is stability. To investigate the stability properties of a Runge–Kutta method, the Dahlquist test equation is conventionally employed:

$$y' = \lambda y$$

where $\lambda \in \mathbb{C}$ and the quantity $z = h\lambda$ is introduced. For a general *s*-stage Runge-Kutta method, the stability function takes the form

$$R(z) = zb^{T}(I - zA)^{-1}e{+}1$$

in which *A* denotes the coefficient matrix of the method, *b* is the weight vector, and $e = (1,\dots,1)^{T}$ is the vector.

Definition 3.2.1 (Absolute Stability) The stability region of a numerical method is defined as the set

$$S = \{z \in \mathbb{C} : |R(z)| \leq 1\}$$

For all values of z that lie within this region, the growth of the numerical solution is prevented, and stable behavior of the method is ensured (Lambert, 1991).

Definition 3.2.2 (A-Stability) A numerical method is called A-stable if its region of absolute stability contains the entire left half of the complex plane, i.e. if the set inclusion

$$\{z \in \mathbb{C} : Re(z) \leq 0\} \subseteq S$$

is satisfied. Equivalently, the stability function must satisfy

$$|R(z)| \leq 1. \qquad Re(z) \leq 0$$

(Hairer, Nørsett, and Wanner, 1993).

Definition 3.2.3 (L-Stability). A method is called L-stable if it is A-stable and, in addition, the condition

$$\lim_{z \to -\infty} R(z) = 0$$

is satisfied (Hairer, Wanner,,1996).

Definition 3.2.4 (B-stability) A numerical method is called B-stable if, for any system for which the inner-product condition

$$\langle f(u) - f(v), u - v \rangle \leq 0$$

is satisfied, the contractivity property

$$\|y_{n+1} - \widetilde{y_{n+1}}\| \leq \|y_n - \widetilde{y_n}\|$$

holds for any two numerical solutions $\{y_n\}$ and $\{\widetilde{y_n}\}$. In other words, it may be expressed equivalently as the condition that the separation between any two numerical solution trajectories is non-increasing throughout the integration interval. (Butcher, 2016).

Definition 3.2.5 (Algebraic stability) In the context of a Runge–Kutta method, let the weights satisfy $b_i \geq 0 \quad (i = 1,2,..,s)$ and let the matrix $M = (m_{ij})$ be defined by

$$m_{ij} = a_{ij}b_i + a_{ji}b_j - b_jb_i.$$

If M is positive semi-definite ($M \geq 0$), the method is called to be algebraically stable (Hairer and Wanner, 1996).

Definition 3.2.6 (AN-stability) A method is called AN-stable if its stability region, while not necessarily covering the entire left half-plane, contains the sector

$$\{z : |\arg(-z)| \leq \alpha\}$$

for some angle $0 < \alpha < 90^o$. In the special case $\alpha = 90^o$, A-stability is recovered (Butcher, 2016).

Definition 3.2.7 (G-stability) A numerical method is called G-stable if there exists a symmetric positive-definite matrix $G = G^T > 0$ such that, in the G-norm $\|y\|_G = \sqrt{y^T Gy}$, the inequality

$$\|y_{n+1}\|_G \leq \|y_n\|_G$$

holds for all numerical solutions (Dahlquist, 1978).

Definition 3.2.8 (Zero-stability). Let the characteristic polynomial be denoted by $\rho(r)$ and suppose that $\rho(r) = 0$. A method is zero-stable if all roots r_i satisfy $|r_i| \leq 1$ and any root for which $|r_i| = 1$ is simple (Lambert,1991).

Definition 3.2.9 (P-stability) A method is called P-stable if, when applied to the oscillator equation $y'' + \omega 2y = 0y'' + \omega 2y = 0$, no artificial numerical damping occurs, i.e., $| R(iy) | = 1$ for all real y (Hairer & Wanner, 1996).

Definition3.2.10 (Padé Approximation) The Padé approximant of order (p, q) to the exponential function e^z is the unique rational function

$$R_{p,q}(z) = \frac{N_{p,q}(z)}{D_{p,q}(z)} = \frac{\sum_{k=0}^{p} z^k \alpha_k}{\sum_{k=0}^{q} z^k \beta_k}$$

where $\beta_0 = 1$, such that, satisfying the interpolation condition

$$e^z - R_{p,q}(z) = O(zp + q + 1), \quad z \to 0.$$

The coefficients are given explicitly by

$$\alpha_k = \frac{(p+q-k)!p!}{(p+q)!k!(p-k)!}, \quad \beta_k = \frac{(p+q-k)!q!}{(p+q)!k!(q-k)!}$$

(Hairer & Wanner, 1996).

Definition3.2.11 (Absolute Stability Boundary) For a given Lobatto method, the absolute stability boundary is defined by the relation $|R(z)| = 1$. The stability region is the set of all points satisfying the condition $|R(z)| \leq 1$. For instance, in the case of the three-stage Lobatto IIIA, IIIB, and IIIC, generalized Lobatto and LobattoIIID methods, the stability function is given by

$$R_{IIIA}(z) = R_{IIIB}(z) = \frac{\frac{1}{12}z^2 + \frac{1}{2}z + 1}{\frac{1}{12}z^2 - \frac{1}{2}z + 1},$$

$$R_{IIIC}(z) = \frac{\frac{1}{2}z + 1}{\frac{1}{6}z^2 - \frac{1}{2}z + 1}$$

$$R_{IIIC^*}(z) = \frac{1}{R_{IIIC}(-z)} = \frac{\frac{1}{6}z^2 + \frac{1}{2}z + 1}{-\frac{1}{2}z + 1}$$

$$R_{GL}(z) = R_{IIID}(z) = \frac{\frac{1}{12}z^2 + \frac{1}{2}z + 1}{\frac{1}{12}z^2 - \frac{1}{2}z + 1}$$

(Dahlquist, 1978; Hairer,, Wanner, 1996; Butcher, 2016).

For the three-stage case, Lobatto IIIA, IIIB and IIID share the same stability function, whereas Lobatto IIIC possesses a distinct stability function associated with its stiffly accurate structure. Generalized Lobatto methods do not admit a unique stability function, since their properties depend on the specific parameter selection.

Table 1. Comparison of Stability and Geometric Properties of Lobatto Families

Property	**IIIA**	**IIIB**	**IIIC**	**IIIC***	**IIID**	**Generalized Lobatto**	
Implicit Method	Yes	Yes	Yes	Yes	Yes	Yes	16,17,23,27,32
Symmetric	Yes	Yes	No	No	No	Parameter-dependent	17,24,25,28
Order (s-stage)	2s−2	2s−2	2s−2	2s−2	2s−2	Depends on construction	15,17,24,28,32
A-Stable	Yes	Yes	Yes	Yes	Yes	Usually Yes	16,17,19,20,23,24
L-Stable	No	No	Yes	No	No	Parameter-dependent	17,20,24,32
AN-Stable	Yes	Yes	Yes	Yes	Yes	Usually Yes	6,17,24
Zero-Stable	Yes	Yes	Yes	Yes	Yes	Yes	11,17,23,31
B-Stable	No	No	Yes	No	Generally no	Parameter-dependent	17,20,24
Algebraically Stable	No	No	Yes	No	Generally no	Parameter-dependent	17,20,24
G-Stable	Yes	Yes	Yes	Generally No	Yes	Parameter-dependent	17,18,23,24
P-Stable	Generally no	Generally no	Generally no	Generally no	Generally no	Usually No	6,17,24
Stiffly Accurate	No	No	Yes	No	Yes	Parameter-dependent	17,20,24,32
Symplectic (single method)	No	No	No	No	No	Parameter-dependent	17,23,25
Symplectic Pair	IIIA–IIIB	IIIA–IIIB	None	None	None	Possible	17,23,25,28
Energy Behavior	Good	Good	Strong damping	Dissipative	Good damping	Parameter-dependent	17,23,24,25
Imaginary-Axis Behavior	Nearly conservative	Nearly conservative	Damped	Damped	Moderately damped	Parameter-dependent	17,18,24,25
High-Frequency Damping	Weak	Weak	Strong	Moderate	Strong	Parameter-dependent	17,20,23,24
Suitable for Stiff ODEs	Moderate	Moderate	Excellent	Moderate	Excellent	Depends on parameters	17,20,24,32
Suitable for DAEs	Good	Moderate	Excellent	Moderate	Excellent	Depends on formulation	17,20,24,32
Suitable for Hamiltonian Systems	Via IIIA–IIIB pair	Via IIIA–IIIB pair	Limited	Limited	Limited	Possible	17,23,25,28
Boundary Value Problems	Excellent	Good	Excellent	Good	Excellent	Excellent	1,17,23,24
Typical Applications	Collocation methods	Partitioned systems	Stiff systems and DAEs	Specialized IRK methods	DAEs and stiff problems	Problem-dependent	6,17,23,24, 25,28,29,32

3.3 Lobatto Families and Absolute Stability Regions

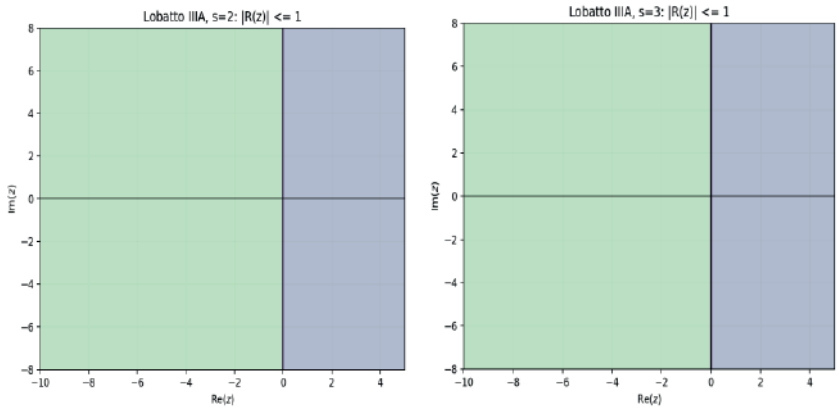

Figure 8: Absolute stability regions for Lobatto IIIA method for s=2 (left) and s=3 (right)

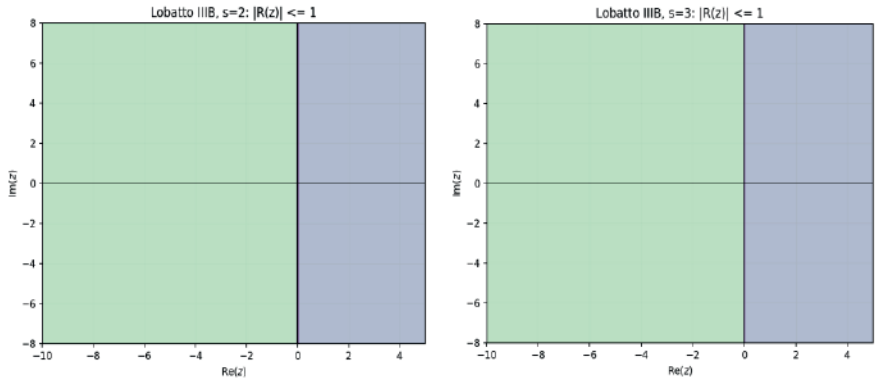

Figure 9: Absolute stability regions for Lobatto IIIB method for s=2 (left) and s=3 (right)

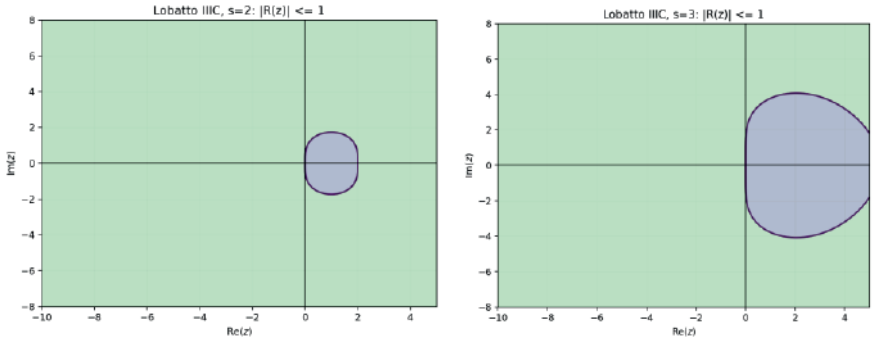

Figure 10: Absolute stability regions for Lobatto IIIC method for s=2 (left) and s=3 (right)

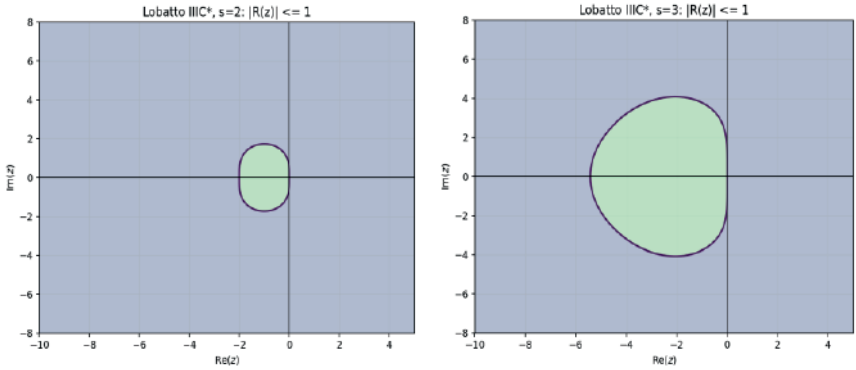

Figure 11: Absolute stability regions for Lobatto IIIC* methods with s=2 (left) and s=3 (right)

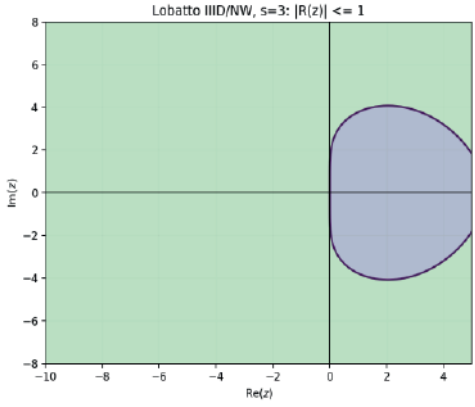

Figure 12: Absolute stability regions for Lobatto IIID/Nørsett-Wanner method for s=3

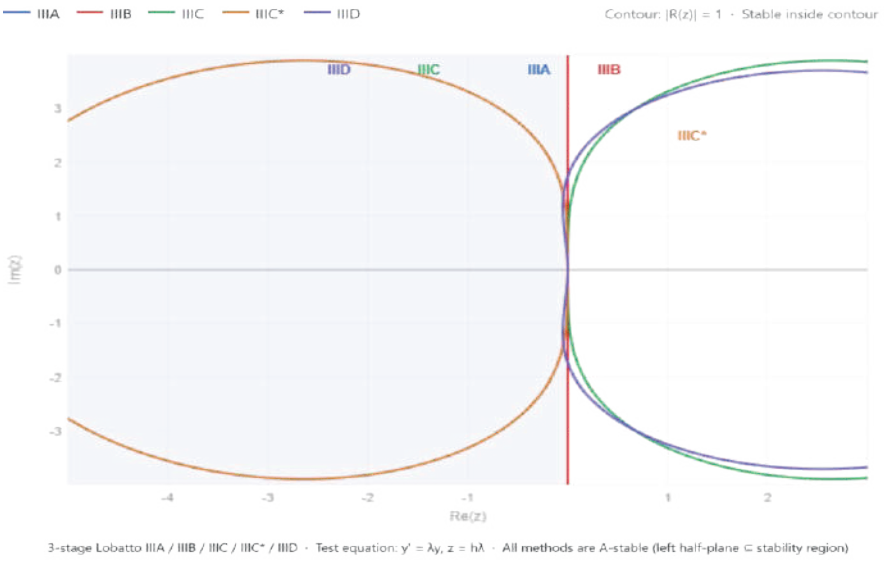

Figure 13: Absolute stability regions of the 3-stage Lobatto IIIA, IIIB, IIIC, IIIC*, and IIID methods

All figures were generated using the Maple software package. As observed in Figure $8-13$, the shaded regions show where $|R(z)| \leq 1$ in the absolute stability plots. Since . $z = h\lambda$ is defined, the point is shifted to the left as either the step size h is increased or λ becomes more negative. Because large negative real values are of primary concern in stiff problems, the behavior within the left half-plane is considered the deciding factor.

In the plots for the Lobatto IIIA and IIIB methods, the left half-plane is fully contained within the stability region; thus, A-stability is implied. However, it is noted that as $|z| \to \infty$ along the negative real axis, $R(z)$ is not driven to zero. Consequently, very stiff modes are not completely suppressed. In the diagrams, this is evidenced by the fact that the method's stability function is shown to approach a magnitude of 1 at infinity, even though the negative real axis remains within the stable region.

In the case of Lobatto IIIC and IIID/NW plots, the behavior $R(z) \to 0$ is observed along the negative real axis. Through this property, stiff modes are suppressed more effectively by these methods. This feature is particularly advantageous for parabolic-type or strongly dissipative systems, allowing more reliable integration with large step sizes.

4. Conclusion

Ordinary differential equations (ODEs) provide a fundamental framework for modeling dynamical systems across a multitude of scientific and engineering disciplines Since analytical solutions are rarely available for such systems, robust numerical methods have become essential in computational mathematics. These methods approximate the solution at discrete nodes over a given interval. The goal is to capture the continuous behavior of the system as accurately as possible. Among the most prevalent numerical frameworks utilized to achieve this are the Runge-Kutta (RK) algorithms. While explicit RK schemes offer computational efficiency for non-stiff problems, the presence of stiff systems stiff systems, characterized by widely separated time scales, require implicit methods mandates the deployment of implicit methods to ensure stability without the computational burden of prohibitively small step sizes. Within the broader class of implicit Runge-Kutta (IRK) schemes, collocation-based methods are distinguished by high-order accuracy coupled with a continuous representation of the analytical solution. Grounded in Gauss-Lobatto quadrature, the Lobatto family occupies a particularly prominent position within this collocation framework. The distinct mathematical signature of Lobatto methods is the explicit requirement that the interpolating polynomial strictly satisfies the differential equation at both the initial and final boundaries of the integration step, formally defined by setting the collocation nodes to $c_1 = 0$ and $c_s = 1$. Because of this deliberate endpoint inclusion, some members of the Lobatto family possess additional properties such as stiff accuracy and enhanced continuity and global continuity, which is particularly useful for boundary value problems and optimal control. Consequently, the distinct subfamilies, namely Lobatto IIIA, IIIB, IIIC, and IIIC*, exhibit a rich spectrum of stability profiles, ranging from the purely A-stable and good geometric properties of the IIIA class to the rigorously L-stable and strongly damped behavior of the IIIC variant.

References

1. Ascher, U. M., Ruuth, S. J., & Wetton, B. T. (1995). Implicit-explicit methods for time-dependent partial differential equations. SIAM Journal on Numerical Analysis, 32(3), 797-823.
2. Atkinson, E., Han, W. ve Stewart, D. (2008). Numerical Solution of Ordinary Differential Equations, 2.Baskı, John Wiley&Sons, New Jersey.
3. Atkinson, K.E., Han W and Stewart D.E., 2009, Numerical Solution of Ordinary Differential Equations, Towa City, IA, 95-109.
4. Boscarino, S. 2007. Error analysis of IMEX Runge-Kutta methods derived from differential-algebraic systems. SIAM Journal on Numerical Analysis, 45(4), 1600-1621.
5. Boscarino, S. 2009. On an accurate third order implicit-explicit Runge-Kutta method for stiff problems. Applied Numerical Mathematics, 59(7), 1515-1528.
6. Boscarino, S., Bürger, R., Mulet, P., Russo, G., & Villada, L. M. 2015. Linearly implicit IMEX Runge-Kutta methods for a class of degenerate convection-diffusion problems. SIAM Journal on Scientific Computing, 37(2), B305-B331.
7. Brugnano, L., & Magherini, C. (2007). Blended implicit methods for solving ODE and DAE problems, and their extension for second-order problems. Journal of computational and applied mathematics, 205(2), 777-790.
8. Brugnano, L., Iavernaro, F., & Trigiante, D. 2012. Energy- and quadratic invariants–preserving integrators based upon Gauss collocation formulae. SIAM Journal on Numerical Analysis, 50(6), 2897–2916.
9. Brugnano, L., & Sun, Y. 2014. Multiple invariants conserving Runge-Kutta type methods for Hamiltonian problems. Numerical Algorithms, 65(3), 611–632.
10. Bulirsch, R., & Stoer, J. 2000. Introduction to numerical analysis. Springer-Verlag.
11. Burden, R.L., Fairs, J.D. 2010. Numerical Analysis. 9th Edition, Boston, MA: Brooks/Cole, Cengage Learning.
12. Burden, R. L., & Faires, J. D. (2011). Numerical differentiation & integration numerical differentiation I. Numerical analysis, 174-184.
13. Burrage, K. (1978a). Stability and efficiency properties of implicit Runge-Kutta methods. Bulletin of the Australian Mathematical Society, 19(2), 297-298.
14. Burrage, K. (1978b). A special family of Runge-Kutta methods for solving stiff differential equations. BIT Numerical Mathematics, 18(1), 22-41.
15. Butcher, J. C. 1987. The numerical analysis of ordinary differential equations I: Runge-Kutta and general linear methods. John Wiley & Sons.

16. Butcher, J. C. 1964. On Runge-Kutta processes of higher order, Journal of the Australian Mathematical Society, 4(2), 179-197.
17. Butcher, J.C., 2016. Numerical Methods for Ordinary Differential Equations, 3rd ed., John Wiley and Sons, Chichester.
18. Dahlquist, G. (1978). G-stability is equivalent to A-stability. BIT Numerical Mathematics, 18(4), 384-401.
19. Ehle, B. L. (1973). A-stable methods and Padé approximations to the exponential. SIAM Journal on Mathematical Analysis, 4(4), 671-680.
20. Frank, R., Schneid, J., & Ueberhuber, C. W. (1985). Stability properties of implicit Runge– Kutta methods. SIAM journal on numerical analysis, 22(3), 497-514.
21. Griepentrog, E., 1978, Gemischte Runge-Kutta-Verfahren für steife Systeme (Mixed Runge-Kutta Methods for Stiff Systems), Seminarberichte, vol. 11, Sektion Mathematik, Humboldt Universität, Berlin, pp. 19–29, in German.
22. Hairer, E., Lubich, C., & Roche, M. (1989). Error of Rosenbrock methods for stiff problems studied via differential algebraic equations. BIT Numerical Mathematics, 29(1), 77-90.
23. Hairer, E. Nørsett, S.P. Wanner, G. 1993. Solving Ordinary Differential Equations, I: Nonstiff Problems, 2 ed., Springer-Verlag, Berlin.
24. Hairer, E., & Wanner, G. 1996. Solving ordinary differential equations. II (2nd ed.). Springer Series in Computational Mathematics, 14. Berlin: Springer-Verlag.
25. Hairer, E., Lubich, C., & Wanner, G. 2006. Geometric numerical integration (2nd ed.). Springer Series in Computational Mathematics, 31. Berlin: Springer-Verlag.
26. Hairer, E., Wanner, G., & Nørsett, S. P. (1993). Solving ordinary differential equations I: Nonstiff problems. Berlin, Heidelberg: Springer Berlin Heidelberg.
27. Iserles, A. (2009). A first course in the numerical analysis of differential equations (No. 44). Cambridge university press.
28. Jay, L. O. (1996). Lobatto methods. chemistry, 29, 298-305.
29. Jay, L. O. (2015). Lobatto methods. Department of Mathematics, The University of Lowa, Lowa City, USA.
30. Kahaner, D., Moler, C., & Nash, S. (1989). Numerical methods and software. Prentice-Hall, Inc..
31. Lambert, J.D. (1991) Numerical Methods for Ordinary Differential Systems: The Initial Value Problem. John Wiley & Sons, Inc., Hoboken, Chapter 2, 21-44.
32. Liu, H., & Sun, G. (2005). Implicit Runge–Kutta methods based on Lobatto quadrature formula. International Journal of Computer Mathematics, 82(1), 77-88.

33. Martín-Vaquero, J. (2010). A 17th-order Radau IIA method for package RADAU. Applications in mechanical systems. Computers & Mathematics with Applications, 59(8), 2464-2472.
34. Pareschi, L., & Russo, G. 2001. Implicit-explicit Runge-Kutta schemes for stiff systems of differential equations. In Recent Trends in Numerical Analysis (Adv. Theory Comput. Math., vol. 3, pp. 269–288).
35. Prince, P.J. Dormand, J.R. 1981. High order embedded Runge–Kutta formulae, J. Comput. Appl. Math. 7 (1) 67–75.
36. Ranocha, H., Sayyari, M., Dalcin, L., Parsani, M., & Ketcheson, D. I. 2020. Relaxation Runge-Kutta methods: fully discrete explicit entropy-stable schemes for the compressible Euler and Navier-Stokes equations. SIAM Journal on Scientific Computing, 42(2), A612–A638.
37. Süli, E., & Mayers, D. F. (2003). An introduction to numerical analysis. Cambridge university press.

Chapter 8

Neimark-Sacker Bifurcation of a Nonstandard Discretized 3D Tigan System

Fatma Iscan[1], Mevlüde Yakıt Ongun[2]

Abstract

This paper presents a comprehensive qualitative investigation into the discrete-time topological transitions and localized phase space dynamics of a three-dimensional T-system. Crucially, rather than employing a conventional Euler discretization scheme, which frequently induces numerical instabilities and unphysical divergence, the continuous-time vector field is systematically mapped into a discrete layout using a non-local Non-Standard Finite Difference framework. Following the formulation of the rational map, the local topological architecture of the system is rigorously investigated at both the trivial equilibrium and the non-trivial interior equilibrium zones.

The primary objective of this work is to establish the precise boundaries governing the emergence of Neimark-Sacker bifurcations. To achieve this, the explicit algebraic Flip and Neimark-Sacker bifurcation criteria is implemented, which bypasses traditional approximation limits by acting directly on the transcendental characteristic polynomials of the system matrices. Under specific parameter configurations, a scheme-induced supercritical Neimark-Sacker bifurcation artifact is exposed at the origin, evaluated via three-dimensional center manifold projections and complex normal form operators. Conversely, under the physical regime, the stability boundaries shift to the interior manifold, revealing a non-degenerate supercritical Neimark-Sacker bifurcation. The same procedure is implemented to the positive fixed point.

All theoretical analyses are seamlessly supported by comprehensive numerical experiments. Finally, high-density bifurcation diagrams and detailed phase space portraits are provided to visually confirm the structural evolution of the trajectories, capturing the birth, contraction, and expansion of the bifurcated discrete manifolds and invariant closed curves.

Keywords: 3D Tigan System, Non-Standard Finite Difference, Yao Explicit Criteria, Neimark-Sacker Bifurcation, Center Manifold Projection, Phase Portraits, Bifurcation Diagrams.

1 Cand.PhD, Graduate School of Natural and Applied Sciences, Süleyman Demirel University, d2040110342@ogr.sdu.edu.tr, Lecturer, Mehmet Akif Ersoy University, mail fatmaiscan@mehmetakif.edu.tr, ORCID ID:0009-0000-9409-8368

2 Prof. Dr, Süleyman Demirel University, mail mevludeyakit@sdu.edu.tr, ORCID ID:0000-0003-2363-9395

https://doi.org/10.58830/ozgur.pub1361.c5498

1. Introduction

Dynamical systems theory constitutes an indispensable mathematical foundation for analyzing, predicting, and controlling the evolution of time-dependent phenomena across a wide spectrum of scientific engineering fields, such as fluid mechanics, population biology, secure communication protocols, and aerospace control networks. Fundamentally, a mathematical description of a real-world physical configuration naturally arises in the form of continuous-time autonomous differential equations. In these continuous frameworks, the primary objective is to characterize the qualitative and topological structures of the phase space, which are strictly governed by geometric invariants such as vector fields, manifolds, and trajectories. However, characterizing non-linear continuous systems presents massive analytical difficulties, as most realistic multi-dimensional models resist exact closed-form integrations. Consequently, researchers must rely heavily on localized linearizations, qualitative geometric theories, and advanced bifurcation analyses to map out long-term asymptotic behaviors and topological transitions [11], [12], [14], [15], [18], [21].

A profound paradigm shift in computational and theoretical non-linear dynamics occurs when transitioning from continuous-time vector fields to discrete-time mappings. In modern computational science, this temporal transition is not merely a matter of convenience but a fundamental prerequisite. Real-time digital signal processing, numerical simulators, and micro-controller-based modern engineering designs operate strictly on discrete temporal iterations rather than continuous time intervals. Nevertheless, this discretization process introduces severe theoretical complications and numerical anomalies due to the divergence in topological constraints between the two domains [12], [15], [21], [27], [28], [29], [30]. For instance, according to the classical Poincaré-Bendixson theorem, continuous autonomous systems require a minimum of three dimensions to exhibit chaotic or strange attractors. Discrete maps, however, are entirely liberated from such dimensional restrictions; they can display highly complex, chaotic trajectories and topological entanglements even within one or two dimensional phase spaces [2].

As a consequence of this fundamental difference, transforming a continuous-time system into a discrete counterpart can severely alter the underlying structural invariants. Classical numerical schemes, most notably the forward explicit Euler method, are notorious for introducing severe numerical artifacts. At larger iteration steps, these standard methods frequently induce non-physical chaotic oscillations, artificially shift or destroy the localized stability boundaries of equilibria, or introduce spurious fixed points that possess no physical meaning in the parent continuous-time model. To overcome these fundamental qualitative deficiencies, the application of the Non-Standard Finite Difference (NSFD) method, pioneered by Mickens, has emerged as a mathematically superior discretization paradigm. By utilizing sophisticated non-local approximations for non-linear terms and designing parameter-dependent complex denominator

functions, the NSFD framework meticulously preserves the structural invariants of the continuous-time system, such as positivity of solutions, boundedness, and elementary stability profiles, regardless of the chosen step size [3], [8], [9], [16], [17].

A significant milestone in modern chaotic dynamics within this domain was achieved by Tigan (2005), who introduced a novel three-dimensional autonomous chaotic system, widely recognized in the literature as the Tigan system or 3D T-system, which is governed by the following set of ordinary differential equations:

$$\begin{aligned} \dot{x} &= a(y - x) \\ \dot{y} &= (c - a)x - axz \\ \dot{z} &= xy - bz \end{aligned} \tag{1}$$

where a, b and c represent positive real parameters. Despite its apparent algebraic simplicity, the Tigan system exhibits an extraordinarily rich topological structure, including complex butterfly-shaped strange attractors, multiple coexisting global bifurcations, and complex manifold structures [23]. While the continuous Tigan system and its classical Euler-discretized variants have been partially explored in literature [20], the systematic discrete-time bifurcation analysis of the Tigan system under a structurally preserved NSFD discretization scheme remains completely unaddressed. Motivated by this distinct research gap, this paper constructs the non-standard discrete-time mapping of the 3D Tigan system by strictly applying Mickens' design rules, yielding the following discrete formulation:

$$\begin{aligned} x_{n+1} &= \frac{1}{1+\varphi a}\left(x_n + a\varphi\, y_n\right) \\ y_{n+1} &= y_n + \left((c - a)x_n - ax_n z_n\right) \\ z_{n+1} &= \frac{1}{1+\varphi b}\left(z_n + \varphi\, x_n y_n\right) \end{aligned} \tag{2}$$

where a, b and c represent the positive continuous system parameters, and $\varphi > 0$ is the non-standard step-size denominator function, which serves as our primary bifurcation parameter throughout this work.

When stable discrete-time systems like the proposed NSFD Tigan system map encounter variations in their parameter space, they face structural instabilities known as bifurcations, where the qualitative nature of the phase space shifts abruptly. In multi-dimensional discrete maps, the primary routes to deterministic chaos are governed by the Flip (period-doubling) and Neimark-Sacker (discrete Hopf) bifurcations. The rigorous classification of these discrete instabilities traditionally requires calculating the exact spectrum (eigenvalues) of the

localized Jacobian matrix and implementing intricate center manifold reductions based on classical projection methods [11]. However, in multi-parameter spaces or systems exhibiting coupled block-diagonal structures, computing exact complex eigenvalues analytically becomes highly tedious or introduces severe numerical singularities. To resolve this computational bottleneck, advanced algebraic frameworks have been developed to evaluate bifurcation criteria explicitly from the coefficients and invariants of the system's characteristic equation, completely bypassing the direct computation of eigenvalues and baseline eigenvectors [4], [5], [6], [7], [10], [11], [13], [19], [24], [25], [26], [30].

The primary novelty and contribution of this work lie in evaluating the NSFD-discretized Tigan system map using the explicit, eigenvalue-free algebraic bifurcation criteria proposed by Yao (2012). A mathematically transparent bridge is established to analyze the localized dynamics and structural stability around the fixed points. By doing so, we explicitly demonstrate how the NSFD scheme structurally outperforms classical Euler discretizations by maintaining strict topological alignment with the continuous Tigan system, while providing closed-form analytical solutions for the first Lyapunov coefficient on the reduced center manifold.

The remainder of this paper is structured as follows. In Section 2, the fixed points of the NSFD Tigan system map are established, and localized linear stability is evaluated via the Jacobian operator. Section 3 is dedicated to the application of the explicit bifurcation criteria and the analytical formulation of the center manifold reduction. Section 4 provides the corresponding numerical simulations, phase portraits, and maximum Lyapunov exponent (MLE) graphs to visually validate our mathematical proofs. Finally, a brief conclusion and future research horizons are presented in Section 5.

2. Local Stability Analysis of Fixed Points

In this section, the fixed points of the discrete-time NSFD Tigan map are characterized, and their local asymptotic stability is examined through a rigorous linear algebraic framework.Setting the right-hand side of system (2) equal to zero yields the following system of nonlinear equations, whose solutions correspond to the equilibrium points of the system:

$$\begin{aligned} x &= \frac{x+a\varphi y}{1+\varphi a} \\ y &= y + \varphi((c-a)x - axz) \\ z &= \frac{z+\varphi xy}{1+\varphi b} \end{aligned} \tag{3}$$

The following lemma can be established through direct algebraic computations.

Lemma 1: For any parameter values, the system (2)

(i) has a unique fixed point given by $E_0(0,0,0)$,

(ii) If $c > a$, system (2) possesses three fixed points $E_1(0,0,0), E_{2,3} = \left(\pm\sqrt{\frac{b(c-a)}{a}}, \pm\sqrt{\frac{b(c-a)}{a}}, \frac{c-a}{a}\right)$.

Performing the analytical differentiation on NSFD formulation yields the following the Jacobian matrix and the characteristic equation given at any fixed point $E(x,y,z)$ are obtained as:

$$J(E) = \begin{pmatrix} \frac{1}{a\varphi+1} & \frac{a\varphi}{a\varphi+1} & 0 \\ \varphi(-az-a+c) & 1 & -a\varphi x \\ \frac{\varphi y}{b\varphi+1} & \frac{\varphi x}{b\varphi+1} & \frac{1}{b\varphi+1} \end{pmatrix} \tag{4}$$

and

$$P(\rho) \coloneqq \rho^3 + \vartheta_2\rho^2 + \vartheta_1\rho + \vartheta_0 = 0 \tag{5}$$

where

$$\begin{gathered} \vartheta_2 = -tr(J), \\ \vartheta_1 = \begin{vmatrix} j_{11} & j_{12} \\ j_{21} & j_{22} \end{vmatrix} + \begin{vmatrix} j_{22} & j_{23} \\ j_{32} & j_{33} \end{vmatrix} + \begin{vmatrix} j_{11} & j_{13} \\ j_{31} & j_{33} \end{vmatrix}, \\ \vartheta_0 = -|J|. \end{gathered} \tag{6}$$

Firstly, the following lemma establishes the necessary and sufficient conditions for the stability of System (2) around its fixed point, which are used to describe the local dynamics near $E(x,y,z)$.

Lemma 2: Suppose that $\varpi_2, \varpi_1, \varpi_0 \in \mathbb{R}$. Then, the necessary and sufficient conditions for all roots μ of the equation

$$\mu^3 + \varpi_2\mu^2 + \varpi_1\mu + \varpi = 0$$

to satisfy $|\mu| < 1$ are

$|\varpi_2 + \varpi_0| < 1 + \varpi_1, |\varpi_2 - 3\varpi_0| < 3 - \varpi_1$ and $\varpi_0^2 + \varpi_1 - \varpi_0\varpi_2 < 1$ [1], [22].

In this section, the local dynamics of System (2) in a neighborhood of the fixed E_0 are studied in accordance with Lemma 2. The Jacobian matrix at E_0 is given by

$$J(E_0) = \begin{pmatrix} \frac{1}{a\varphi+1} & \frac{a\varphi}{a\varphi+1} & 0 \\ \varphi(-a+c) & 1 & 0 \\ 0 & 0 & \frac{1}{b\varphi+1} \end{pmatrix} \tag{7}$$

The characteristic equation of matrix $J(E_0)$ is

$$P \coloneqq \rho^3 + \kappa_2\rho^2 + \kappa_1\rho + \kappa_0 \tag{8}$$

where,

$$\kappa_2 = -\frac{ab\varphi^2+2a\varphi+2b\varphi+3}{(a\varphi+1)(b\varphi+1)}$$
$$\kappa_1 = \frac{a^2b\varphi^3 - abc\varphi^3 + a^2\varphi^2 - ac\varphi^2 + a\varphi + b\varphi + 3}{(a\varphi+1)(b\varphi+1)} \quad (9)$$
$$\kappa_0 = -\frac{a^2\varphi^2 - ac\varphi^2 + 1}{(a\varphi+1)(b\varphi+1)}$$

The Jacobian matrix $J(E_0)$ have eigenvalues $\rho_1 = \frac{1}{\varphi b+1}, \rho_{2,3} = \frac{1}{2}\left[B \mp \sqrt{B^2-4C}\right]$ where $\mu_{2,3}$ satisfy the equation $\rho^2 - B\rho + C = 0$, where $B = -\frac{a\varphi+2}{1+\varphi a}, C = \frac{a^2\varphi^2-ac\varphi^2+1}{1+\varphi a}$.

So in the following lemma the local stability classification of E_0 presented is obtained:

Lemma 3: If $c < a$ the fixed point $E_0$is a

(i) sink if $-3a^2+4ac \geq 0$ and $\varphi < min\left\{\frac{2}{b}, -\frac{a+\sqrt{-3a^2+4ac}}{a^2-ac}\right\}$ or $-3a^2+4ac < 0$ and $\varphi < min\left\{\frac{2}{b}, \frac{1}{a-c}\right\}$.

(ii) source if $-3a^2+4ac \geq 0$, $\varphi > max\left\{\frac{2}{b}, -\frac{a-\sqrt{-3a^2+4ac}}{a^2-ac}\right\}$ and $-3a^2+4ac < 0$ and $\varphi > max\left\{\frac{2}{b}, \frac{1}{a-c}\right\}$.

(iii) saddle if $-\frac{a+\sqrt{-3a^2+4ac}}{a^2-ac} < \varphi < -\frac{a-\sqrt{-3a^2+4ac}}{a^2-ac}$.

(iv) Non-hyperbolic if

a) $-3a^2+4ac \geq 0, \varphi = \frac{2}{b}$ or $\varphi = -\frac{a\pm\sqrt{-3a^2+4ac}}{a^2-ac}$,

b) $-3a^2+4ac < 0, \varphi = \frac{1}{a-c}$.

Let,

$$NSB_{E_0} = \left\{(a,b,c,\varphi): \varphi = \frac{1}{a-c}, -3a^2+4ac < 0\right\}.$$

If parameters change in small vicinity of NSB_{E_0}, then system (2) meets a Neimark-Sacker bifurcation at E_0.

The Jacobian matrix for E_+ is

$$J(E_+) = \begin{pmatrix} \frac{1}{a\varphi+1} & \frac{a\varphi}{a\varphi+1} & 0 \\ 0 & 1 & -\varphi\sqrt{-ba^2+abc} \\ \varphi\sqrt{\frac{-ba+bc}{a(b\varphi+1)^2}} & \varphi\sqrt{\frac{-ba+bc}{a(b\varphi+1)^2}} & \frac{1}{b\varphi+1} \end{pmatrix} \quad (10)$$

and the characteristic equation of matrix $J(E_+)$ is

$$P := \rho^3 + \kappa_2\rho^2 + \kappa_1\rho + \kappa_0 \tag{11}$$

where,

$$\begin{aligned} \kappa_2 &= -\frac{ab\varphi^2+2a\varphi+2b\varphi+3}{(a\varphi+1)(b\varphi+1)} \\ \kappa_1 &= -\frac{a^2b\varphi^3 - abc\varphi^3 + ab\varphi^2 - bc\varphi^2 - a\varphi - b\varphi - 3}{(a\varphi+1)(b\varphi+1)} \\ \kappa_0 &= -\frac{a^2b\varphi^3 - abc\varphi^3 - ab\varphi^2 + bc\varphi^2 + 1}{(a\varphi+1)(b\varphi+1)} \end{aligned} \tag{12}$$

According to the Lemma 2 following Lemma is written for stability requirement of E_+.

Lemma 4: The fixed point E_+ is locally asymptotically stable if and only if the coefficients $\kappa_2, \kappa_1, \kappa_0$ satisfy

$$|\kappa_2 + \kappa_0| < 1 + \kappa_1, |\kappa_2 - 3\kappa_0| < 3 - \kappa_1 \text{ and } \kappa_0^2 + \kappa_1 - \kappa_0\kappa_2 < 1.$$

3. Analysis of Neimark-Sacker Bifurcation

In this section, the existence, direction, and stability of the Neimark–Sacker bifurcation of System (2) near the fixed points E_0 and E_+ is studied employing the explicit flip and Neimark–Sacker bifurcation criteria, Kuznetsov's normal form method, and center manifold theory, where φ is considered as the bifurcation parameter[11], [24], [26].

3.1. Neimark-Sacker Bifurcation:Existence, Direction and Stability

In this section, topological classification of the codimension-one local bifurcations occurring at the fixed points is presented E_0 and E_+ of the non-standard finite difference Tigan system mapping. To establish analytical closed-form boundaries without executing direct, parameter-dependent complex root extractions, we deploy the explicit algebraic criteria within the setting of the generalized center manifold projection framework [11], [24], [26].

The existence of the Neimark–Sacker bifurcation is established using the explicit flip and Neimark–Sacker bifurcation criteria, as stated in the following lemma [26].

Lemma 5: Consider the following non-dimensional discrete-time dynamical system

$$\aleph_{k+1} = \mathrm{P}_\eta(\aleph_k)$$

where $\eta \in \mathbb{R}$ is regarded as a bifurcation parameter. Let $J(\aleph^*) = (\theta_{ij})_{n\times n}$ denote the Jacobian matrix of P_η evaluated at a fixed point $\aleph^* \epsilon\, \mathbb{R}^n$. The local

dynamical behavior of the system in a neighborhood of $\aleph^*$ is primarily determined by the eigenvalues of $J(\aleph^*)$. $\eta \in \mathbb{R}$ is being taken as a bifurcation parameter. Furthermore, The equation of the Jacobian matrix $J(\aleph^*) = (\theta_{ij})_{n\times n}$ at fixed point $\aleph^* \epsilon\ \mathbb{R}^n$ for P_η is written as follows

$$D_\eta(\lambda) = \lambda^n + \xi_1\lambda^{n-1} + \cdots + \xi_{n-1}\lambda + \xi_n = 0 \tag{13}$$

where $\xi_i = \xi_i(\eta, \upsilon), i = 1,2, \ldots, n$ and υ is being taken as the control parameter unless stated which is to be determined.We define a sequence of determinants $\left(N_i^{\pm}(\eta,\upsilon)\right)_{i=0}^{n}$ with $N_0^{\pm}(\eta,\upsilon) = 1$ which is to be defined as

$$N_i^{\pm} = det(T_1 \pm T_2) \tag{14}$$

where

$$T_1 = \begin{pmatrix} 1 & \xi_1 & \xi_2 & \cdots & \xi_{i-1} \\ 0 & 1 & \xi_1 & \cdots & \xi_{i-2} \\ 0 & 0 & 1 & \cdots & \xi_{i-3} \\ \cdots & \cdots & \cdots & \cdots & \cdots \\ 0 & 0 & 0 & \cdots & 1 \end{pmatrix} \tag{15}$$

$$T_2 = \begin{pmatrix} \xi_{n-i+1} & \xi_{n-i+2} & \cdots & \xi_{n-1} & \xi_n \\ \xi_{n-i+2} & \xi_{n-i+3} & \cdots & \xi_n & 0 \\ \vdots & \vdots & \cdots & \vdots & \vdots \\ \xi_{n-1} & \xi_n & \cdots & 0 & 0 \\ \xi_n & 0 & \cdots & 0 & 0 \end{pmatrix}. \tag{16}$$

Moreover, assuming that the following conditions are satisfied:

(i) $N_{n-1}^{-}(\eta_0,\upsilon) = 0,\ N_{n-1}^{+}(\eta_0,\upsilon) > 0,\ D_{\eta_0}(1) > 1,\ (-1)^n$

$D_{\eta_0}(-1) > 0, N_i^{\pm}(\eta_0,\upsilon) > 0$ for $i = n-3,\ n-5, \ldots, 2(or\ 1)$ when n is odd(or even respectively).

(ii) $\left(\frac{d}{dv}\left(N_{n-1}^{-}(\eta,\upsilon)\right)\right)_{\upsilon=\upsilon_0} \neq 0,$

(iii) $cos\left(\frac{2\pi}{\ell}\right) \neq \delta,$ where $\ell = 3,4,5, \ldots$ and $\delta = 1 - 0.5\, D_{\eta_0}(1)N_{n-3}^{-}(\eta_0,\upsilon) \Big/ N_{n-2}^{+}(\eta_0,\upsilon)$

Therefore, a Neimark–Sacker bifurcation takes place at the critical value η_0.

3.1.1. Neimark-Sacker bifurcation around E_0

Let $\mathcal{G}: \mathbb{R}^3 \times \mathbb{R}^+ \to \mathbb{R}^3$ represent the smooth discrete-time mapping generated by the NSFD scheme. The localized transcendental flow around the invariant hyper-

surface E_0 is completely governed by the spectrum Spec(J(E_0))which corresponds to the roots of the cubic characteristic equation (8). Suppose the parameters $(a, b, c, \varphi) \in NSB_{E_0}$, the eigenvalues of system (2) are :

$$\rho_1 = \frac{1}{\varphi b+1}, \rho_{2,3} = \frac{2+a\varphi \pm i\sqrt{4(1+a\varphi)^2-(2+a\varphi)^2)}}{2(1+a\varphi)} \tag{17}$$

Let $\varphi = \varphi_{NS} = \frac{1}{a-c}$. Obviously,

$$\left|\rho_{2,3}(\varphi_{NS})\right| = \sqrt{\frac{1-a\varphi^2(c-a)}{1+a\varphi}} = 1, \rho_1(\varphi_{NS}) = \frac{a-c}{1+b-c}$$

and

$$\frac{d|\rho_i(\varphi)|}{d\varphi}\Big|_{\varphi=\varphi_{NS}} = \frac{a(a-c)}{4a-2c} \neq 0, i = 2,3. \tag{18}$$

Moreover,

$$\frac{a}{a-c} \neq -2, -\frac{3}{2} \tag{19}$$

implies that $\rho_{2,3}^k \neq 1, k = 1,2,3,4$.

To isolate the non-linear dynamics on the critical two-dimensional invariant surface at $\varphi = \varphi_{NS}$ we define a formal projection operator using the bi-orthogonalization framework of [11].

The non-standard map in a localized perturbational vector form around E_0 is expressed as:

$$X = A(\varphi)X + F \tag{20}$$

where $A(\varphi) = J(E_0; \varphi_{NS})$ represent the critical linear operatör and $F = (0, -\frac{\varphi}{2}xz, \frac{\varphi}{2}xy)^T$ with $\varphi = \varphi_{NS}$. The system (15) can be written as

$$X_{n+1} = AX_n + \frac{1}{2}B(X_n, X_n) + \frac{1}{6}C(X_n, X_n, X_n) + O({X_n}^4)$$

where,

$$B(x,y) = \begin{pmatrix} B_1(x,y) \\ B_2(x,y) \\ B_3(x,y) \end{pmatrix}, \; C(x,y,z) = \begin{pmatrix} C_1(x,y,z) \\ C_2(x,y,z) \\ C_3(x,y,z) \end{pmatrix} \tag{21}$$

The symmetric multilinear functions $B: \mathbb{R}^3 \times \mathbb{R}^3 \longrightarrow \mathbb{R}^3$ and $C: \mathbb{R}^3 \times \mathbb{R}^3 \longrightarrow \mathbb{R}^3$are defined, respectively, as follows:

$$B_i(x,y) = \sum_{j,k=1}^{3} \frac{\partial^2 X_i(v,0)}{\partial v_j \partial v_k}\Big|_{v=0} x_j y_k, \;\; i = 1,2,3$$

$$C_i(x,y,z) = \sum_{j,k,l=1}^{3} \left.\frac{\partial^2 X_i(\nu,0)}{\partial \nu_j \partial \nu_k \partial \nu_l}\right|_{\nu=0} x_j y_k u_l, \quad i = 1,2,3$$

For the system (15)

$$B(x,y) = \begin{pmatrix} 0 \\ -\frac{\varphi_{NS}}{2}(x_1y_3 + x_3y_1) \\ \frac{\varphi_{NS}}{2}(x_1y_2 + x_2y_1) \end{pmatrix}, \; C(x,y,z) = \begin{pmatrix} 0 \\ 0 \\ 0 \end{pmatrix} \tag{22}$$

Let $q\epsilon\mathbb{C}^3$ be the right eigenvector of $A(\varphi_{NS})$ corresponding to $\lambda_1 = e^{i\theta_0}$, and let $p\epsilon\mathbb{C}^3$be the adjoint left eigenvector of $A^T(\varphi_{NS})$ satisfying $A^T p = e^{-i\theta_0}p$. Due to the uncoupled block tracking along the stable transversal dimension, the exact algebraic structures are parametrized as:

$$q = (\upsilon_1, 1, 0)^T, p = (p_1, p_2, 0)^T$$

where υ_1 and p_1 are complex parameters uniquely determined by the linear kernels, and the bi-orthogonality normalization condition under the Hermitian inner product is strictly enforced:

$\langle p, q\rangle = \bar{p}^T \cdot q = \bar{p}_1\upsilon_1 + \bar{p}_2 = 1.$

The state vector $X_n = (x_n, y_n, z_n)^T \in \mathbb{R}^3$of the NSFD Tigan system map is decomposed within the local coordinate system of the center manifold W^c. Let $z \in \mathbb{C}$ define the complex coordinates of the two-dimensional critical eigenspace $Y^c = span\{q, \bar{q}\}$. The embedding operator $H\colon \mathbb{C} \to \mathbb{R}^3$ maps the localized flow via the second-order Taylor approximation:

$$X_n = z_n q + \bar{z}_n \bar{q} + W(z_n, \bar{z}_n)$$

where

$$W(z_n, \bar{z}_n) = \frac{1}{2}w_{20}z_n^2 + w_{11}z_n\bar{z}_n + \frac{1}{2}w_{02}\bar{z}_n^2 + \mathcal{O}(|z_n|^3).$$

By substituting the coordinate restrictions into the global map and executing the bi-orthogonal inner product projections with the adjoint left eigenvector $p\epsilon\mathbb{C}^3$ the restricted dynamic tracking equation reduces to the standard Poincaré-Birkhoff normal form:

$$z_{n+1} = \lambda_1 z_{n+1} + \frac{1}{2}g_{20}z_n^2 + g_{11}z_n\bar{z}_n + \frac{1}{2}g_{02}\bar{z}_n^2 + \frac{1}{2}g_{21}z_n^2\bar{z}_n + \mathcal{O}(|z_n|^3).$$

The second-order complex Taylor coefficients $g_{ij}\epsilon\mathbb{C}$ are computed directly from the symmetric bilinear form contractions:

$$\begin{aligned} g_{20}(\varphi_{NS}) &= \langle p, B(q,q)\rangle = \bar{p}^T \cdot \; B(q,q) \\ g_{11}(\varphi_{NS}) &= \langle p, B(q,\bar{q})\rangle = \bar{p}^T \cdot B(q,\bar{q}) \\ g_{02}(\varphi_{NS}) &= \langle p, B(\bar{q},\bar{q})\rangle = \bar{p}^T \cdot \; B(\bar{q},\bar{q}) \\ g_{21}(\varphi_{NS}) &= \langle p, C(q,q,q)\rangle \end{aligned} \tag{23}$$

By some tedious calculation, this coefficients are obtained as g_{20}=0, $g_{11}=0$, $g_{02}=0$ and $g_{21}=-\varphi_{NS}a\bar{p}_2\left[2v_1\left(\frac{v_1+\bar{v}_1}{b}\right)+\bar{v}_1\left(\frac{\varphi_{NS}v_1}{2\lambda_1-1+\varphi_{NS}b}\right)\right]$. To determine the topological stability and orientation of the bifurcating closed invariant curves, we construct the First Lyapunov Coefficient(l_1). By leveraging the fact that $g_{20}=g_{11}=g_{02}=0$, the generalized invariant mapping simplifies to the following analytical kernel:

$$l_1=-\frac{\varphi_{NS}a}{2}Re\left(e^{-i\theta_0}\bar{p}_2\left[2v_1\left(\frac{v_1+\bar{v}_1}{b}\right)+\bar{v}_1\left(\frac{\varphi_{NS}v_1}{2\lambda_1-1+\varphi_{NS}b}\right)\right]\right). \tag{24}$$

Theorem 1: Suppose that the condition (12) is satisfied and $\ell_1(\varphi_{NS})\neq 0$. Then, a Neimark-Sacker bifurcation occurs at the fixed point $E_0(0,0,0)$ of system (2) when the bifurcation parameter φ passes through the critical value φ_{NS}. Moreover, if $\ell_1(\varphi_{NS})<0$,the bifurcation is supercritical and a stable invariant closed curve emerges from E_0; whereas if resp. $\ell_1(\varphi_{NS})>0$, the bifurcation is subcritical and an unstable invariant closed curve is generated.

3.1.2. Neimark-Sacker bifurcation around E_+

In this section, the localized bifurcation dynamics of the 3D Tigan system discretized via the Non-Standard Finite Difference (NSFD) scheme (2) are investigated. The critical threshold of the step-size parameter φ, where the system loses its asymptotic stability and transitions into a stable limit cycle, is rigorously analyzed by employing the Lemma 5.

For n=3, the following lemma establishes the necessary and sufficient parametric conditions under which System (2) undergoes a Neimark–Sacker bifurcation as the bifurcation parameter crosses its critical value.

Lemma 6: System (2) undergoes a Neimark–Sacker bifurcation near the fixed point E_0 at $\varphi=\varphi_{NS}$ if and only if the following conditions hold:

$$\begin{aligned}
&1-\kappa_1+\kappa_0(\kappa_2-\kappa_0)=0\\
&1+\kappa_1-\kappa_0(\kappa_2+\kappa_0)>0\\
&1+\kappa_2+\kappa_1+\kappa_0>0\\
&1-\kappa_2+\kappa_1-\kappa_0>0\\
&\frac{d}{d\varphi}\left(1-\kappa_1+\kappa_0(\kappa_2-\kappa_0)\right)_{\varphi=\varphi_{NS}}\neq 0\\
&cos\left(\frac{2\pi}{\ell}\right)\neq 1-\frac{1+\kappa_2+\kappa_1+\kappa_0}{2(1+\kappa_0)},\ell=3,4,5,\ldots
\end{aligned}$$

where $\kappa_2,\kappa_1,\kappa_0$ are given as in (12).

Set

$$NSB_{E_2}=\{(a,b,c,\varphi):\varphi=\varphi_{NS},a,b,c>0\ \}$$

and for parameter perturbation in a small neighborhood of NSB_{E_+} two roots of (12) equation are complex conjugate having modulus one and magnitude of other root is not equal to one, then the system (2) experiences Neimark-Sacker bifurcation around E_+ as given:

$$\varphi_{NSB_{E_2}} = \frac{1}{6(-c+a)ab}\sqrt[3]{b^2\left(H + 12a\sqrt{-\frac{1}{ab}\mathrm{K}}\right)} + \frac{L}{3((-c+a)a)\Theta} + \frac{2(2a-c)}{3a(-c+a)} \qquad (25)$$

$$\mathrm{H} = 648a^4 + 944a^3b - 972a^3c - 1020a^2bc + 324a^2c^2 + 204abc^2 + 8bc^3$$

$$\begin{aligned}\mathrm{K} = 3(&108a^8 - 72a^7b - 324a^7c - 332a^6b^2 + 432a^6bc + 324a^4c^2 \\ &+ 252a^5b^3 + 1008a^5b^2c - 855a^5bc^2 - 108a^5c^3 \\ &- 820a^4b^3c - 1174a^4b^2c^2 + 702a^4bc^3 + 989a^3b^3c^3 \\ &+ 628a^3b^2c^3 - 207a^3bc^4 - 510a^2b^3c^3 - 114a^2b^2c^4 \\ &+ 113ab^3c^4 - 16ab^2c^5 - 16b^3c^5\end{aligned}$$

$$\mathrm{L} = 2(9a^3 + 25a^2\mathrm{b} - 9a^2\mathrm{c}) - 19\mathrm{abc} + \mathrm{b}c^2.$$

Set

$$NSB_{E_+} = \{(a, b, c, \varphi): \varphi = \varphi_{NS}, a, b, c > 0\ \}$$

and for a parameter perturbation in a small neighborhood of NSB_{E_+}, two roots of (11) are complex conjugate having modulus one and the magnitude of other root is not equal to one, the system (2) experiences NS bifurcation around E_+. Let $\kappa_1, \kappa_2 \epsilon \mathbb{C}^3$ be the right and left eigenvectors of $A(\varphi_{NS})$, respectively, corresponding to the critical conjugate eigenvalues $\rho_1(\varphi_{NS})$ and $\rho_2(\varphi_{NS})$, such that

$$A(\varphi_{NS})\kappa_1 = \rho_1(\varphi_{NS})\kappa_1, A^T(\varphi_{NS})\kappa_2 = \rho_2(\varphi_{NS})\kappa_2 \; and < \kappa_2, \kappa_1 >= \sum_{i=1}^{3} \bar{\kappa}_{2i}\kappa_{1i} = 1$$

The coefficient $\ell_2(\varphi_{NS})$, obtained from equation (24), characterizes both the direction and the stability of the Neimark–Sacker bifurcation. The corresponding results are stated in the following theorem.

Theorem 2: Suppose that condition (12) holds and $\ell_2(\varphi_{NS}) \neq 0$. Then the positive equilibrium point E_+ of system (2) experiences a Neimark–Sacker bifurcation when the parameter φ crosses the critical threshold φ_{NS}. In addition, if $\ell_2(\varphi_{NS}) < 0$, the bifurcation is supercritical and gives rise to an attracting invariant closed curve in a neighborhood of E_+. On the other hand, if $\ell_2(\varphi_{NS}) > 0$, the bifurcation is subcritical and an unstable invariant closed curve is generated near E_+.

4. Numerical Simulations

In this section, comprehensive numerical experiments to validate the theoretical bifurcation thresholds and normal form classifications derived in the previous sections are presented. The simulations illustrate how the Non-Standard Finite

Difference (NSFD) scheme behaves under different step-size parameters φ across two distinct parametric regimes.

Case 1: Parameter values are taken as $a = 12, b = 8, c = 4$. By some calculation, the bifurcation point is obtained as $\varphi_{NS} = 0{,}125$ at fixed point $E_0(0,0,0)$ of the system (2). The Jacobian matrix at E_0 have eigenvalues $\rho_1 = 0.5$ and $\rho_{2,3} = 0.7 \pm 0.714142842854285i$ with $|\rho_i| = 1, i = 2{,}3$. Furthermore

$$\frac{d|\rho_i(\varphi)|}{d}\Big|_{\varphi=\varphi_{NS}} = \frac{a(a-c)}{2(2a-c)} = 2.4 \neq 0, i = 2{,}3.$$

$$\frac{a}{a-c} = \frac{3}{2} \neq -2, -\frac{3}{2}.$$

Therefore, the conditions for the existence of a Neimark–Sacker bifurcation are satisfied for $(a, b, c, \varphi) \epsilon NSBE_0$, which confirms Lemma 3. Consequently, a Neimark–Sacker bifurcation occurs in a neighborhood of the fixed point E_0 as the parameter φ crosses its critical value φ_{NS}.

Let $q_1, p_1 \epsilon \mathbb{C}^3$ be eigenvectors of $A(\varphi_{NS})$ and $A^T(\varphi_{NS})$ corresponding to the eigenvalues corresponding to $\rho_{1,2}$ respectively. By straightforward algebraic computations, the eigenvectors are obtained as follows:

$q_1 \sim (0.5 - 1.190238i, 1{,}0)^T$, and $p_2 \sim (1, -0.3 - 0.7141428i)^T$. Calculating the coefficient g_{20}, g_{21}, g_{11} and g_{02} with (23), The Lyapunov coefficient $l_1(\varphi_{NS}) < 0$. So, the NS bifurcation is supercritical according to the Theorem 1.

The NS diagram are displayed in Figure 1(i) which reveal that the conditions of stability for the fixed point E_0 occurs when $\varphi < \varphi_{NS}$, loses its stability at $\varphi = \varphi_{NS}$ and there appears an attracting closed invariant curve when $\varphi > \varphi_{NS}$. The MLEs related Figure1(i) are shown Figure 1(ii). The phase portraits of system (2) are plotted for different values of φ in Figure 2.

Case 2: By taking $a = 10, b = 8$ and $c = 28$. the positive fixed point is found as $E_+ = (3.7947331922, 3.7947331922, 1.8)$ of system and bifurcation parameter $\varphi_{NS_+} = 0.01278893113$. The Jacobian matrix is obtained at E_+ as

$$A(\varphi_{NS}) = \begin{pmatrix} 0.8866118246 & 0.1133881756 & 0 \\ 0 & 1 & -0.48530581464 \\ 0.04402619739 & 0.04402619739 & 0.9071846264 \end{pmatrix},$$

and the eigenvalues of $A(\varphi_{NS})$ are $\rho_{1,2} = 0.9864774997 \mp 0.1638967173i$, $\rho_3 = 0.8208414516$ with $|\rho_{1,2}| = 1$. Furthermore

$$1 - \kappa_1 + \kappa_0(\kappa_2 + \kappa_0) = 0$$

$$1 + \kappa_1 - \kappa_0(\kappa_2 + \kappa_0) = 0.652438648 > 0$$

$$1 + \kappa_2 + \kappa_1 + \kappa_0 = 0.0048453427 > 0$$

$$1 - \kappa_2 + \kappa_1 - \kappa_0 = 7.234121133 > 0$$
$$1 + \kappa_0 = 0.1791585557 > 0$$
$$1 - \kappa_0 = 1.820841444 > 0$$
$$\frac{\partial}{\partial \varphi}\left(1 - \kappa_1 + \kappa_0(\kappa_2 - \kappa_0)\right) \neq 0$$

and

$$1 - \frac{1+\kappa_2+\kappa_1+\kappa_0}{2(1+\kappa_0)} = 0.98647750122.$$

From the resonance condition $cos\left(\frac{2\pi}{l}\right) = 0.98647750122$, we get $l = \pm 6.36931435274$.

By Lemma 6, the transversality and non-resonance conditions required for a Neimark–Sacker bifurcation are satisfied at E_+. Hence, the system exhibits a Neimark–Sacker bifurcation at the fixed point φ_{NS} when $\varphi = \varphi_{NS}$, and an invariant closed curve is generated in a neighborhood of E_+.

Let $m_1, m_2 \epsilon \mathbb{C}^3$ denote the right and left eigenvectors of $A(\varphi_{NS})$ associated with the critical eigenvalues $\rho_{1,2}$ respectively. These eigenvectors are computed explicitly as follows:

$m_1 \sim (-0.2541 - 0.4170i, 0.8265, 0.0230 - 0.2791)^T$,$m_2 \sim (0.1093 + 0.1793i, -0.1496 + 0.3091i, 09154)^T$. For $< m_1, m_2 > = 1$, normalized vector is taken as $m_2 \sim (0.2380 - 0.2486i, 0.5417 + 0.1139i, -0.3556 - 1.4319i)^T$. Calculating the coefficient g_{20}, g_{21}, g_{11} and g_{02} with (23), The Lyapunov coefficient $l_1(\varphi_{NS}) > 0$. So, the NS bifurcation is subcritical according to the Theorem 2.

Figure 3(i), shows the Neimark–Sacker bifurcation diagram for $a = 10, b = 8$ and $c = 28$, where the critical bifurcation value is $\varphi_{NS_+} = 0.01278893113$ at the equilibrium point $E_+ = (3.7947331922, 3.7947331922, 1.8)$. The bifurcation diagram is represented in the (x, y, z) −space. Figure 4-5 depicts the corresponding phase portraits of System (2) for several values of φ, illustrating the evolution of the system dynamics before and after the onset of the Neimark–Sacker bifurcation. Figure (6) illustrates chaotic attractor and the corresponding Poincaré section of system (2) in the (x, y, z) −space and (x, y, z) −plane, respectively, demonstrating the chaotic dynamics around the equilibrium point E_+.

Case 3: By taking $a = 2, b = 0.4$ and $c = 5$ the positive fixed point is found as $E_+ = (0.7745966692, 0.7745966692, 1.5)$ of system and bifurcation parameter $\varphi_{NS_+} = 0.047815$. The Jacobian matrix is obtained at E_+ as

$$A(\varphi_{NS}) = \begin{pmatrix} 0.9131064341 & 0.08689356591 & 0 \\ 0 & 1 & -0.07371261905 \\ 0.03616794258 & 0.03616794258 & 0.9813229552 \end{pmatrix},$$

and the eigenvalues of $A(\varphi_{NS})$ are $\rho_{1,2} = 1.00033816443896 \mp 0.066035538269995i$, $\rho_3 = 0.893753060422073$ with $|\rho_{1,2}| = 1$. Furthermore

$$1 - \kappa_1 + \kappa_0(\kappa_2 + \kappa_0) = 0$$
$$1 + \kappa_1 - \kappa_0(\kappa_2 + \kappa_0) = 0.386349936 > 0$$
$$1 + \kappa_2 + \kappa_1 + \kappa_0 = 0.0004633218 > 0$$
$$1 - \kappa_2 + \kappa_1 - \kappa_0 = 7.585832136 > 0$$
$$1 + \kappa_0 = 0.1017449838 > 0$$
$$1 - \kappa_0 = 1.898255016 > 0$$
$$\frac{\partial}{\partial \varphi}\left(1 - \kappa_1 + \kappa_0(\kappa_2 - \kappa_0)\right) \neq 0$$

and

$$1 - \frac{1+\kappa_2+\kappa_1+\kappa_0}{2(1+\kappa_0)} = 0.9977231222.$$

From the resonance condition $cos\left(\frac{2\pi}{l}\right) = 0.9977231222$, we get $l = \pm 6.29752399977$.

In view of Lemma 6, the necessary and sufficient conditions for the existence of a Neimark–Sacker bifurcation are fulfilled for $(a, b, c, \varphi) \in NSB_{E_2}$. Hence, the fixed point E_+ experiences a Neimark–Sacker bifurcation as the parameter φ crosses the critical threshold φ_{NS}.

Let $t_1, t_2 \epsilon \mathbb{C}^3$ be two eigenvectors of $A(\varphi_{NS})$ and $A^T(\varphi_{NS})$ corresponding to $\rho_{1,2}$ respectively. By some algebraic calculation t_1, t_2 can be found as follows, $t_1 \sim (0.405941170103580 - 0.307302670365212i, 0.6410583723889, -0.0029409231097 - 0.57429291251)^T$ and $t_2 \sim (-0.18739031 + 0.14185686i, 0.183402262868 + 0.63691474i, -0.710960419)^T$.

Some calculation via help of (17) MLEs is obtained positive. So, according to the theorem, the Neimark-Sacker bifurcation is subcritical.

Figure 7(i) presents the Neimark–Sacker bifurcation diagram and the corresponding maximum Lyapunov exponents (MLEs) of System (2) for a=2, b=0.4,c=5 in the (φ, x)-plane. The critical bifurcation value is found to be $\varphi_{NS_+} = 0.047815$ at the equilibrium point $E_+ = (0.7745966692, 0.7745966692, 1.5)$. Figure 8 depicts the corresponding

phase portraits for several values of φ, illustrating the evolution of the system dynamics as the bifurcation parameter varies. Furthermore, Figure 9 shows the phase portraits of System (2) in the (x, y), (x, z) and (y, z)-planes, respectively, confirming the presence of chaotic dynamics in the vicinity of the equilibrium point E_+.

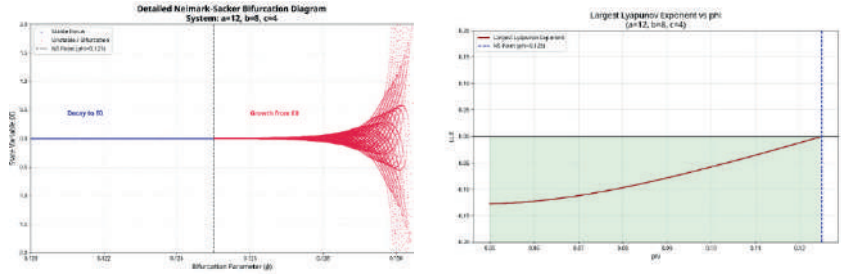

(i) (ii)

Figure 1: (i) Neimark-.sacker Bifurcation Diagram with respect to phi for a=12, b=8 and c=4(ii) Corresponding Maximum Lyapunov Exponents

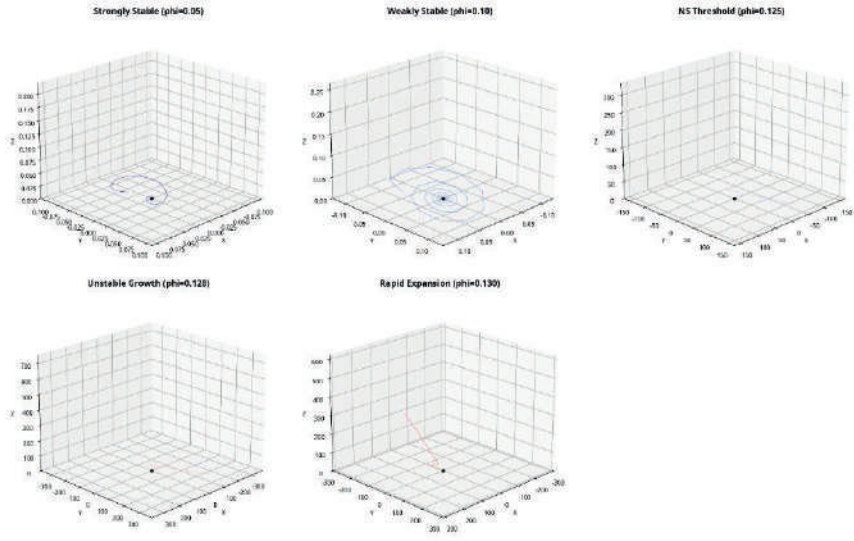

Figure 2:Phase Portraits of System (2) with a=12, b=8,c=4 in (x, y, z) plane for different φ values.

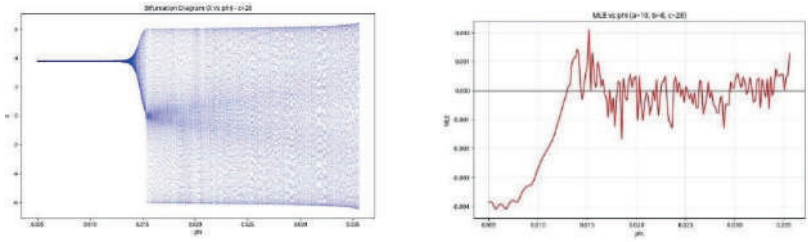

(i) (ii)

Figure 3:Neimark Sacker Bifurcation Diagram with a=10, b=8,c=28 in (φ, x) plane and MLEs.

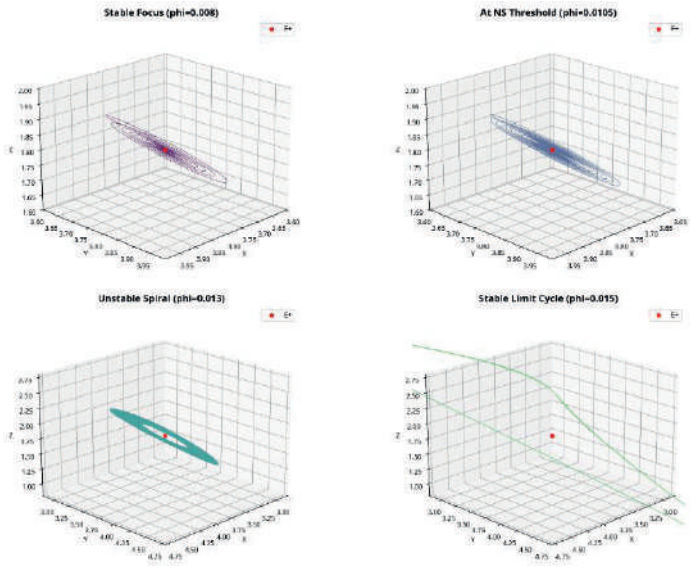

Figure 4: Phase Portraits of System (2) with a=10, b=8,c=28 in (x, y, z) plane for different φ values.

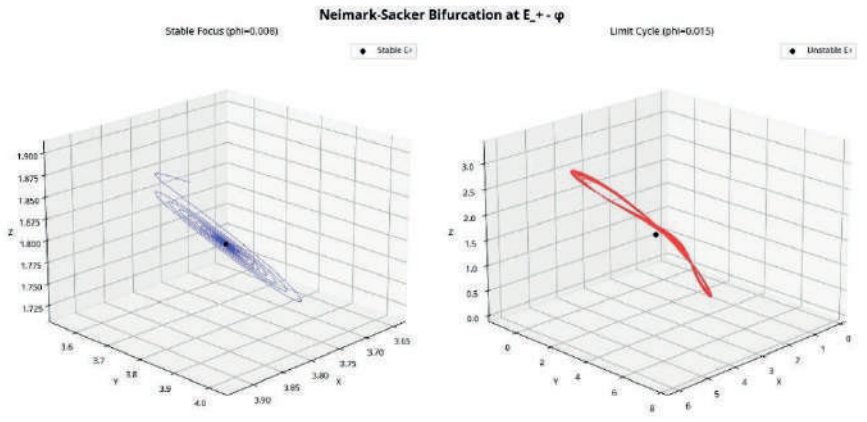

Figure 5:Neimark Sacker Bifurcation Diagram with a=10, b=8,c=28 in (x, y, z) plane.

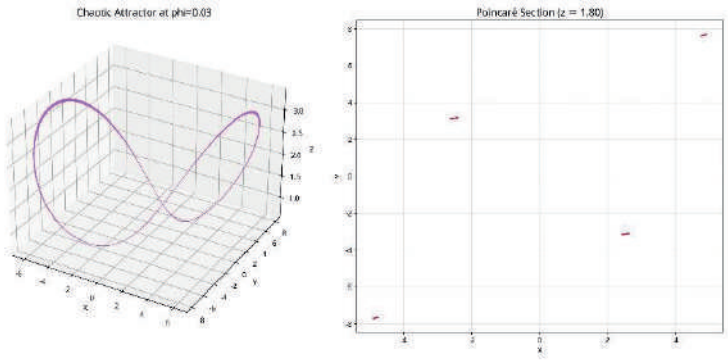

Figure 6: Chaotic attractor in the (x, y, z)-space and its corresponding Poincaré section in the (x, y, z) $-$plane for the equilibrium point E_+ with a=10, b=8,c=28.

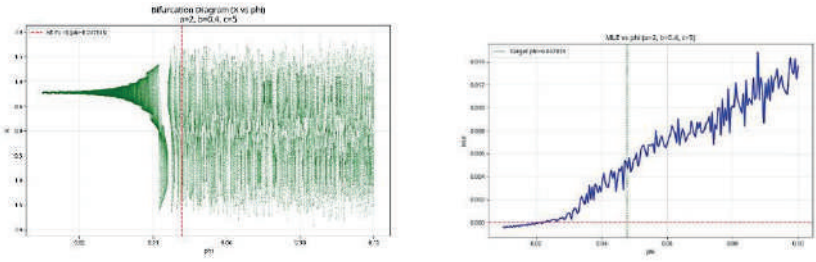

(i) (ii)

Figure 7:Neimark Sacker Bifurcation Diagram with a=2, b=0.4,c=5 in (φ, x) plane and MLEs.

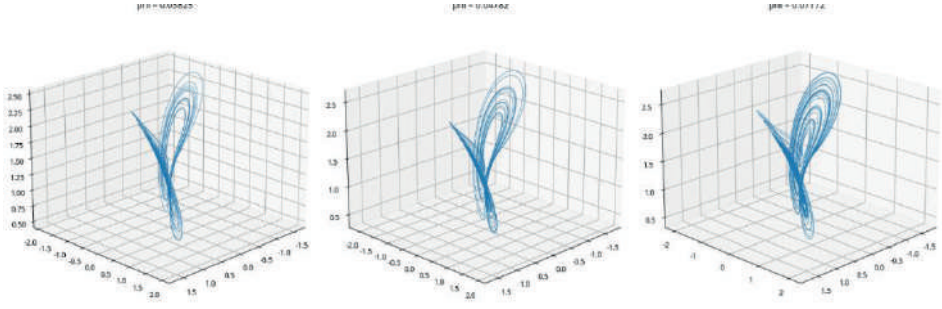

Figure 8: Phase Portraits of System (2) with a=2, b=0.4, c=5 in (x, y, z) plane for different φ values.

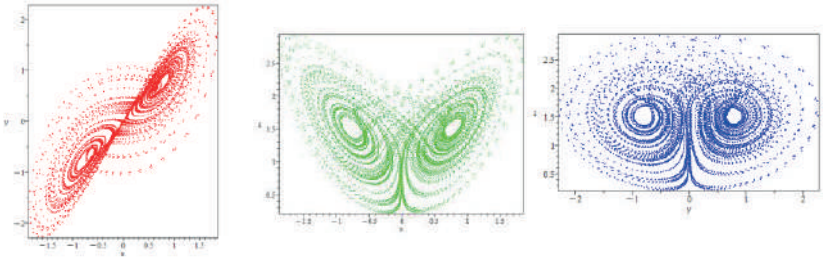

Figure 9: Phase Portraits of System (2) with a=2, b=0.4, c=5 in (x, y), (x,z) and (y,z) plane $\varphi = 0.0475815$ value.

5. Conclusion

In this study, the discrete-time dynamics and bifurcation behaviors of a three-dimensional Tigan system are comprehensively investigated. Instead of employing traditional discretization schemes such as the standard Euler method,which often introduce numerical instabilities and artificial chaos, Non-Standard Finite Difference (NSFD) scheme is utilized to construct a topologically consistent discrete model. This approach successfully preserved the essential structural properties and positivity of the original continuous system.

The primary focus of our mathematical analysis was centered on the local stability and the occurrence of a Neimark-Sacker bifurcation at the positive equilibrium point. By choosing the step size φ as the main bifurcation parameter, we rigorously determined the critical thresholds where the system transitions from a stable steady state to quasi-periodic oscillations. The topological classification and existence conditions for the Neimark-Sacker bifurcation were explicitly derived using Yao's bifurcation criteria, alongside the evaluation of the first Lyapunov coefficient to determine the direction and stability of the emerging invariant closed curve.

To validate the theoretical framework, extensive numerical simulations—including bifurcation diagrams, Lyapunov exponent spectra, and phase portraits—were presented. The numerical results demonstrated an excellent agreement with our analytical findings, confirming that the step size φ plays a crucial role in controlling the complex, chaotic dynamics of the system.

In conclusion, the application of the NSFD method combined with rigorous bifurcation analysis provides a robust framework for understanding and predicting the long-term behavior of 3D chaotic systems in a discrete domain. Future research directions may include the exploration of global bifurcations, chaos control strategies, or the extension of this methodology to fractional-order discrete Tigan systems.

6. References

[1] Camouzis, E., & Ladas, G. (2007). Dynamics of third-order rational difference equations with open problems and conjectures. Chapman and Hall/CRC.

[2] Ciesielski, K. (2012). The Poincaré-Bendixson theorem: from Poincaré to the XXIst century. Central European Journal of Mathematics, 10(6), 2110-2128.

[3] Çetinkaya, İ. T., Kocabıyık, M., & Ongun, M. Y. (2021). Stability analysis of discretized model of glucose–insulin homeostasis. *Celal Bayar University Journal of Science*, *17*(4), 369-377.

[4] Din, Q., Elsadany, A. A., & Khalil, H. (2017). Neimark-Sacker Bifurcation and Chaos Control in a Fractional-Order Plant-Herbivore Model. *Discrete Dynamics in Nature and Society*, *2017*(1), 6312964.

[5] Feng, G., Yin, D., & Jiacheng, L. (2021). Neimark–Sacker Bifurcation and Controlling Chaos in a Three-Species Food Chain Model through the OGY Method. *Discrete Dynamics in Nature and Society*, *2021*(1), 6316235.

[6] He, Z., & Lai, X. (2011). Bifurcation and chaotic behavior of a discrete-time predator–prey system. *Nonlinear Analysis: Real World Applications*, *12*(1), 403-417.

[7] Kangalgil, F., & Işık, S. (2020). Controlling chaos and Neimark-Sacker bifurcation in a discrete-time predator-prey system. *Hacettepe Journal of Mathematics and Statistics*, *49*(5), 1761-1776.

[8] Kocabıyık, M., & Ongun, M. Y. (2023). Discretization and stability analysis for a generalized type nonlinear pharmacokinetic models. *Gazi University Journal of Science*, *36*(4), 1675-1691.

[9] Kocabiyik, M., & Ongun, M. Y. (2025). Distributed order hantavirus model and its nonstandard discretizations and stability analysis. *Mathematical Methods in the Applied Sciences*, *48*(2), 2404-2420.

[10] Kulenović, M. R., Moranjkić, S., Nurkanović, M., & Nurkanović, Z. (2018). Global Asymptotic Stability and Naimark-Sacker Bifurcation of Certain Mix Monotone Difference Equation. *Discrete Dynamics in Nature and Society*, *2018*(1), 7052935.

[11] Kuznetsov, Y. A. (1998). *Elements of applied bifurcation theory*. New York, NY: Springer New York.

[12] Li, X. F., Chu, Y. D., Zhang, J. G., & Chang, Y. X. (2009). Nonlinear dynamics and circuit implementation for a new Lorenz-like attractor. *Chaos, Solitons & Fractals*, *41*(5), 2360-2370.

[13] Liu, W., & Jiang, Y. (2020). Flip bifurcation and Neimark–Sacker bifurcation in a discrete predator–prey model with harvesting. *International Journal of Biomathematics*, *13*(01), 1950093.

[14] Lorenz, E. N. (1963). Deterministic nonperiodic flow, journal of the atmospheric sciences vol. 20. *No. In. XX*.

[15] Luo, W., Ou, Q., Yu, F., Cui, L., & Jin, J. (2020). Analysis of a new hidden attractor coupled chaotic system and application of its weak signal detection. *Mathematical Problems in Engineering*, *2020*(1), 8849283.

[16] E. Mickens, R. (1994). *Nonstandard finite difference models of differential equations*.

[17] Mickens, R. E. (2002). Nonstandard finite difference schemes for differential equations. *Journal of Difference Equations and Applications*, *8*(9), 823-847.

[18] Kocabıyık, M. (2022). Nonstandard discretization and stability analysis of a novel type Malaria-Ross model. Journal of the Institute of Science and Technology, 12(2), 1023-1033.

[19] Qin, S., Zhang, J., Du, W., & Yu, J. (2016). Neimark–sacker bifurcation in a new three–dimensional discrete chaotic system. *ICIC-EL*, *10*(4), 1-7.

[20] Rana, S. M. S. (2023). Bifurcation analysis and 0-1 chaos test of a discrete T system. *Chaos Theory and Applications*, *5*(2), 90-104.

[21] Rössler, O. E. (1976). An equation for continuous chaos. *Physics Letters A*, *57*(5), 397-398.

[22] Jury, E. I. (1962). A simplified stability criterion for linear discrete systems. *Proceedings of the IRE*, *50*(6), 1493-1500.

[23] Tigan, G. (2005). Analysis of a dynamical system derived from the Lorenz system. *Sci. Bull. Politehnica Univ. Timisoara Tomul*, *50*(64), 61-72.

[24] Wen, G. (2005). Criterion to identify Hopf bifurcations in maps of arbitrary dimension. *Physical Review E—Statistical, Nonlinear, and Soft Matter Physics*, *72*(2), 026201.

[25] Xin, B., Chen, T., & Ma, J. (2010). Neimark-Sacker Bifurcation in a Discrete-Time Financial System. *Discrete Dynamics in Nature and Society*, *2010*(1), 405639.

[26] Yao, S. (2012). New bifurcation critical criterion of Flip-Neimark-Sacker bifurcations for two-parameterized family of n-dimensional discrete systems. *Discrete Dynamics in Nature and Society*, *2012*(1), 264526.

[27] Yousef, A. M., Salman, S. M., & Elsadany, A. A. (2018). Stability and bifurcation analysis of a delayed discrete predator–prey model. *International Journal of Bifurcation and Chaos*, *28*(09), 1850116.

[28] Yousef, A. M., Rida, S. Z., & Arafat, S. (2020). Stability, analytic bifurcation structure and chaos control in a mutual interference host-parasitoid model. *International Journal of Bifurcation and Chaos*, *30*(15), 2050237.

[29] Zhang, Y., Cheng, Q., & Deng, S. (2023). Qualitative structure of a discrete predator-prey model with nonmonotonic functional response. *Discrete & Continuous Dynamical Systems-Series S*, *16*.

[30] Zhao, M. (2021). Bifurcation and chaotic behavior in the discrete BVP oscillator. *International Journal of Non-Linear Mechanics*, *131*, 103687.

Interdisciplinary Applications of Applied Mathematics

Editor:
Prof. Dr. Mevlüde YAKIT ONGUN

ÖZGÜR PRESS